LUND UNIVERSITY

Impacts of climate change on surface hydrology in the source region of the Yellow River

Yuan, Feifei

2015

Link to publication

Feifei Yuan

Impacts of climate change on surface hydrology in the source region of the Yellow River

Impacts of climate change on surface hydrology in the source region of the Yellow River

FEIFEI YUAN | WATER RESOURCES ENGINEERING | LUND UNIVERSITY SWEDEN

LUND
UNIVERSITY

Report No 1064

Impacts of climate change on surface hydrology in the source region of the Yellow River

Feifei Yuan

Organization	Document name
LUND UNIVERSITY	DOCTORAL DISSERTATION
Water Resources Engineering, Box 118, SE-221 00 Lund , Sweden	**Date of issue** April 28, 2015
Author: Feifei Yuan	**Coden:** LUTVDG/TVVR-1064 (2015)

Title: Impacts of climate change on surface hydrology in the source region of the Yellow River

Abstract The source region of the Yellow River contributes about 35% of the total water yield in the Yellow River basin playing an important role for meeting the downstream water resources requirements. The declining water availability caused by climate change in the source region of the Yellow River is expected to have severe repercussions for the 110 million basin inhabitants in terms of water resources affecting agricultural productivity, municipal, and industrial water supply. Thus, this study investigated the impacts of climate change on surface hydrology in the source region of the Yellow River. The presented results have important implications for water resources management in the Yellow River.

Hydroclimatic trend and periodicity during the last 50 years were investigated to identify significant changes in time and space over the study area. Results showed that mean annual temperature increased for all stations and it had an accelerated increasing trend during the last decade. Mean annual precipitation trends varied depending on station location; however, they were generally slightly decreasing. Annual streamflow decreased markedly especially from the 1990s but showed recovery during recent years. Statistically significant changes in trend occurred for temperature in 1998 and for streamflow in 1990. Based on the streamflow change point, seasonal analysis results showed that precipitation mainly decreased during the summer monsoon period (July-September) and temperature increased throughout the year. Corresponding to the weakened monsoon period the average runoff depth is decreasing by 0.74 mm/year over the whole area. Statistically significant 2 to 4-year periodicities for mean areal precipitation and temperature occurred over the area. For streamflow, an even stronger 8-year periodicity was revealed from the end of the 60s to the beginning of the 90s. Frequency analysis investigated the magnitudes of mean annual precipitation and discharge corresponding to a given frequency. Hydroclimatic trends and linkages at each sub-basin were investigated to further improve the understanding of observed streamflow changes.

The summer precipitation (June-September) in the source region of the Yellow River accounts for approximately 70% of the annual total playing an important role for water availability, and its decreasing trend will cause water shortage in the whole river basin. Hence, summer precipitation trends and teleconnections with global sea surface temperature (SST) and Southern Oscillation Index (SOI) from 1961 to 2010 were investigated. Results show that the precipitation has a strongly decreasing gradient from southeast to northwest due to the weakening summer monsoon, and a division of the region into three homogeneous precipitation zones shows marked spatial variability. The northwest part (zone 1) had a non-significantly increasing trend, and the middle and southeast parts (zone 2 and 3) that receive the most precipitation displayed a statistically significant decreasing trend. The summer precipitation in the whole region shows statistically significant negative correlations with the central Pacific SST for 0-4 month lags and with the southern Indian and Atlantic Ocean SST for 5-8 month lags. Analyses of sub-regions reveal intricate and complex correlations with different SST areas that further explain the summer precipitation variability. The SOI had significant positive correlations mainly for 0-2 month lag with summer precipitation. It is seen that El Niño Southern Oscillation (ENSO) events have an influence on the summer precipitation, and the predominant negative correlations indicate that higher SST in equatorial Pacific areas corresponding to El Nino coincides with less summer precipitation in the source region of the Yellow River.

The linkages between the precipitation and global teleconnection patterns were identified, and summer precipitation was predicted based on revealed teleconnections. It was found that precipitation in the study area is positively related to North Atlantic Oscillation, West Pacific Pattern and El Nino Southern Oscillation, and inversely related to Polar Eurasian pattern. Summer precipitation was overall well predicted using these significantly correlated climate indices, and the Pearson correlation coefficient between predicted and observed summer precipitation was in general larger than 0.6.

The performance of the Xinanjiang model for daily rainfall-runoff simulation in the source region of the Yellow River was evaluated. The Blaney–Criddle method was used to calculate the potential evapotranspiration as model input due to data scarcity of this area. The Monte Carlo method was used to optimize the sensitive model parameters. The resulting Pearson correlation coefficient between observed and simulated runoff for the calibration period was up to 0.87, and 0.85 for the validation period. Accordingly, the Xinanjiang model simulated the daily runoff series well in general. Thus, the Xinanjiang model can be a proper tool for further water resources management involving runoff simulation and flood forecasting in the source region of the Yellow River.

Key words: Source region of the Yellow River, climate change, summer precipitation, ENSO, teleconnection pattern, sea surface temperature, Xinanjiang model, Rainfall-Runoff process

Classification system and/or index terms (if any)		
Supplementary bibliographical information		**Language:** English
ISSN and key title: 1101-9824		**ISBN:** 978-91-7623-311-5
Recipient's notes	Number of pages 156	Price
	Security classification	

Doctoral Thesis

Impacts of climate change on surface hydrology in the source region of the Yellow River

by

Feifei Yuan

LUND
UNIVERSITY

June 2015

ACKNOWLEDGEMENTS

POPULÄRVETENSKAPLIG SAMMANFATTNING

Nästan 35% av den totala avrinningen i Gula floden härstammar från dess källområde och vattenförsörjningen nedströms är därför beroende av de rådande förhållandena i detta område. Minskad vattenföring i floden på grund av klimatförändringar förväntas leda till negativa konsekvenser för de 110 miljoner invånarna i avrinningsområdet och problem uppstår för såväl jordbruket som vattenförsörjningen av hushåll och industri. Denna studie behandlar därför klimatförändringars påverkan på källregionens ytvattenhydrologi. Målsättningen är att resultatet ska kunna användas för vattenresursplanering och bättre hantering av vattenresurserna i Gula flodens avrinningsområde. Hydroklimatiska trender och variationer i klimatologi under de senaste 50 åren undersöktes för att identifiera förändringar över tid och rum. Analysen pekar på en årlig ökning i medeltemperatur över hela området och under de senaste decenniet har ökningen eskalerat. Förändringar i den årliga medelnederbörden varierade mellan stationerna, och generellt kunde en viss minskning ses. Årsflödet i floden har minskat påtagligt, allra mest sedan 1990-talet, men under de senaste åren har det synts tecken på en återgång mot högre flöden. En tydlig förändring av temperaturentrenden identifierades för 1998 och en liknande trendförändring av vattenflödet för 1990. Utifrån en säsongsanalys av vattenflödet kan sägas att en minskning har inträffat av nederbörden under sommarmonsunen (juli till september) samtidigt som medeltemperaturen har ökat för årets alla månader. På grund av den försvagade monsunen har medelavrinningen minskat med 0.74 mm/år över hela källregionen. Utöver detta kunde en statistiskt fastställd periodicitet av områdets medelnederbörd och temperatur på 2 till 4 år konstateras. En ännu tydligare 8-årsperiodicitet för vattenflödet var uppenbar från slutet av 1960-talet till början av 1990-talet. För en fördjupad förståelse av förändringarna i vattenflödet har hydroklimatiska trender och kopplingar mellan olika delavrinningsområden undersökts. Nederbörden under sommarmånaderna (juni till september) motsvara i Gula flodens källregion för ungefär 70% av den årliga avrinningen och är därför av stor betydelse för vattentillgången och därmed kommer de minskade flödena under monsunen att medföra vattenbrist för befolkningen i området. Därför har förändringarna av källregionens sommarnederbörd från 1961 till 2010 analyserats och satts i förhållande till jordens havsytvattentemperaturer, likaså till det kopplade systemet som beskrivs av Southern Oscillation Index (SOI). Nederbörden uppvisar en tydligt minskande gradient, från sydväst till nordöst, på grund av den försvagade sommarmonsunen. En uppdelning av regionen i tre områden med homogen nederbörd visar på en tydlig areell variation. Det nordvästra området (zon 1) hade en svagt ökande trend, medan mittendelen och området i sydöst (zon 2 och zon 3), där mest nederbörd faller, hade en statistiskt fastställd minskande trend. Hela regionens sommarnederbörd har visat på en statistiskt fastställd omvänd korrelation till yttemperatur i centrala Indiska oceanen med en fördröjning på 0-4 månader, och liknande relation till yttemperaturen i södra Indiska oceanen och Atlanten, med en fördröjning på 5-8 månader.

Analyser av delområden visar på komplexa samband med olika havsområdens yttemperaturer som kan ytterligare förklara variationer i nederbörden. En korrelation konstaterades mellan sommarnederbörden i källregionen och SOI med en fördröjning på 0-2 månader. El Niño-Southern Oscillation (ENSO) påverkar sommarnederbörden i källregionen, och en övervägande omvänd korrelation tyder på att högre yttemperaturer i ekvatoriella Indiska oceanen under El Niño sammanfaller med mindre nederbörd i Gula floden källregion. Kopplingar mellan nederbörden i Gula floden källregion och andra kända globalt kopplade system har identifierats, för att kunna förutsäga sommarnederbörden med hjälp av dessa samband. Nederbörden är kopplad till den Nordatlantiska oscillationen, West Pacific Pattern, och ENSO, samt en omvänd relation till Polar Eurasian Pattern. Prognoserna för källregionens sommarnederbörd utifrån dessa samband är överlag bra och korrelationen mellan prognosen och den observerade nederbörden var generellt större än 0.6. En delvis modifierad nederbörds-avrinningsmodell (Xinanjiangmodellen) applicerades på Gula flodens källregion för att undersöka relationen mellan nederbörd och avrinning. Den potentiella evapotranspirationen i modellen beräknades med Blaney-Criddle-metoden och Monte Carlo-simulering användes för att optimera känsliga parametrar. Pearson-korrelationskoefficienten mellan observerad och simulerad avrinningen var upp till 0.87 under kalibrering och upp till 0.85 för validering. Således gav Xinanjiang-modellen generellt bra simulering av relationen mellan nederbörd och avrinning. Xinanjiang-modellen kan därför vara ett lämpligt verktyg för framtida vattenresurshantering rörande avrinningssimulering och översvämningsprognoser i Gula Flodens källregion.

ABSTRACT

The source region of the Yellow River contributes about 35% of the total water yield in the Yellow River basin playing an important role for meeting the downstream water resources requirements. The declining water availability caused by climate change in the source region of the Yellow River is expected to have severe repercussions for the 110 million basin inhabitants in terms of water resources affecting agricultural productivity, municipal, and industrial water supply. Thus, this study investigated the impacts of climate change on surface hydrology in the source region of the Yellow River. The presented results have important implications for water resources management in the Yellow River.

Hydroclimatic trend and periodicity during the last 50 years were investigated to identify significant changes in time and space over the study area. Results showed that mean annual temperature increased for all stations and it had an accelerated increasing trend during the last decade. Mean annual precipitation trends varied depending on station location; however, they were generally slightly decreasing. Annual streamflow decreased markedly especially from the 1990s but showed recovery during recent years. Statistically significant changes in trend occurred for temperature in 1998 and for streamflow in 1990. Based on the streamflow change point, seasonal analysis results showed that precipitation mainly decreased during the summer monsoon period (July-September) and temperature increased throughout the year. Corresponding to the weakened monsoon period the average runoff depth is decreasing by 0.74 mm/year over the whole area. Statistically significant 2 to 4-year periodicities for mean areal precipitation and temperature occurred over the area. For streamflow, an even stronger 8-year periodicity was revealed from the end of the 60s to the beginning of the 90s. Frequency analysis investigated the magnitudes of mean annual precipitation and discharge corresponding to a given frequency. Hydroclimatic trends and linkages at each sub-basin were investigated to further improve the understanding of observed streamflow changes.

The summer precipitation (June-September) in the source region of the Yellow River accounts for approximately 70% of the annual total playing an important role for water availability, and its decreasing trend will cause water shortage in the whole river basin. Hence, summer precipitation trends and teleconnections with global sea surface temperature (SST) and Southern Oscillation Index (SOI) from 1961 to 2010 were investigated. Results show that the precipitation has a strongly decreasing gradient from southeast to northwest due to the weakening summer monsoon, and a division of the region into three homogeneous precipitation zones shows marked spatial variability. The northwest part (zone 1) had a non-significantly increasing trend, and the middle and southeast parts (zone 2 and 3) that receive the most precipitation displayed a statistically significant decreasing trend. The summer precipitation in the whole region shows statistically significant negative correlations with the central Pacific SST for 0-4 month lags and with the southern Indian and Atlantic Ocean

SST for 5-8 month lags. Analyses of sub-regions reveal intricate and complex correlations with different SST areas that further explain the summer precipitation variability. The SOI had significant positive correlations mainly for 0-2 month lag with summer precipitation. It is seen that El Niño Southern Oscillation (ENSO) events have an influence on the summer precipitation, and the predominant negative correlations indicate that higher SST in equatorial Pacific areas corresponding to El Nino coincides with less summer precipitation in the source region of the Yellow River.

The linkages between the precipitation and global teleconnection patterns were identified, and summer precipitation was predicted based on revealed teleconnections. It was found that precipitation in the study area is positively related to North Atlantic Oscillation, West Pacific Pattern and El Nino Southern Oscillation, and inversely related to Polar Eurasian pattern. Summer precipitation was overall well predicted using these significantly correlated climate indices, and the Pearson correlation coefficient between predicted and observed summer precipitation was in general larger than 0.6.

The performance of the Xinanjiang model for daily rainfall-runoff simulation in the source region of the Yellow River was evaluated. The Blaney–Criddle method was used to calculate the potential evapotranspiration as model input due to data scarcity of this area. The Monte Carlo method was used to optimize the sensitive model parameters. The resulting Pearson correlation coefficient between observed and simulated runoff for the calibration period was up to 0.87, and 0.85 for the validation period. Accordingly, the Xinanjiang model simulated the daily runoff series well in general. Thus, the Xinanjiang model can be a proper tool for further water resources management involving runoff simulation and flood forecasting in the source region of the Yellow River.

摘要

黄河源区产流量占整个黄河流域的 35%，在整个流域的水资源需求中具有重要的角色。气候变化引起的黄河源区水资源供应量的减少对黄河流域内一亿一千万居民的饮用水及工农业用水有重要的影响。为此，本文研究了气候变化对黄河源区地表水文的影响，研究成果对黄河流域水资源的管理具有重要应用价值。

本文研究了黄河源区过去五十年内水文气象的趋势性和周期性。结果显示研究区域内所有观测站点的年平均温度均有所上升，并且过去十年内有更为显著的趋势。年平均降水量的趋势具有时空不均一性，但是总体有轻微的下降。年径流量自上世纪 90 年代初有显著的下降，但是近年有所回升。黄河源区温度和径流的趋势性分别于 1998 年和 1990 年有统计上显著的突变。基于径流的突变点，季节性分析表明黄河源区降水的减少主要发生于夏季六月到九月，而温度则是全年均有所增加。随着夏季降雨的减少，黄河源区的径流深过去五十年内平均每年减少 0.74 毫米。整个区域内年平均降水和温度具有 2 到 4 年的显著性统计周期，而径流自 60 年代末至 90 年代初具有 8 年的显著性统计周期。通过年平均降水和径流的频率分析计算，得到相对应频率的设计值，此外，本文还进一步研究了黄河源区各子流域水文气象的趋势性和关联性，以便进一步理解径流的变化。

黄河源区夏季六月至九月的降雨占全年的 70%左右，夏季降雨的减少将会引起整个流域内水资源的短缺。因此，本文进一步研究了黄河源区夏季降雨的趋势性及其和全球海平面温度以及南方涛动指数的关系。结果显示黄河源区的降水由于逐渐减弱的季风影响，自东南至西北部呈递减趋势。由于降水时空分布的差异性，黄河源区被划分为三个同质子区域。西北部的降水成非显著的增加趋势，而降水较多的东南部和中部则成显著的下降趋势。整个源区的夏季降雨和太平洋中部的海平面温度有 0-4 个月滞后的负相关，而和南印度洋及南大西洋的海平面温度具有 5-8 个月滞后的负相关。黄河源区各子区域夏季降雨都与不同区域的海平面温度相关，显示出黄河源区降水空间分布的差异性。黄河源区的夏季降雨和南方涛动指数具有 0-2 个月滞后的正相关。从而进一步证明厄尔尼诺南方涛动现象对黄河源区的夏季降雨具有显著的影响，而海平面温度的负相关性表明太平洋中部较高的海平面温度相对应的厄尔尼诺现象会引起黄河源区较少的夏季降雨。

本研究还进一步揭示了黄河源区的降水和全球遥相关模式的关系，从而利用统计上显著相关的气候因子对夏季降雨进行预测。结果表明黄河源区的降水和北大西洋涛动，西太平洋遥相关型以及厄尔尼诺南方涛动成正相关，而与极地欧亚遥模式成负相关。利用统计上显著相关的气候因子，夏季降雨的预报结果有较理想的精度。观测值和预测值的皮尔逊相关系数整体大于 0.6。

本文评估了新安江水文模型对黄河源区的日降水和径流的模拟精度。由于该区域资料的短缺，采用 Blaney-Criddle 方法计算潜在蒸散发作为模型的输入。采用蒙特卡洛方法优化模型的敏感性参数。结果显示校准阶段模型的径流模拟相关系数达到

0.87，验证阶段径流模拟的相关系数达到 0.85，达到了较好的模拟结果。因此，新安江模型可用于黄河源区的径流模拟和洪水预报，对黄河流域内的水资源管理具有重要的应用价值。

PAPERS

Appended papers

I. **Yuan, F.**, Berndtsson, R., Zhang, L., Uvo, C., Hao, Z., Wang, X. and Yasuda, H., 2015. Hydro Climatic Trend and Periodicity for the Source Region of the Yellow River. *Journal of Hydrologic Engineering. DOI: 10.1061/ (ASCE) HE. 1943-5584.0001182.*

II. **Yuan, F.**, Yasuda, H., Berndtsson, R., Uvo, C., Zhang, L., Hao, Z. and Wang, X., 2015. Regional sea surface temperatures explain spatial and temporal variation of summer precipitation in the source region of the Yellow River. *Hydrological Sciences Journal. DOI: 10.1080/02626667.2015.1035658.*

III. **Yuan, F.**, Berndtsson, R., Uvo, C., Zhang, L. and Jiang, P., 2015. Summer precipitation prediction in the source region of the Yellow River using climate indices. *Hydrology Research* (under review).

IV. **Yuan, F.**, Berndtsson, R., Wang, L. and Zhang, L., 2015. Modelling daily rainfall-runoff in the source region of the Yellow River using the Xinanjiang model. (Manuscript)

Author's contributions to the appended papers

Paper I. The author planned the work together with the co-authors, performed the statistical analysis, analysed the results and wrote the paper together with the co-authors. The co-authors participated in discussions and helped to revise the paper.

Paper II. The author planned the work together with the co-authors, performed the statistical analysis, analysed the results and wrote the paper together with the co-authors. The co-authors supervised the work and participated in discussions.

Paper III. The author planned the work together with the co-authors, performed the statistical analysis, analysed the results and wrote the paper. The co-authors participated in discussions and helped to revise the paper.

Paper IV. The author planned the work, performed the hydrological model, analysed the results and wrote the paper. The co-authors participated in discussions and helped to revise the paper.

Related publications not included in this dissertation

Journal papers

I.   **Yuan, F**., Berndtsson, R., Hao, Z., Zhang, L., Jiang, P. and Yasuda, H., 2015. Mass balance in Glacier No.1 at the headwater of the Urumqi River, in relation to climate variability. *Water Resources Management* (submitted).

Conference papers and presentations

I.   **Yuan, F.**, Zhang, L., Hao, Z., 2011. Runoff prediction under different climate scenarios in the source region of the Yellow River. Water and Society 2011. Las Vegas, USA

II.   **Yuan, F.**, Berndtsson, R., Zhang, L., 2012. The effect of climate change on Glacier No.1 at the source region of the Urumqi River, Tianshan, China. XXVII Nordic Hydrological Conference 13-15 August, 2012 in Oulu, Finland

III. **Yuan, F.**, Zhang, L., Berndtsson, R., 2013. Identifying the relationship between the precipitation in the source region of the Yellow River and climatic patterns.European Geosciences Union .General Assembly 2013. 07 – 12 April 2013, Vienna, Austria.

IV.   **Yuan, F.**, Berndtsson, R., Zhang, L., 2013. The relationship between global sea surface temperature and summer precipitation in the source region of the Yellow River. 9-13 December 2013 AGU fall meeting, San Francisco, USA.

ABBREVIATIONS AND SYMBOLS

ANN   Artificial Neural Network

CMA   China Meteorological Administration

CPC   Climate Prediction Centre

CSI   Consortium for Spatial Information

CV   Coefficient of Variation

DEM   Digital Elevation Model

E   Actual Evapotranspiration

EA   East Atlantic Pattern

EA/WR   East Atlantic/West Russia Pattern

EM   Potential Evapotranspiration

ENSO   El Nino Southern Oscillation

GCMs   General Circulation Models

IOD   India Ocean Dipole

NAO   North Atlantic Oscillation

NOAA   National Oceanic and Atmospheric Administration

P   Precipitation

PCA   Principal Component Analysis

PDO   Pacific Decadal Oscillation

PNA   Pacific/North American Pattern

POL   Polar/Eurasia Pattern

Q   Discharge

SCA   Scandinavia Pattern

SD   Standard Deviation

SOI   Southern Oscillation Index

SST   Sea Surface Temperature

SRTM	Shuttle Radar Topography Mission
SVD	Singular Value Decomposition
T	Temperature
WP	West Pacific Pattern

CONTENTS

1 INTRODUCTION

1.1 Background and problem statement

The Yellow River is of immense importance to China. It is 5,464 km long, has a basin area of 752,440 km^2, and is the main source of surface water in northwest and northern China. The Yellow River originates in the Qinghai-Tibetan plateau and empties into the Bohai Gulf in the Yellow Sea. The basin has more than 110 million inhabitants and 12.6 million ha cultivated land, representing about 8 and 13% of the national totals, respectively (Wang et al. 2006). The Yellow River is mainly used for irrigation, domestic and industry, electricity generation and supporting ecological health of areas of high conservation value. However, the Yellow River is currently facing several key issues, including water shortage, continued threat of floods, water quality and environment, land degradation in the Loess plateau, and severity of groundwater exhaustion (Liu and Xia 2004, Giordano et al. 2004). For instance, the lower Yellow River has increasingly suffered from low-flow conditions and parts of the lower reaches have often been dry since the 1970s. The situation has been directly linked to the effects of climate change and human activities (Tang et al. 2008).

The source region of the Yellow River contributes about 35% of the total water yield in the Yellow River basin (Lan et al. 2010). Consequently, it is an extremely important area in terms of water resources affecting agricultural productivity, municipal, and industrial water supply for the whole basin. The last 50 years have witnessed generally decreasing trends in annual precipitation and streamflow for the Yellow River source region, and it is mainly due to a weakening of the summer monsoon rainfall. Corresponding to the weakened monsoon rainfall the average runoff depth is decreasing by 0.74 mm/year over the entire study area (Yuan et al. 2015a). The precipitation and streamflow decrease may cause further water shortage problems in the downstream of the Yellow River.

Climate change refers to a change in the state of the climate that can be identified (e.g. using statistical tests) by changes in the mean and/or the variability of its properties and that persists for an extended period, typically decades or longer. It refers to any change in climate over time, whether due to natural variability or as a result of human activity (IPCC 2007). Many studies have shown that climate change has strong impact on basin water resources through changes in temperature and hydrologic variables (Westmacott and Burn 1997, Lorenzo et al. 2008, Milly et al. 2005). For example, the frequency and severity of drought events could increase as a result of changes in both precipitation and temperature. Changes in the hydrologic regime that do occur are expected to be spatially and temporally variable (Burn and Elnur 2002). The interannual periodicity in local hydroclimatic variables (temperature, precipitation, and streamflow) could be a reflection for low-frequency climatic

fluctuations. It is important to understand the underlying dynamics of the hydrological cycle for investigated basins.

It has been shown that sea surface temperature (SST) can provide important predictive information about hydrologic variability in many regions of the world (Tootle and Piechota 2006, Yasuda et al. 2009). For example, El Nino Southern Oscillation (ENSO) events are closely linked to patterns of flood and drought in different areas of the world and strongly affect local and regional scale climates through teleconnections between the coupled ocean-atmosphere and land systems (Wang *et al.* 2006). Understanding the linkage between local precipitation and global teleconnection patterns is essential for water resources management, and it could also improve the ability to predict the local precipitation based on physical understanding (Redmond and Koch 1991, Hartmann et al. 2008). Thus, improving the knowledge regarding the relationship between precipitation in the source region of the Yellow River and global SST and teleconnection patterns would have important implications for water resources management.

Hydro-meteorological processes have a dynamic and complex structure in space and time, and the rainfall-runoff process is a well-known highly complex and nonlinear phenomenon in hydrology with obvious relevance for water resource management (Modarres and Ouarda 2013). Comprehensive hydrological models are expected to be effective tools for flood simulation and forecasting. However, proper runoff simulation is often one of the most challenging tasks in theoretical and operational hydrology due to the lack of hydrologic observations (Yao et al. 2014). Data scarcity or inconsistency for the model input is one of reasons for high uncertainty in hydrological modelling (Sood and Smakhtin 2014). The source region of the Yellow River is an important area for water supply in the entire basin but with limited observational data. It is essential to evaluate suitable hydrological model in view of data scarcity to investigate the impact of climate change on regional water resources.In this respect, the performance of the Xinanjiang model for daily rainfall-runoff simulation in the source region of the Yellow River was evaluated to improve the understanding of the dynamic hydroclimatic features.

1.2 Objectives and scope

In view of above, this research aimed at investigating the impact of climate change on surface hydrology in the source region of the Yellow River. The current understanding of hydroclimatic processes is largely based on time series analysis of observations. The local hydroclimatic variability is closely associated with coupled ocean-atmosphere system, and exploring these relationships is essential for regional water resources management. Thus, the overall objectives of the research were:

To improve the physical understanding of hydroclimatic change in the source region of the Yellow River from the impacts of global sea surface temperature and teleconnection patterns, and to promote the application of hydrological modelling and forecasting techniques for water resources management.

To achieve the overall objective of this thesis, different statistical methods and a partly modified hydrological model were employed and the following research problems were addressed:

➢ To investigate the hydroclimatic trend and periodicity for the source region of the Yellow River during last 50 years (**Paper I**).

➢ To identify the spatial and temporal variation of summer precipitation in the source region of the Yellow River in relation to global sea surface temperature (**Paper II**).

➢ To explore the influence of teleconnection patterns on precipitation in the source region of the Yellow River and to predict summer precipitation using significantly correlated climate indices (**Paper III**).

➢ To evaluate the performance of the Xinanjiang model for daily rainfall-runoff simulation in the source region of the Yellow River. (**Paper IV**).

1.3 Thesis structure and appended papers

This thesis is based on the research work presented in the four appended papers. After introduction in Chapter 1, the theoretical background of the appended papers is presented in Chapter 2. In Chapter 3, an overview of study area and data as well as statistical methods and hydrological model are presented. In Chapter 4, the main results from the appended papers are summarized and discussed. Finally, conclusions as well as future studies are presented in Chapter 5.

Paper I investigated trend for temperature, precipitation, and streamflow from 1960 to 2010. Change-point analysis was applied to identify the potential significant hydroclimatic changes in recent years. Based on the change point results, seasonal analysis was examined indicating a new possible hydrometeorological regime. The hydroclimatic periodicity was investigated by wavelet analysis giving insight in periodicity and severity of drought and connections to the climate system. Besides, hydrological frequency analysis

was examined to determine the magnitudes of mean annual precipitation and discharge corresponding to a given frequency or recurrence interval. This study also explored the hydro-climatic trends and linkages at each sub-basin to further improve the understanding of observed streamflow changes. Based on these analyses the paper is closed with a discussion on practical applications of the results.

Paper II further investigated precipitation variability in the source region of the Yellow River and summer precipitation teleconnections with global SST. Cluster analysis was used to separate the precipitation stations in the source region of the Yellow River into homogeneous zones. Linear regression and Mann-Kendall tests for each zone further revealed the spatial variability of summer precipitation. Correlation analysis examined the links between summer precipitation in the source region of the Yellow River and global SST and Southern Oscillation Index (SOI). The significantly correlated SST areas identified the influence of climate patterns on precipitation variability in the source region of the Yellow River.

Paper III examined the relationships between precipitation in the source region of the Yellow River and global teleconnection patterns, and predicted the summer precipitation using significantly correlated climate indices. Spatial variability of precipitation was investigated based on three homogeneous sub-regions. Principal component analysis (PCA) and singular value decomposition (SVD) were used to find significant relations between the precipitation in the source region of the Yellow River and global teleconnection patterns using climate indices. A back-propagation neural network was developed to predict the summer precipitation using significantly correlated climate indices.

Paper IV evaluated the performance of the Xinanjiang model for daily rainfall-runoff simulation in the source region of the Yellow River. The Blaney–Criddle method was used to calculate the potential evapotranspiration as model input due to data scarcity of this area. The Monte Carlo method was used to optimize the sensitive model parameters. Rainfall-runoff relationships for the source region of the Yellow River were quantified to understand the dynamic hydro-meteorological processes influence on runoff. The simulation can be used for further investigating water resources management involving runoff simulation and flood forecasting in the source region of the Yellow River.

2 THEORETICAL BACKGROUND

This chapter provides the background and a literature review about the Asian summer monsoon and teleconnection patterns used in the following chapters. It is not intended to present a full account of the state of the art, but the necessary facts to familiarize the reader with the context in which the investigations were performed.

2.1 The Asian summer monsoon

The Asian summer monsoon is driven by the differential seasonal adiabatic heating of the Asian continent and tropical Indo-Pacific Ocean, and it is associated with changes in the large-scale atmospheric circulation over substantial parts of Asia (Fan et al. 2009). The boreal summer phase of the monsoon is associated with surface convergence of moisture, and hence precipitation, over large parts of South and Southeast Asia, providing water resources over these densely populated regions (Fan et al. 2009). The Asian summer monsoon system can be divided into two subsystems, the south Asian (or India) and the East Asian summer monsoon system that are independent of each other and, at the same time, interact with each other (Yihui 1994). The Asian monsoon region attains the most distinct variation of the annual cycle and the alternation of dry and wet seasons which is in concert with the seasonal reversal of the monsoon circulation features(Webster et al. 1998). However, the duration of dry and wet seasons might be different for different areas of the Asian monsoon influenced region, depending on their climate regions.

The climate of the source region of the Yellow River is greatly influenced by the southwest monsoon and the East Asian summer monsoon (Ding and Chan 2005). The earliest onset of the East Asian summer monsoon occurs in the central and southern Indochina Peninsula. It displays a distinct stepwise northward and north-eastward movement and then finally penetrates in to the upper Yellow River from the south of China (Ding and Chan 2005). The effects of atmospheric circulation are in general different for the upper and lower Yellow River. The monsoon rain belt in the upper part is caused by south-easterly flow while the corresponding monsoon rain belt in the lower parts is influenced by south-westerly flow (Qian et al. 2002). This causes differences in spatial distribution of summer precipitation between the two parts of the Yellow River.

2.2 Teleconnection patterns

The atmospheric circulation exhibits substantial variability, which reflects climate patterns and circulation systems occurring at different time and space scales. Teleconnection patterns are recurring, persistent, and large-scale oscillating circulation systems in the atmosphere,

which are identified as modes of low-frequency pressure variability, typically lasting for weeks or longer (Barnston and Livezey 1987). They affect the temperature, precipitation and jet stream patterns over large areas. Understanding precipitation and temperature anomalies associated with the dominant teleconnection patterns of climate variability is essential to understanding many regional climate anomalies and why these may differ from those at the global scale (Solomon et al. 2007). Here ten prominent teleconnection patterns were used.

El Nino-Southern Oscillation (ENSO)

The El Nino-Southern oscillation is a coupled ocean-atmosphere phenomenon in the equatorial Pacific (Chiew et al. 1998). It involves fluctuating sea surface temperature in the equatorial Pacific. El Nino representing the warm phase of the ENSO refers to the above-average sea surface temperatures that periodically develop across the east- central equatorial Pacific. La Nina representing the cold phase of the ENSO refers to the cooling of sea surface temperatures that periodically develop across the east- central equatorial Pacific. The fluctuations in ocean temperatures during El Nino and La Nina are accompanied by even larger-scale fluctuations in air pressure between the western and eastern tropical Pacific known as the Southern Oscillation. Sea Surface Temperature and the Southern Oscillation Index are the most common used indicators to quantify the strength of an ENSO event (Chiew et al. 1998), which is measured by the difference in surface pressure anomalies between Tahiti and Darwin and the SSTs in the central and eastern equatorial Pacific (Solomon et al. 2007).

North Atlantic Oscillation (NAO)

The North Atlantic Oscillation is one of the dominant modes of Northern Hemisphere climate variability and it is present in all seasons (Barnston and Livezey 1987). The NAO consists of two pressure centres over Greenland/Iceland with low pressure and the Azores with high pressure. The positive phase is defined as a strengthening of the Icelandic low and the Azores high. This results in an enhanced Atlantic storm track and anomalously high transport of moisture and heat by transient eddies, corresponding to changed precipitation and temperature patterns extending from eastern North America to western and central Europe and into Scandinavia, Siberia and Central Russian (Hurrell 1995). The negative phase indicates weakening of the Icelandic low and Azores high that decreases the pressure gradient across the North Atlantic.

Polar/Eurasia Pattern (POL)

The positive phase of POL consists of negative height anomalies over the polar region and positive anomalies over northern China and Mongolia. This pattern is associated with fluctuations in the strength of the circumpolar circulation, with the positive phase reflecting an enhanced circumpolar vortex and the negative phase reflecting a weaker than average polar vortex (CPC 2008). The Polar/Eurasian pattern is mainly associated with above-average temperatures in eastern Siberia and below-average temperatures in eastern China.

East Atlantic Pattern (EA)

The East Atlantic pattern is the second prominent mode of low-frequency variability over the North Atlantic. The EA pattern is structurally similar to the NAO, and consists of a north-south dipole of anomaly centres spanning the North Atlantic from east to west, and it is most prominent in winter, nor found at all in the summer months (Barnston and Livezey 1987). The anomaly centres of the EA pattern are displaced south-eastward to the approximate nodal lines of the NAO pattern.

West Pacific Pattern (WP)

The WP pattern is a primary mode of low-frequency variability over the North Pacific in all months. It is characterized by a spatial-anomaly distribution as a north-south dipole during winter and spring, with one centre located over the Kamchatka Peninsula and another broad centre of opposite sign covering portions of south-eastern Asia and the western subtropical North Pacific (Barnston and Livezey 1987). The strong positive and negative WP patterns are related to the east-west and north-south movements of the East Asian jet stream, indicating that the change from cold to warm season results from the northward movement of the East Asian jet stream and thus affects aspects of the East Asian climate such as precipitation and temperature (Choi and Moon 2012, Barnston and Livezey 1987). The positive phase of the WP pattern is associated with above-average temperatures over the lower latitudes of the western North Pacific in both winter and spring, while the negative phase is connected with below-average temperatures over eastern Siberia in all seasons (Choi and Moon 2012). The WP pattern is also associated with above-average precipitation in all seasons over the high latitudes of the North Pacific, and below-average precipitation across the central North Pacific especially during the winter and spring (Choi and Moon 2012).

Pacific/North American Pattern (PNA)

The positive phase of the PNA pattern features above-average heights in the vicinity of Hawaii and over the intermountain region of North America, and below-average heights located south of the Aleutian Islands and over the south-eastern United States (Barnston and Livezey 1987). The PNA pattern is associated with strong fluctuations in the strength and location of the East Asian jet stream. It is also strongly influenced by the El Nino-Southern Oscillation phenomenon. The positive phase of the PNA pattern tends to be associated with Pacific warm episodes (El Nino), and the negative phase tends to be associated with Pacific cold episodes (La Nina).

East Atlantic/West Russia Pattern (EA/WR)

The East Atlantic/ West Russia pattern consists of four main anomaly centres. The positive phase is associated with positive height anomalies located over Europe and northern China, and negative height anomalies located over the central North Atlantic and north of the Caspian Sea (Barnston and Livezey 1987). The main surface temperature anomalies associated with the positive phase of the EA/ WR pattern reflect above-average temperatures

over eastern Asia, and below-average temperatures over large portions of western Russia and north-eastern Africa (CPC 2008). The main precipitation departures reflect generally above-average precipitation in eastern China and below-average precipitation across central Europe.

India Ocean Dipole (IOD)

Indian Ocean SST plays an important role in tropical climate variability. India Ocean Dipole is defined by opposite signs of sea surface temperature anomalies in the western tropical Indian Ocean and that in the eastern tropical India ocean (Saji et al. 1999). A positive IOD period is characterised by cooler than normal water in the tropical eastern Indian Ocean and warmer than normal water in the tropical western Indian Ocean, and a negative IOD period is characterised by warmer than normal water in the tropical eastern Indian Ocean and cooler than normal water in the tropical western Indian Ocean (Saji et al. 1999).

Scandinavia Pattern (SCA)

Scandinavia pattern has the primary centre of influence around the Scandinavian Peninsula, with two other centres of action with the opposite sign, one over the north-eastern Atlantic and the other over central Siberia to the southwest of Lake Baikal (Bueh and Nakamura 2007). Its positive phase is characterized by prominent anticyclone anomalies around the Scandinavian Peninsula, giving rise in winter to below-normal temperatures across central Russia and western Europe, above-normal precipitation across southern Europe, and dry conditions over the Scandinavian region (CPC 2008).

Pacific Decadal Oscillation (PDO)

The Pacific Decadal Oscillation is a pattern of Pacific climate variability similar to ENSO in character, but which varies over a much longer time scale. The PDO can remain in the same phase for 20 to 30 years, while ENSO cycles typically only last 6 to 18 months (SCO 2015). The PDO consists of a warm and cool phase which alters upper level atmospheric winds. The broad area of above average water temperatures off the coast of North America from Alaska to the equator is a classic feature of the warm phase of the Pacific Decadal Oscillation, and the expansive area of below average water temperatures off the coast of North America from Alaska to the equator signals the cold phase of the PDO (SCO 2015).

3 EXPERIMENTAL AREA AND METHODS

This chapter gives an overview of the study area, data collection and methodology used including different statistical analysis and the partly modified hydrological model in this research.

3.1 Experimental area and data

The source region of the Yellow River is located on the northeast Qinghai-Tibet Plateau between 32º12´-35º48´N and 95º50´-103º28´E and includes the area upstream of the Tangnaihai runoff observation station. The area is 12.2×10^4 km^2, occupying approximately 16% of the Yellow River Basin, and it has a great elevation change from 2,670 m in the east to 6,253 m in the west. Grassland covers 80% of the catchment and it includes typical alpine swamp, steppe, and shrub meadows. In recent years, the alpine grasslands in this area have suffered from severe degradation (Zhou et al. 2005). The grassland degradation is thought to be a joint effect of long-term overgrazing and climate warming. The area of lakes and swamps is about 2,000 km^2. There is a permanent snowpack and glaciers in the southern Animaqing, Bayankala, and Northern Qilian mountains. The area has a comparably low population density and a total of approximately half a million inhabitants. The area is therefore regarded as relatively unaffected by human activities (Hu et al. 2011, Zheng et al. 2009). Neither large irrigation projects nor large dams exist in the area even though the population increase of humans and domestic livestock is increasingly affecting the grass cover and soil erosion.

Climatologically the area belongs to the semi humid region of the Tibetan Plateau sub Frigid Zone and about 70% of the annual precipitation in this area fall during the wet summer season (June-September). The upper part of the Yellow River is characterized by low-temperatures, sharp day-night temperature contrasts, long-cold and short-warm seasons, and intense sunlight (Liang et al. 2010). Annual average temperature varies between -4 and 2°C from southeast to northwest. The precipitation in this region is generally of low intensity (<50 mm/day), long duration (10-30 days), and covers a large area (>100,000 km^2) (Hu et al. 2011, Zheng et al. 2007). Snowfall is concentrated from November to March, when more than 78% of the total precipitation falls in the form of snow. However, total amount of annual snowfall accounts for less than 10% of the annual precipitation (Hu et al. 2011). The potential evaporation is 1,300-1,400 mm/year (Liang et al. 2010).

Daily precipitation and temperature observations from 1961 to 2010 collected at ten meteorological stations (Fig. 3.1); Xinghai, Tongde, Zeku, Henan, Maduo, Dari, Jiuzhi, Maqu, Ruoergai, and Hongyuan, were obtained from the China Meteorological Administration (CMA), and data quality has previously been checked by the CMA. Daily

streamflow data from 1960 to 2009 at four runoff observation stations, including Huangheyan, Jimai, Maqu, and Tangnaihai, were obtained from the Yellow River Conservancy Commission. Runoff data from 1968 to 1975 at Huangheyan station were not available. The missing data were interpolated based on the linear regression with Jimai station because this station has the highest correlation with the Huangheyan station. The shuttle radar topography mission (SRTM) 90 m digital elevation data were downloaded from the Consortium for Spatial Information (CGIAR-CSI). Table 3.1 and Table 3.2 show a summary of these data.

Table 3.1 Observation stations for precipitation and temperature.

Station	Altitude (m)	Longitude (ºE)	Latitude (ºN)	Mean annual P (mm/year)	Mean annual T (°C)	Min. annual P (mm/year)	Max. annual P (mm/year)	Min. annual T (°C)	Max. annual T (°C)
Xinghai	3323	99.98	35.58	365.3	1.44	214.1	530.9	0.2	2.9
Tongde	3289	100.39	35.16	411.2	0.67	199.0	598.7	-0.5	3.4
Zeku	3663	101.28	35.02	418.1	-2.16	214.6	651.8	-3.7	2.7
Henan	3500	101.36	34.44	562.9	-0.23	384.1	835.3	-1.7	1.0
Maduo	4272	98.13	34.55	318.5	-3.63	184.0	485.6	-5.5	-2.0
Dari	3967	99.65	33.75	551.8	-0.78	413.1	698.7	-2.2	0.8
Jiuzhi	3629	101.48	33.43	744.7	0.71	562.6	1030.8	-0.5	2.3
Maqu	3471	102.08	34.00	589.2	1.58	448.4	924.7	0.5	3.4
Ruoergai	3440	102.97	33.58	649.7	1.20	464.8	862.9	0.1	2.8
Hongyuan	3492	102.55	32.80	747.1	1.52	508.1	996.3	0.5	2.8

Table 3.2 Observation stations for streamflow

Station	Altitude (m)	Longitude (ºE)	Latitude (ºN)	Mean discharge (m^3/s)	Min. discharge (m^3/s)	Max. discharge (m^3/s)	Drainage area (km^2)
Huangheyan	4221	98.17	34.88	23.4	0.6	78.2	20,930
Jimai	3969	99.65	33.77	130.2	62.0	263.0	45,019
Maqu	3471	102.08	33.97	456.3	228.3	707.0	86,048
Tangnaihai	2546	100.15	35.50	641.1	335.4	1040.0	121,972

In **Paper II**, monthly global sea surface temperature (1×1°) version HadISST 1.1 from 1960 to 2010 obtained by courtesy of the British Atmospheric Data Centre was used (Rayner et al. 2003). The monthly Southern Oscillation Index data was from the Climate Prediction Centre (CPC, NOAA) (http://www.cpc.ncep.noaa.gov/data/indices/soi).

In **Paper III**, global monthly climate indices data representing teleconnection patterns, including North Atlantic Oscillation (NAO), East Atlantic Pattern (EA), West Pacific Pattern (WP), Pacific/North American Pattern (PNA), East Atlantic/West Russia Pattern (EA/WR), India Ocean Dipole (IOD), El Nino-Southern Oscillation (NINO3.4), Scandinavia Pattern (SCA), Polar/Eurasia Pattern (POL) and Pacific Decadal Oscillation (PDO), were obtained from the National Weather Service, Climate Prediction Centre (CPC, NOAA). Further physical explanation for each climate pattern could be seen here (Washington et al. 2000, Barnston and Livezey 1987).
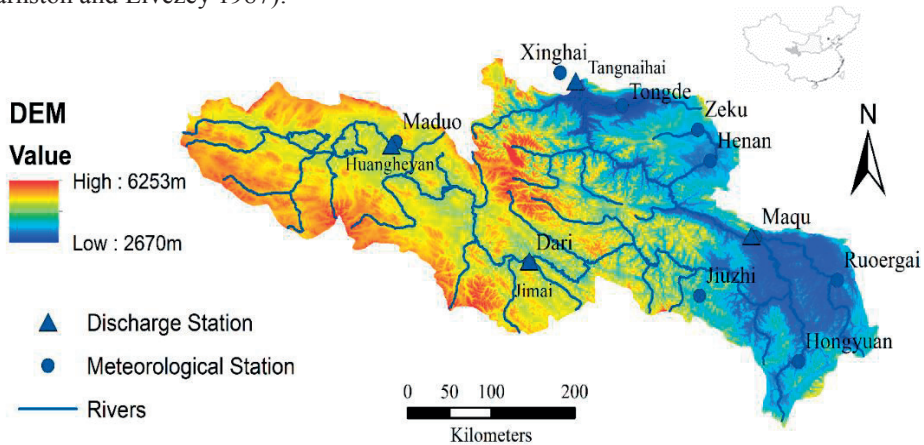
Fig. 3.1 The Yellow River source region topography, river network, and hydroclimatic stations.

3.2 Statistical methods

Mann-Kendall

Trends in precipitation, temperature, and streamflow time series were examined by the non-parametric Mann-Kendall test (**Paper I, II and III**). The Kendall statistic was originally devised as a non-parametric test for trend by Mann (1945). Later Kendall (1975) derived the exact distribution of the test statistic. The method has been widely used in hydroclimatic time series analysis for identifying trend (Burn and Elnur 2002, Rana et al. 2012, Westmacott and Burn 1997). The Mann-Kendall test is independent of the statistical distribution of the data. Statistical significance of the trend was evaluated at the 0.05 level of significance against the null hypothesis that there is no trend for the data series. A detailed procedure for this statistical test can be found in Burn and Elnur (2002).

Change-Point Analyzer

Change-Point Analyzer (Taylor 2000) was used to investigate the potential abrupt hydroclimatic changes in the source region of the Yellow River and to detect the change

points (**Paper I**). Change-Point Analyzer is a software package for analysing time-ordered data to determine whether a change has taken place, and it detects multiple changes and provides confidence levels for each change. It iteratively uses a combination of time varying cumulative sum charts (cusums) and bootstrapping to detect changes (Taylor 2000). It has been widely used for detecting change points in hydroclimatic areas (Collins et al. 2008, Fischer et al. 2012, Mavromatis and Stathis 2011).

Wavelet Analysis

Wavelet analysis is a common tool for signal processing. It is an effective method to identify the dominant modes of periodicity by decomposing time series into time-frequency space (Coulibaly and Burn 2004, Jiang et al. 2013) . The wavelet power spectrum is defined as the absolute value squared by the wavelet transform and gives a measure of the time series´ variance at each scale and at each time and there is no need for a predetermined scale that might limit the frequency range (Coulibaly and Burn 2004, Torrence and Webster 1999). For a more detailed description of wavelet analysis in hydrology, see further Torrence and Compo (1998) and Labat et al. (2000). The method applied here was the Morlet wavelet that consists of a complex exponential Gaussian modulation $\Psi_0(\eta) = \pi^{-1/4} e^{iw_0\eta} e^{-\eta^2/2}$, where w_0 is the non-dimensional frequency, here taken to be 6. To reduce wrap-around effects each time series was padded with zeros. The cone of influence is the region of the wavelet spectrum in which edge effects become important. The background spectrum was chosen as red noise, which means that power increases with decreasing frequency (**Paper I**).

Frequency Analysis

Hydrological frequency analysis is examined to determine the magnitudes of mean annual precipitation and discharge corresponding to a given frequency or recurrence interval (**Paper I**). The Log-Pearson Type III distribution is a statistical technique for fitting frequency distribution data to predict the design flood that has been widely used in hydrology (Griffis and Stedinger 2007, Vogel and Wilson 1996). It is a three-parameter distribution; the parameters are the mean, standard deviation, and skew coefficient (Costa 1978). A detailed procedure for this statistical technique can be found in Griffis and Stedinger (2007).

Cluster Analysis

Due to the large and diverse topography of the area and marked spatial variability of precipitation, a division into homogeneous precipitation areas was done by cluster analysis using monthly precipitation data (**Paper II**). The results were used to investigate the spatial dependence and influence of different SST areas on the summer precipitation within the source region. Cluster analysis is primarily an exploratory data analysis tool to separate data into groups whose identities are not known in advance (Wilks 2011). The number of groups is defined by the degree of similarity and difference between individual observations (Wilks 2011). A correlation matrix was calculated to discern the levels of dependence among the precipitation stations. This method produces a dendrogram in which the correlations between all precipitation stations are shown as a tree-like hierarchical diagram. The cluster

analysis is a widely used pre-analysis technique in hydrological and meteorological areas (Gong and Richman 1995, Uvo 2003).

In our case, we have an n×p data matrix X, where n is the number of variables and p is the number of precipitation stations. Preprocessing of the variables before calculation of the distance measures is necessary since different variables may be measured on different scales and may also contain irrelevant or redundant information (Fovell and Fovell 1993, Parajka et al. 2010, Kingston et al. 2011). The means of the variables were removed, and then the data matrix was standardized. Principal component analysis was applied to create new variables composed of mutually orthogonal linear combinations of the original variables, each accounting for a specific fraction of the original total variance as indicated by the size of its associated eigenvalue. Retention of only the most significant components presenting more than 90% of the total variance accomplished variable reduction. These created new variables were used to generate component scores that were clustered in place of the raw precipitation data for cluster analysis. Euclidean distance was used here for measuring similarity between pairs of the ten precipitation stations. The Ward method was chosen as a clustering technique, which is commonly used and is based on mutually exclusive subsets of the data set and does not assume normality (Bonell and Sumner 1992).

Pearson Product-Moment Correlation Analysis

To identify potential teleconnections or covariabilities between global SST and the summer precipitation (June, July, August, and September) in the source region of the Yellow River, 0-11 month lagged Pearson product-moment correlation coefficients r between monthly SST and precipitation were calculated (**Paper II**). The summer precipitation normal distribution was tested by the Kolmogorov-Smirnov test in Matlab. The SST data follow the normal distribution (Rayner et al. 2003, Kodera 2004, Yasuda et al. 2009). Statistical significance is assessed using the Student's *t*-test against the null hypothesis of no correlation(Lloyd-Hughes and Saunders 2002). Correlations $|r|>0.36$ and $|r|>0.46$ correspond to a statistical significance level of 0.01 and 0.001, respectively.

The Southern Oscillation Index was used to further reveal the correlated SST influence on summer precipitation in the source region of the Yellow River (**Paper II**). The 0-11 month lagged Pearson product-moment correlation coefficients r between monthly SOI and precipitation were calculated. The statistical significance was assessed at the 0.05 level.

Principal Component Analysis

Principal component analysis (PCA) was used to find relationships between precipitation in the source region of the Yellow River and teleconnection patterns using climate indices (**Paper III**). PCA is a multivariate data analysis tool that offers a way to present complex data in a simplified way to identify relations between different parameters. It maximizes variance explained by weighted sum of elements in two or more fields and identifies linear transformations of the dataset that concentrate as much of the variance as possible into a small number of variables (Rana et al. 2012, Uvo 2003). The PCA biplot is used to visualize

the magnitude and sign of each variable's contribution to the first two principal components, and how each observation is represented in terms of those components.

Singular Value Decomposition

SVD is performed on the cross-covariance matrix of fields of two datasets and isolates the combinations of variables with the fields that tend to be linearly related to one another by maximizing the covariance between them (Rana et al. 2012, Wallace et al. 1992). Here, SVD was conducted on the cross-covariance matrix of the climate indices and precipitation data sets for three homogenous precipitation zones (**Paper III**). The SVD of the cross-covariance matrix of two fields yields two matrices of singular vectors and one set of singular values. A singular vector pair describes spatial patterns for each field which have overall covariance given by the corresponding singular value (Uvo et al. 1998). Heterogeneous correlation maps of the left and right fields from SVD show correlation coefficients between the values of one field and the singular vector of the other field (Uvo et al. 1998). In our case, the patterns shown by the heterogeneous correlation maps for the k_{th} SVD expansion mode indicate how well the pattern of the precipitation anomalies relate to the k_{th} singular vector of climate indices. The correlation coefficients are a good indication of strength of the relationship between the two fields. A detailed procedure for this statistical test can be found here (Bretherton et al. 1992, Wallace et al. 1992).

Artificial Neural Network (ANN)

A back propagation neural network was applied for predicting summer precipitation in the source region of the Yellow River using the significantly correlated global climate indices in **Paper III**. ANN is a powerful tool for prediction of meteorological phenomena involving many complex and nonlinear physical processes (Hartmann et al. 2008, Sahai et al. 2003, Uvo et al. 2000, Yasuda et al. 2009). The significantly correlated global climate indices were used as input variables, and the summer precipitation (June-September) in the source region of the Yellow River will be used as output variable in the ANN. The architecture of the neural network is determined by a 'trial and error' approach. Two hidden layers were placed between the input and output layers. The function 'tansig' in Matlab was used for this purpose. The four-layer ANN was connected by weights. A training period (1961-1995) and a validation period (1996-2010) were selected for optimization of the weights.

3.3 Xinanjiang model

The Xinanjiang model was originally developed by Zhao (1992). The model applied to the source region of the Yellow River consists of two components (**Paper IV**): a three-layer evapotranspiration component and a runoff generating component (Fig. 3.2). The input data are daily precipitation and potential evapotranspiration, and the outputs are discharge and actual evapotranspiration. The model parameters and their ranges are listed in Table 3.3. The parameters are usually defined by specifying lower and upper limits. These limits are chosen

according to physical and mathematical constraints, information about physical characteristics of the system, and from modelling experiences (Cheng et al. 2006).

Table 3.3 Parameters of the Xinanjiang model. Parameters in bold indicate high sensititivy.

Parameter	Definition	Range
UM (mm)	Soil moisture storage capacity of the upper layer	0-50
LM(mm)	Soil moisture storage capacity of the lower layer	0-150
WM (mm)	Areal mean soil moisture storage capacity	50-300
B	Exponential parameter with a single parabolic curve representing the non-uniformity of the spatial distribution of the soil moisture storage capacity	0-1
IM (%)	Percentage of impervious and saturated areas	0-1
K	Ratio of potential evapotranspiration to pan evaporation	0-2
C	Evapotranspiration coefficient of deeper layer	0-0.5
SM (mm)	Free water capacity of the surface soil layer representing the maximum possible deficit of free water storage	0-200
EX	Exponent of the free water capacity curve influencing the development of the saturated area	0.5-2.5
KG	Outflow coefficient of the free water storage to groundwater flow	0.01-1
KI	Outflow coefficient of the free water storage to interflow	0.01-1
CG	Recession constant of the groundwater storage	0.5-1
CI	Recession constant of the lower interflow storage	0.1-1
CS	Recession constant in the lag and route method for routing through the channel system	0.01-1
L (d)	Lag in time for runoff routing period	0-4

The evapotranspiration component acts on three vertical layers identified as upper, lower, and deeper soil layers. The upper layer refers to the vegetation, water surface and the very thin topsoil. The lower layer refers to the soil in which the vegetation roots dominate and the moisture transportation is mainly driven by the potential gradient. The deep layer refers to the soil beneath the lower layer where only the deep-rooted vegetation can absorb water and the potential gradient is very small (Jayawardena and Zhou 2000). Evapotranspiration takes place at the potential rate in the upper layer. On exhaustion of moisture content in the upper layer, evapotranspiration proceeds to the lower layer at a decreased rate that is proportional to the moisture content in that layer. Only when the total evapotranspiration in the upper and lower layers is less than a pre-set threshold, represented as a fraction of the potential evapotranspiration, does it further proceed to the deep layer to keep this pre-set minimum value (Jayawardena and Zhou 2000). Evaporation is first subtracted during the rainfall process, and the runoff generation is computed by considering

the respective soil moisture states and the storage capacities of the three layers. The runoff is separated into three components: surface runoff, interflow, and groundwater flow. A more detailed conceptual hydrological process description is found in Zhao (1992).

Fig. 3.2 Flowchart of the Xinanjiang model

Blaney–Criddle Method The Blaney–Criddle method has been widely used to calculate the potential evapotranspiration as model input (Xu and Singh 2002, Kingston et al. 2009, Sperna Weiland et al. 2012). It is a temperature-based method that requires temperature as input variable. The Blaney-Criddle equation is:

ET = KP (0.46T +8.13)

where

ET = potential evapotranspiration from a reference crop, in mm, for the period in which p is expressed;

T = mean temperature in °C;

K= monthly consumptive use coefficient, depending on vegetation type, location and season. Here it was taken to be 1.

P= percentage of total daytime hours for the used period out of total daytime hours of the year; The daylight hours here are based on the calculation of sunset hour angels that depend on the calculation of solar declination. It can be calculated as N=M $(24/\pi)$, where M is the sunset hour angle in radians.

Monte Carlo Method. The process of model calibration is normally performed either manually or by using computer based automatic procedures. In this study, the Monte Carlo method was used to generate 10000 sets of the 8 sensitive parameters for calibration. The other 7 parameters were pre-set as initial values and adjusted manually during the calibration process. The parameters for best fit between observed and simulated discharge were used for validation.

Model Performance Measure. The Pearson product-moment correlation coefficients r between observed and simulated discharge data were used to measure model performance. The normal distribution of observed and simulated discharge data were tested by the Kolmogorov-Smirnov test in Matlab

4 RESULTS AND DISCUSSION

4.1 Hydroclimatic trend and periodicity analysis

4.1.1 Trend and variability analysis

Annual Trend Analysis

The hydroclimatic annual trend analysis was investigated in **Paper I**. Figure 4.1 shows the mean areal precipitation and temperature depending on time for the study area. The Thiessen polygon method was used to calculate the mean areal precipitation and temperature over the experimental area. The area as a whole has a slight decreasing non-significant trend in precipitation and a significant increasing trend in temperature. The mean annual precipitation decrease is approximately 0.6 mm/year (30 mm for the entire 50-year period) and the mean annual temperature increase is about 0.03°C/year (1.5°C for the entire 50-year period). Both temperature and precipitation have displayed above average annual values during the last 10-year period.
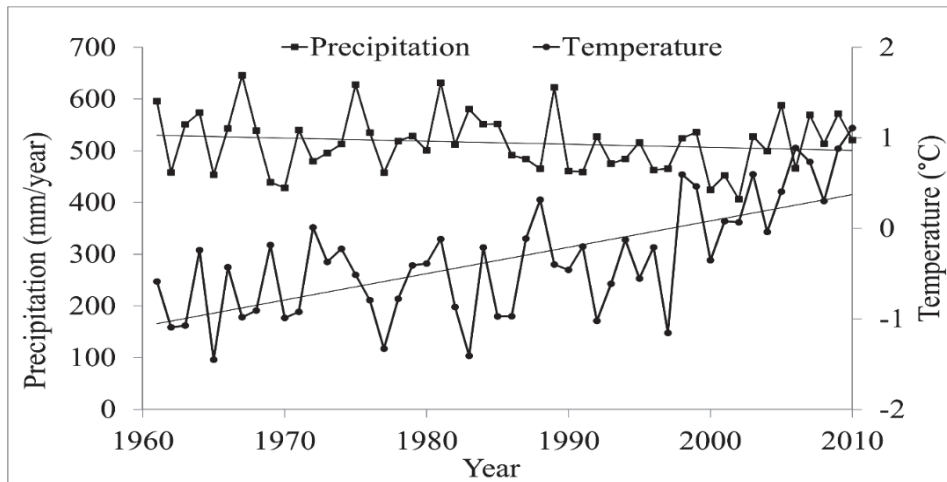
Fig. 4.1 Mean areal annual precipitation and temperature trend in the Yellow River source region.

Figure 4.2 shows linear trends for mean annual precipitation and temperature at each observation station. The trend is quantified in Table 4.1 and as noted 9 out of 10 stations show statistically significant increasing trend for temperature. For precipitation the trend is

less clear. Seven precipitation stations display a decreasing trend while three show an increasing trend. All decreasing stations are located in the eastern and north-eastern part of the Yellow River source area. Since this area is much affected by the summer monsoon it is rather clear that the declining rainfall is related to weakening of the monsoon rainfall.

The linear trend results are corroborated by the Mann-Kendall Test in Table 4.1. Standard deviation (SD) and coefficient of variation (CV) were calculated to examine the variation. The coefficient of variation for precipitation ranges from 0.13 to 0.27. It is seen that four stations display a statistically significant trend. The precipitation stations Tongde, Zeku, and Maqu exhibit a significantly decreasing trend at the 0.05 significance level while Maduo station shows an increasing trend at the 0.05 significance level. The precipitation stations with significantly decreasing trends are all confined to the north-eastern parts of the catchment (Tongde, Zeku, and Maqu) and Maduo with increasing trend is located in the north-western part of the catchment. There is, thus, a geographical dependence for the trend and annual data.

Table 4.1 Precipitation and temperature linear trends and Mann-Kendall statistics (Z); Values in bold are statistically significant at the 0.05 level

Station	Prec. trend (mm/year)	Temp. trend (°C/year)	Prec. SD	Temp. SD	Prec. CV	Prec. Z	Prec. P	Temp. Z	Temp. P
Xinghai	1.13	0.034	69.6	0.66	0.19	1.56	0.120	**5.68**	1.35E-08
Tongde	-1.74	0.037	88.4	0.78	0.21	**-1.99**	0.047	**5.17**	2.35E-07
Zeku	-3.28	0.018	114.9	1.00	0.27	**-2.94**	0.003	1.68	0.093
Henan	-0.04	0.015	93.8	0.88	0.16	-1.47	0.141	**2.53**	0.011
Maduo	1.32	0.039	65.1	0.89	0.20	**2.27**	0.023	**4.88**	1.08E-06
Dari	0.36	0.032	71.8	0.74	0.13	0.67	0.503	**4.90**	9.50E-07
Jiuzhi	-1.56	0.040	99.3	0.72	0.13	-1.44	0.150	**6.35**	2.17E-10
Maqu	-3.36	0.034	111.0	0.68	0.18	**-2.44**	0.015	**5.21**	1.88E-07
Ruoergai	-1.21	0.033	98.4	0.66	0.15	-1.49	0.137	**5.47**	4.48E-08
Hongyuan	-1.01	0.029	101.5	0.62	0.14	-0.75	0.452	**5.05**	4.36E-07
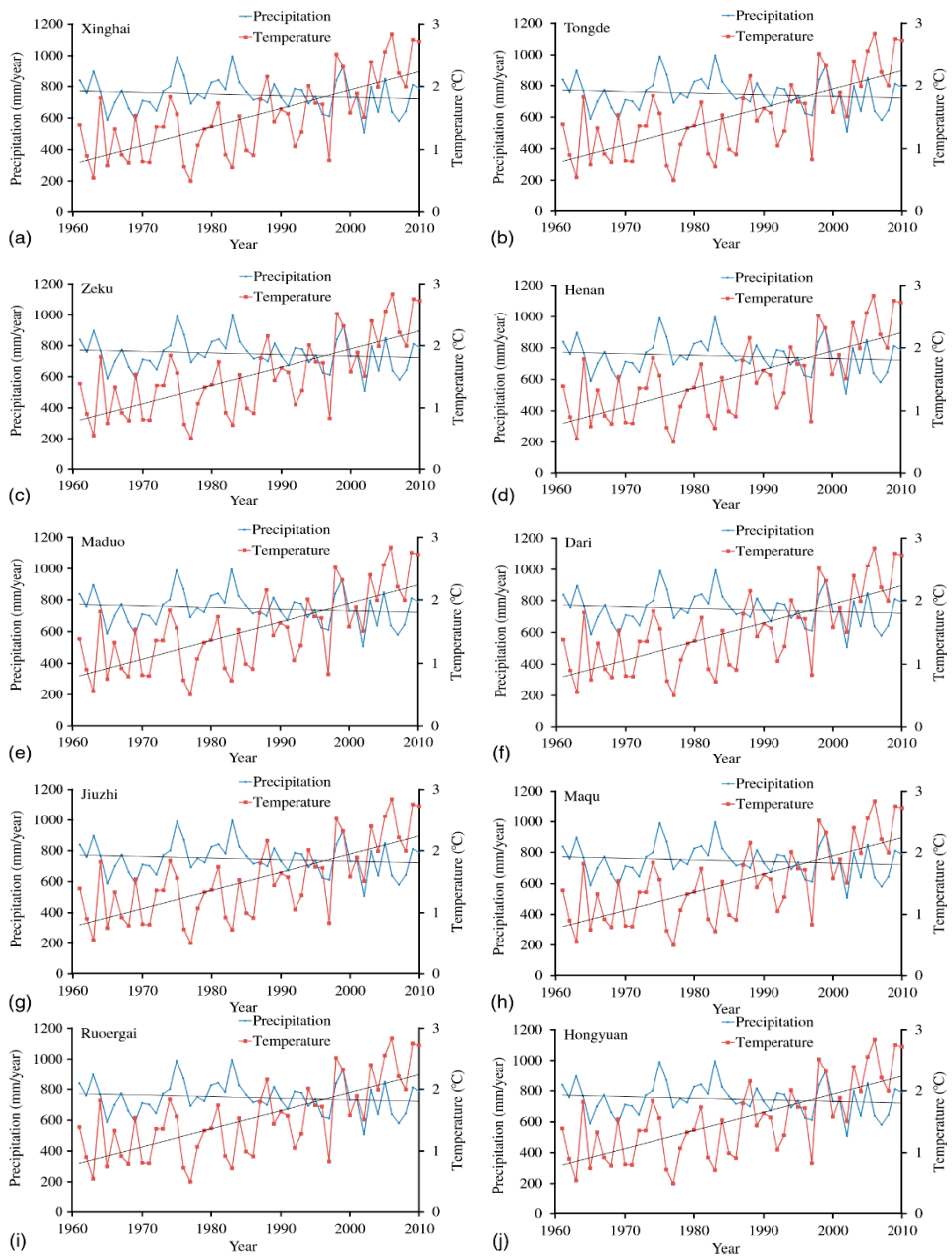
Fig. 4.2 Precipitation and temperature trends depending on station: (a) Xinghai; (b) Tongde; (c) Zeku; (d) Henan; (e) Maduo; (f) Dari; (g) Jiuzhi; (h) Maqu; (i) Ruoergai; (j) Hongyuan
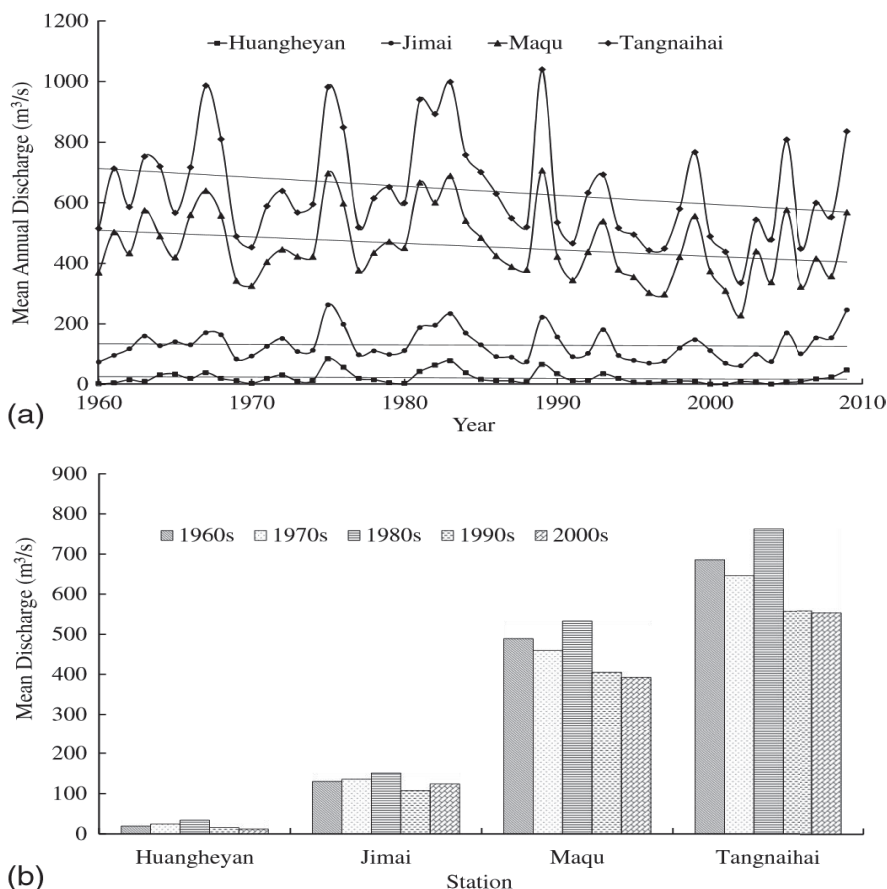
Fig. 4.3 (a) Annual and (b) decadal mean discharge at the four discharge stations

Figure 4.3 shows the corresponding streamflow at the four runoff stations during 1960-2009. When comparing decadal streamflow at the four investigated runoff stations, the last two decades streamflow has been significantly lower than corresponding streamflow during 1960-90 (Fig. 4.3(b)). The decadal mean streamflow at Tangnaihai station decreased by about 28% from 1980s to 2000s. Consequently, there is a clear decreasing trend for streamflow considering the entire 50-year investigated period (Table 4.2). According to Fig. 4.3(a) there is also a pronounced periodicity in annual streamflow that decreases towards the end of the 1990s. It is noticed that the streamflow showed an increasing trend during the last 10-year period. The decreasing linear trend is statistically significant for three of the four runoff stations as seen from Table 4.2. The coefficient of variation for Huangheyan station is highest, followed in order by Jimai, Tangnaihai and Maqu.

22

Table 4.2 Streamflow linear trends and Mann-Kendall statistics (Z); Values in bold are statistically significant at the 0.05 level

Station	Streamflow trend (m^3/s/year)	Mann-Kendall Z	P	SD	CV
Huangheyan	-0.75	**-2.19**	0.028	20.5	0.96
Jimai	-0.18	-1.47	0.239	49.1	0.38
Maqu	-2.15	**-2.40**	0.017	115.2	0.25
Tangnaihai	-2.95	**-2.31**	0.021	169.8	0.26

Seasonal Trend Analysis

Change-Point Analyzer was applied on annual precipitation, temperature and streamflow data series to further explore the potential abrupt hydro-climatic change points in the source region of the Yellow River in **Paper I**. The analysis results are summarized in Table 4.3. No change point was detected for precipitation. Temperature change occurred in 1998 with 99% confidence level, and streamflow change occurred in 1990 with 96% confidence level. The mean annual temperature was -0.58°C during 1961-1998, and it increased to 0.43°C during 1999-2010. The mean annual runoff depth was 179.2 mm during 1960-1990, and it decreased to 143.9 mm during 1991-2009. Hydrological systems act as spatial and temporal integrators of precipitation and temperature over certain watersheds, and streamflow observations can serve as a pertinent index of interannual hydroclimatic variability at regional scale, hence two periods before and after 1990 were divided to further investigate the change.

Table 4.3 Results and confidence levels of change point analysis

Hydroclimatic variables	Change point	Confidence (%)
Precipitation	None	----
Temperature	1998	99
Streamflow	1990	96

The seasonal analysis corroborates the above annual trend and change-point analysis. Figure 4.4 shows the monthly change for precipitation, temperature, and runoff by comparing the periods 1960-90 and 1991-2010. As seen from the comparison in Fig. 4.4 temperature has increased rather evenly throughout the year and all months except for January. Regarding precipitation it is mainly the monsoon period (July to September) that
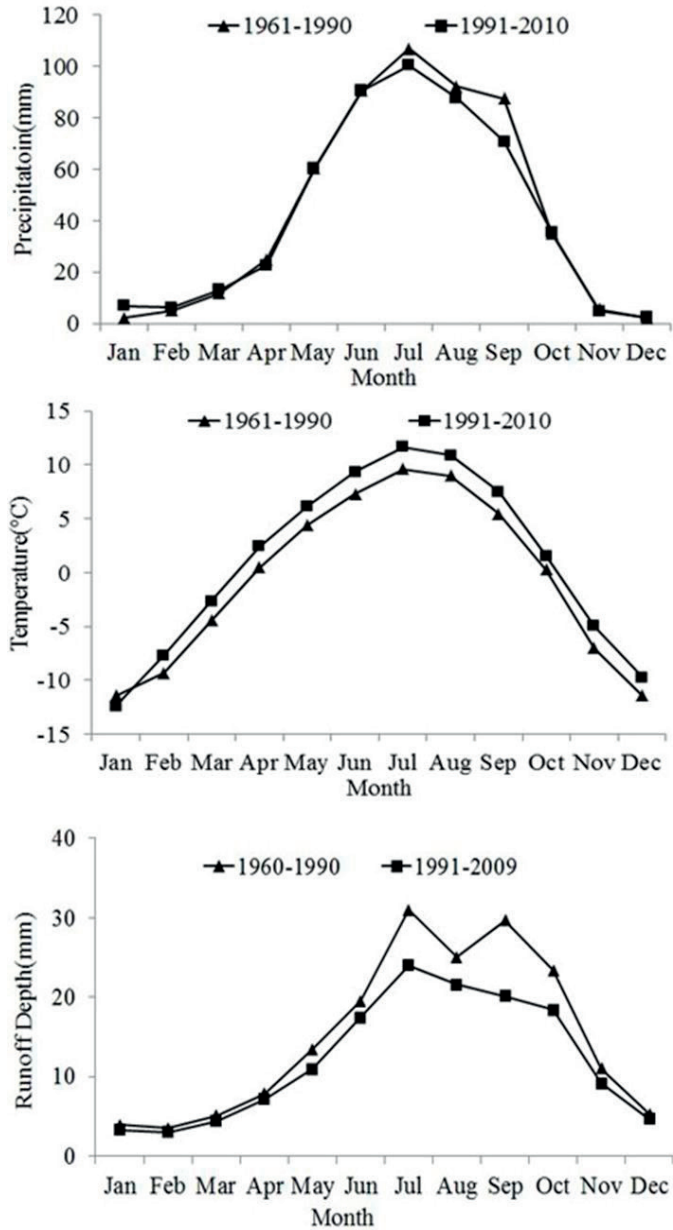
Fig.4.4 Monthly variation of precipitation, temperature, and runoff.

has displayed a decrease. In general, the monsoon period (June-September) accounts for about 62% of the annual total precipitation. September is the month with largest relative

decrease in precipitation. The streamflow displays the largest decrease from July to October as a result from decreasing monsoon rainfall, and there is also a general smaller decrease for the rest months.

Increasing temperature causes more glacier and snow melt, and it increases the portion of snowmelt runoff to the total runoff. However, the clear decrease in streamflow as seen from Fig. 4.4 indicates that the melt water has only limited impact on the total streamflow. The decreasing trend in monsoon precipitation is the major reason for the reduced streamflow in the 1990s and 2000s, but also increasing evapotranspiration due to increasing temperature for other parts of the year is a significant factor. Zheng et al. (2009) reported that the land use change played a more important role than the climate in reducing streamflow in the 1990s. Due to the complexity of temperature influence, topography, land use change, and precipitation variability, further investigations are necessary to gain a deeper understanding of the linkages among hydro-climatic variables and land use for the area.

Hydroclimatic Variability Analysis

Figure 4.5 shows the spatial variation of mean annual precipitation over the Yellow River source region (**Paper I**). The mean areal precipitation over the catchment is 515.1 mm/year. There is a strongly increasing gradient from the northwest parts with approximately 309 - 755 mm/year in the southeast. The topographical gradient of rainfall and the annual rainfall variability are greatly influenced by the south-easterly summer monsoon flow. This makes annual precipitation amount decline with altitude as a general pattern in the region from the southeast to the northwest as seen from Fig. 3.1 and 4.5. The Maduo station receives 319 mm annual mean precipitation only in spite of its high location (4272 m). The reason is partly rain shadow effects due to the high mountain peaks in the central parts of the catchment and partly effects of the spatial extension of the summer monsoon.
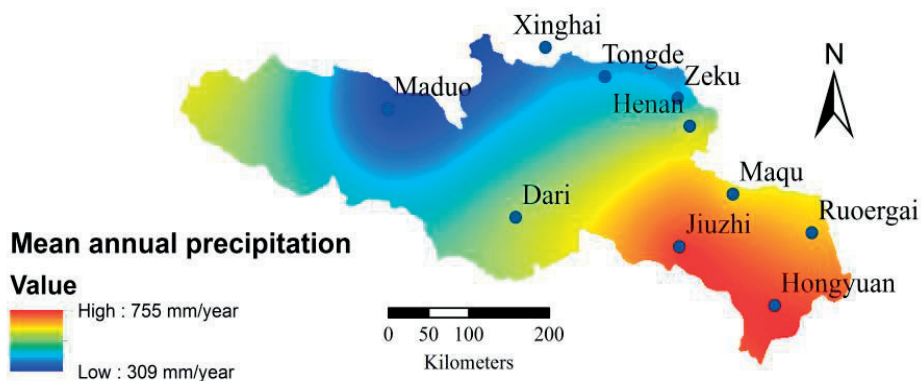

Fig. 4.5 Spatial variation of mean annual precipitation over the Yellow River source region.

In order to further identify the precipitation spatial variability in the source region of the Yellow River, cluster analysis was performed to separate the precipitation stations into homogeneous regions using monthly precipitation data (**Paper II**). Fig. 4.6 shows the outcome of this analysis. The precipitation stations were thus divided into three zones, namely, 1: Xinghai, Tongde, and Maduo; 2: Zeku, Henan, and Dari, and 3: Jiuzhi, Maqu, Ruoergai, and Hongyuan. The summer monsoon rainfall in China is concentrated in about four months from June to September, and the monsoon rain belt in the upper Yellow River is caused by south-easterly flow (Qian *et al.* 2002). Prevailing south easterlies converge along the east edge of the Tibetan Plateau causing rainfall to generally decrease with topography. Thus, the cluster analysis results are mainly characterized by different average annual precipitation amount. The mean annual precipitations are 365, 518, and 692 mm/year for zone 1, zone 2, and zone 3, respectively. This is shown in Table 4.4 that further quantifies the precipitation trend and variability for the three identified zones.
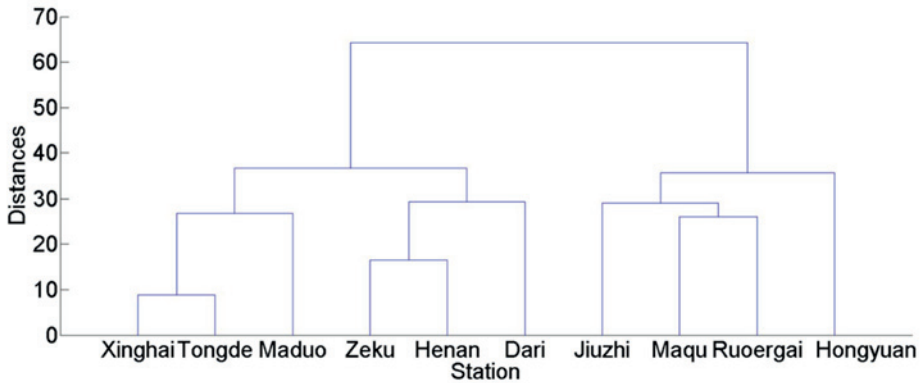
Figure 4.6 Cluster analysis of precipitation stations in the source region of the Yellow River.

The precipitation linear trends were quantified using the Mann-Kendall test (Table 4.4, Fig. 4.7) in **Paper III**. As seen from Table 4.4 and Fig. 4.7, zone 1 had a non-significantly increasing trend during 1961 to 2010. On the contrary, both zone 2 and 3 had significantly decreasing annual precipitation. The decrease is 1.49 and 1.79 mm/year for zone 2 and zone 3, respectively. Previous studies have indicated a small but a statistically non-significant trend for precipitation in the source region of the Yellow River (Tang et al. 2008, Zheng et al. 2007). However, dividing the region into homogeneous zones displays clear differences in precipitation and a clearer picture of the spatially dependent trend. This trend is the strongest for the wettest area of the Yellow River source region and gradually decreases with decreasing annual precipitation. The trend analysis indicates that the summer monsoon is gradually becoming weaker resulting in less summer rainfall. Figure 4.8 shows the monthly

average precipitation for different zones in the source region of the Yellow River. The general monthly distribution pattern is similar for all three zones. Precipitation in July represents the maximum. Table 4.5 shows the contribution of the wet season precipitation to the annual total for the different zones. June to September precipitation represents 68-75% of annual total. There is a general increase in the contribution of summer monsoon rainfall to the total annual amount as the climate becomes dryer. This was also noted for middle part of the Yellow River by Yasuda *et al.* (2009).
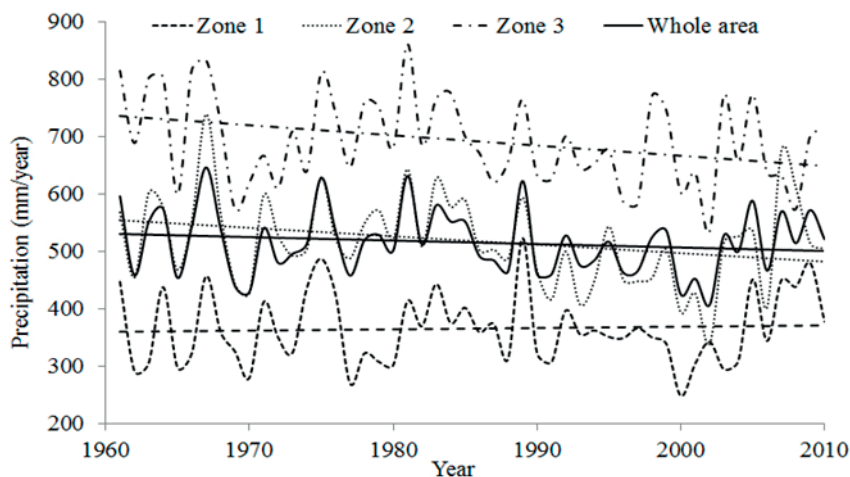
Figure 4.7 Annual precipitation for different zones and the whole area in the source region of the Yellow River.

Table 4.4 Precipitation linear trends and Mann-Kendall statistics (Z); NS: no significant trend; * is statistical significance at the 0.05 level.

Zone	Mean annual precipitation (mm/year)	Min. Annual precipitation (mm/year)	Max. annual precipitation (mm/year)	Linear Trend (mm/year)	Mann-Kendall Trend
Zone 1	365.0	247.9	522.5	0.24	NS
Zone 2	517.9	337.3	738.5	-1.49	*
Zone 3	692.4	533.9	860.5	-1.79	*
Whole area	515.3	406.0	645.8	-0.60	NS

Table 4.5 Contribution of the wet season (June to September) to annual rainfall (%)

Zone	1	2	3
%	74.9	72.6	67.7
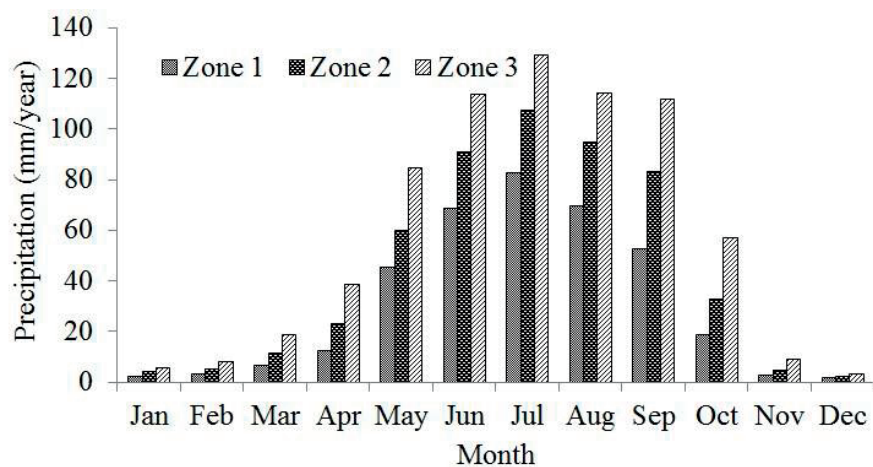
Fig. 4.8 Monthly average precipitation for different zones in the source region of the Yellow River

4.1.2 Hydroclimatic Periodicity Analysis

To further investigate the observed annual periodicity in streamflow according to Fig. 4.3, a wavelet analysis was performed on annual areal precipitation, temperature, and streamflow (**Paper I**). The results are shown in Fig. 4.9 and 4.10. From Fig. 4.9 it can be seen that there are statistically significant 2 to 4-year periodicities especially for precipitation in the beginning of the experimental period (1960-80). For temperature there are significant 2 to 4-year periodicities during 1961-70 and 1980-2010, and an intense 8-year periodicity was found during 1975-1990. The precipitation also showed an intense 8-year periodicity during 1965-85.
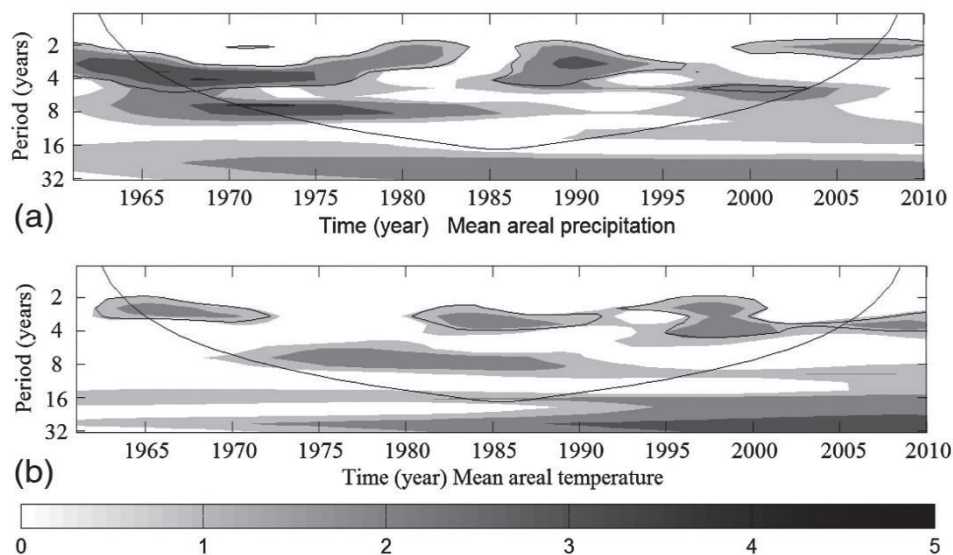
Fig. 4.9 Wavelet power spectrum for annual areal (a) precipitation and (b) temperature; power units are mm^2 and $°C^2$; the black line shows statistical significance at the 0.05 level

     Dominant periodicities for the annual streamflow at each station are shown in Fig. 4.10. As seen from the figure there is a strong statistically significant 8-year periodicity for all stations between the ends of the 1960s until the beginning of the 1990s. The significant change point for streamflow in 1990 (Table 4.3) confirmed the time scale of strong 8-year periodicity. Less strong but still significant is also the 4-year periodicity for mainly Jimai, Maqu, and Tangnaihai stations. When comparing Fig. 4.9 and 4.10 we note that the annual periodicity of precipitation and streamflow is overlapping especially for the 8-year periodicity during the early part of the experimental period. However, the wavelet power spectrum of 8-year periodicity for the streamflow is much stronger than that for the precipitation and temperature during the same period.

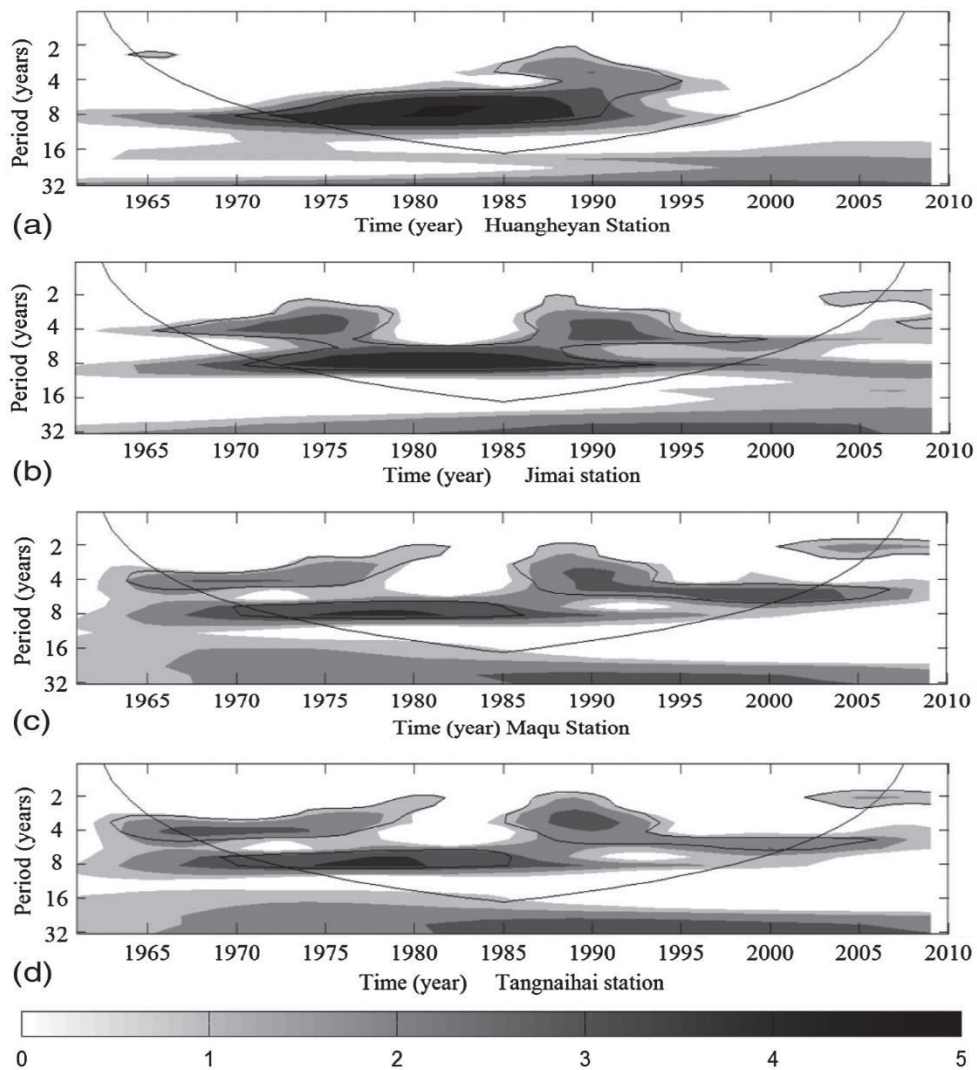Fig. 4.10 Wavelet power spectrum of annual streamflow for each station; power unit is mm^2; the black line shows statistical significance at the 0.05 level: (a) Huangheyan station; (b) Jimai station; (c) Maqu station; (d) Tangnaihai station.

30

Frequency analysis for mean annual precipitation and discharge in the source region of the Yellow River were analysed using Log-Pearson type III probability distribution as seen in Fig. 4.11. It is seen that Log-Pearson type III probability distribution is a suitable pattern due to the general good fitting. The probabilities for mean annual precipitation at 1, 5, 10, and 20% are corresponding to 670, 616, 590 and 561 mm, respectively. The probabilities for mean annual discharge at 1, 5, 10, and 20% are corresponding to 1250, 982, 872 and 763 m^3/s, respectively.
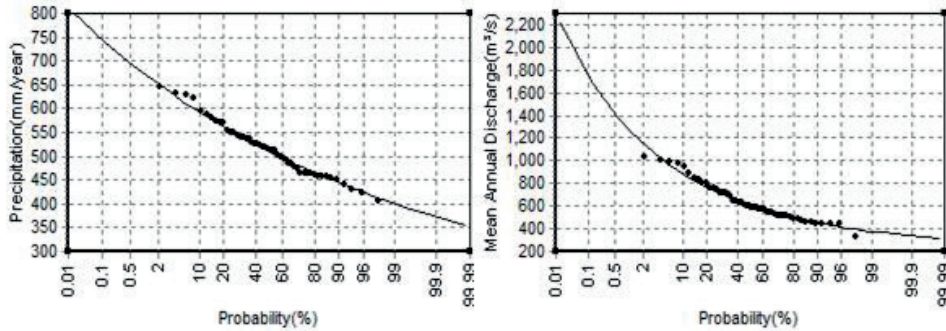
Fig. 4.11 Frequency analysis for mean annual precipitation and discharge in the source region of the Yellow River

4.1.3 Correlation analysis

The streamflow in the Yellow River source region is greatly affected by the changing climate. Due to the vast area and spatial variation in the source region of the Yellow River, water balances were first analysed at sub-basin level (**Paper I**). Annual areal precipitation and temperature trend analysis for each sub-basin is shown in Table 4.6. Temperature significantly increased corresponding to the station analysis, and precipitation in the Huangheyan and Jimai sub-basins also showed increasing trend having an opposite trend with the whole basin. Correlations between annual streamflow at the four discharge stations and annual areal precipitation and temperature for each sub–basin are shown in Table 4.7. Streamflow at all four hydrologic stations are positively correlated with precipitation and negatively correlated with temperature. The significance of the correlations indicates that the streamflow is much more sensitive to precipitation and that the dependence increases from upstream to downstream. Similarly, the highest correlation between temperature and streamflow is for the most upstream station (Huangheyan). Thus, it suggested that temperature effects on runoff are more important for upstream stations due to glacier melting.

To assess the relative contribution of precipitation and temperature to streamflow, a multivariate linear regression analysis was investigated here: R=0.66 P-15.1 T-177.1, where R represents annual runoff depth in the Yellow River source region, P and T represent mean annual areal precipitation and temperature, respectively. The R^2 is equal to 0.76. The bias was insignificant with a value of -2.5E-13, and root mean square error is 21.9 mm. All

coefficients were statistically tested for significance at the 0.05 level (Table 4.8). Both the increasing temperature and the decreasing precipitation are reasons for decrease in natural streamflow. The globally averaged surface temperature showed a warming of 0.85 (0.65 to 1.06) °C over the period 1880 to 2012, and 1983-2012 was likely the warmest 30-year period of the last 1400 years (IPCC 2013). The temperature change for the source region of the Yellow River for the last 50 years is even larger based on our analysis. It is estimated that the global mean surface temperature change for the period 2016-2035 relative to 1986-2005 will likely be in the range of 0.3 to 0.7°C (IPCC 2013). Immerzeel et al. (2010) predicted that the rainfall in the Yellow River upstream will increase about 14% over the period 2046 to 2065. However, we should treat regional precipitation predictions with caution, because most climate models experience difficulties in simulating mean monsoon and interannual precipitation variation. The changing climate will have significant effects on the downstream water availability in the Yellow River.

Table 4.6 Annual areal precipitation and temperature for each sub-basin Mann-Kendall statistics (Z); Values in bold are statistically significant at the 0.05 level

Station	Huangheyan		Jimai		Maqu		Tangnaihai	
	Z	P	Z	p	Z	P	Z	P
Precipitation	**2.27**	0.023	1.34	0.182	-0.54	0.581	-0.97	0.332
Temperature	**4.88**	1.08E-06	**4.58**	4.71E-06	**5.20**	2.02E-07	**4.87**	1.13E-06

Table 4.7 Correlation coefficients between annual streamflow and annual areal precipitation and temperature for each sub–basin. Values in bold are statistically significant at the 0.05 level

Station	Huangheyan	Jimai	Maqu	Tangnaihai
Precipitation	**0.343**	**0.576**	**0.821**	**0.849**
Temperature	**-0.286**	-0.066	-0.178	-0.190

Table 4.8 Summary for multiple linear regression

Variable	Coefficients	Standard Error	t Stat	P-value
Intercept	-177.1	28.7	-6.17	1.63E-07
P	0.66	0.055	11.9	1.29E-15
T	-15.1	5.23	-2.89	0.0059

4.2 Relationship between summer precipitation and global sea surface temperature

The relationship between summer precipitation and global SST was identified in **Paper II**. Figure 4.12 shows the 0-11 month lagged cross-correlation between global SST and the summer precipitation (June to September) for the source region of the Yellow River as a whole. The figure shows statistically significant negative correlations with different SST areas of various lags. For lag 0-4 month it is the large area in the central Pacific that is dominating. However, with increasing lag new areas in the southern Indian and Atlantic Ocean become a dominant influence. The predominant negative correlations mean that lower SST in these areas coincides with more summer rainfall over the source region of the Yellow River. El Nino events occur in the eastern Pacific Pattern and the central Pacific pattern according to the location of the onset of warm SST anomalies (Lin and Yu 1993, Feng et al. 2011). Xu et al. (2007) found that the La Nina phase (lower SST of the eastern tropical Pacific Ocean) corresponds to a relatively rainier season in the Yellow River basin. The results here reveal the correlated SST areas and confirm the importance of ENSO events for the summer precipitation in the source region of the Yellow River. The results also suggest significant relationships with southern Indian and Atlantic Ocean especially for lags between 5 to 8 months. Feng et al. (2013) examined that the SST anomalies over the southern Indian Ocean could induce consistent atmosphere circulation and precipitation anomalies over China, and the warm SST anomalies could decrease the rainfall that is generally in agreement with the negative correlations we found above.

Figure 4.13 shows correlation between summer precipitation in zone 1 and global SST. Different correlated SST areas emerge when dividing the Yellow River source region into homogeneous precipitation areas. Zone 1 rainfall is correlated with SST in mainly central and only partly eastern Pacific. Significant negative correlation remains for a lagged period up to 9 months in this area. It is also seen that a small area with positive correlations (blue area in Fig. 4.13) appears in the central Pacific Ocean for a lag up to about 8 months. The significant positive correlation corroborates with non-significantly increasing precipitation trend in zone 1 during the last 50-year period. It is quite clear that rainfall in zone 1 (western and northwestern parts of the source region of the Yellow River) is mainly governed by central and eastern Pacific SST.

Fig. 4.12 Correlation between summer precipitation in Yellow River source region and global SST for the period 1961–2010 (|r| > 0.36 and |r| > 0.46 correspond to a statistical significance level of 0.01 and 0.001, respectively).

Fig. 4.13 Correlation between summer precipitation in zone 1 and global SST for the period 1961–2010 (|r| > 0.36 and |r| > 0.46 correspond to a statistical significance level of 0.01 and 0.001, respectively).

Fig. 4.14 Correlation between summer precipitation in zone 2 and global SST for the period 1961–2010 (|r| > 0.36 and |r| > 0.46 correspond to a statistical significance level of 0.01 and 0.001, respectively).
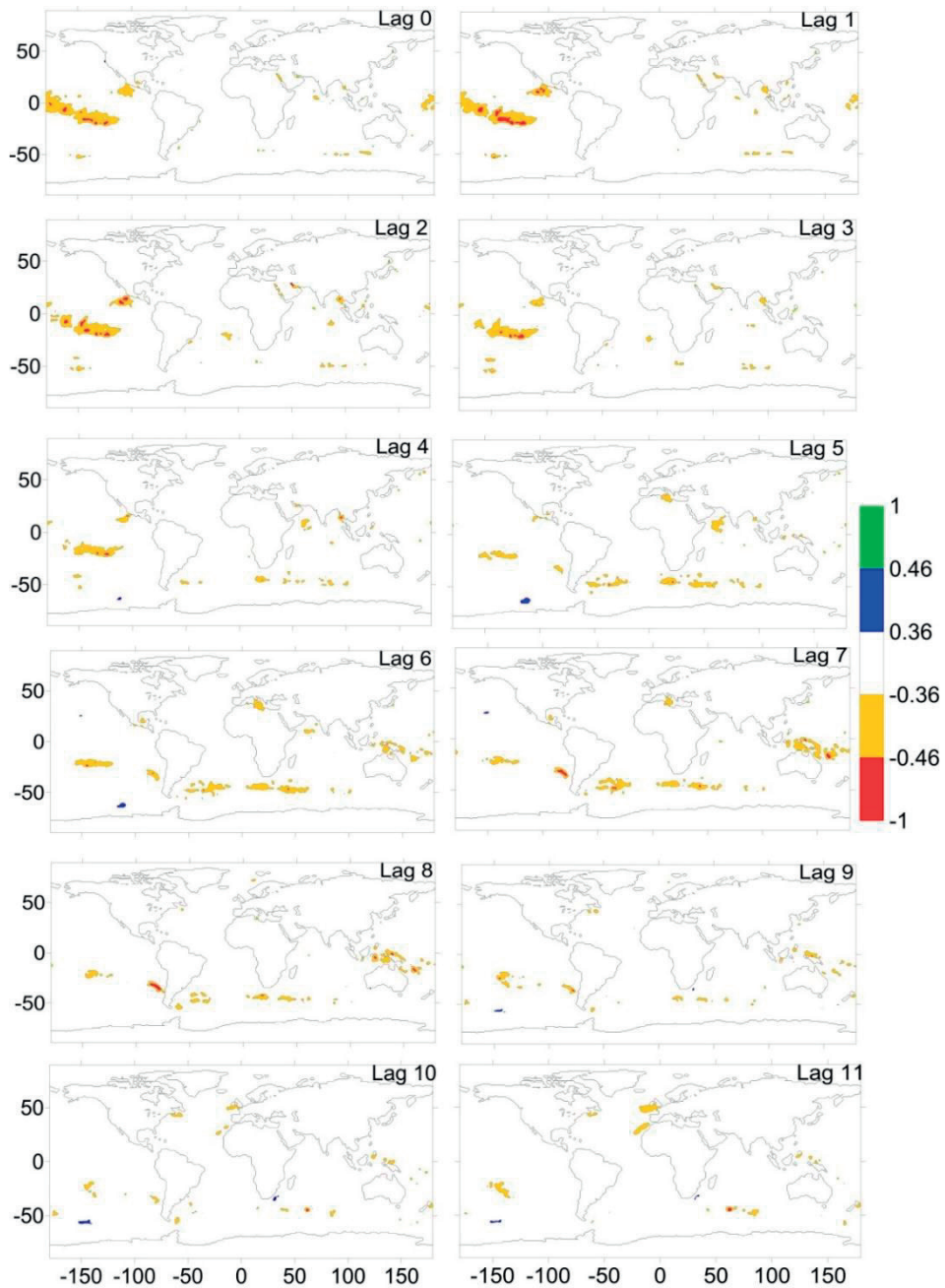
Fig. 4.15 Correlation between summer precipitation in zone 3 and global SST for the period 1961–2010 (|r| > 0.36 and |r| > 0.46 correspond to a statistical significance level of 0.01 and 0.001, respectively).
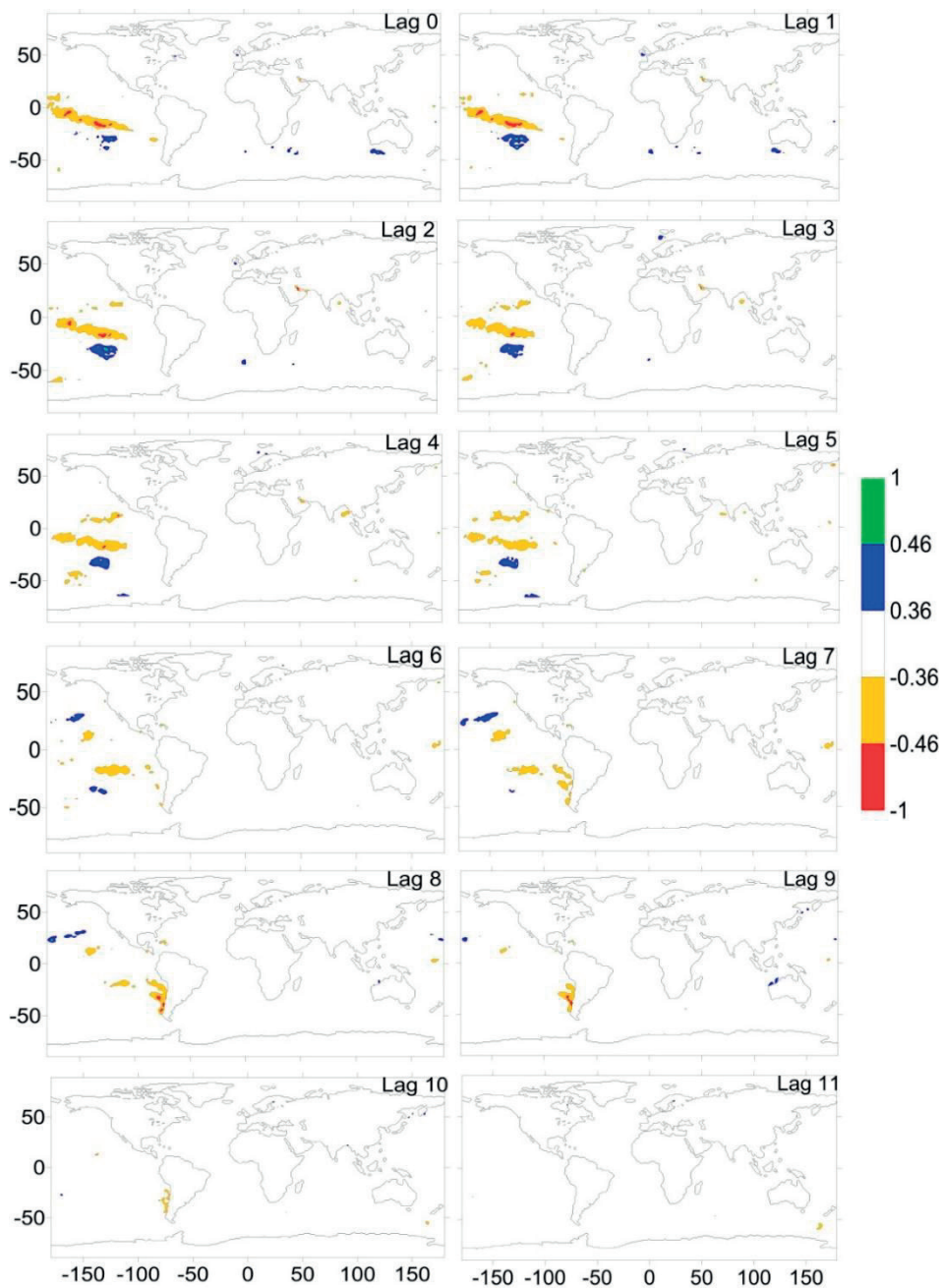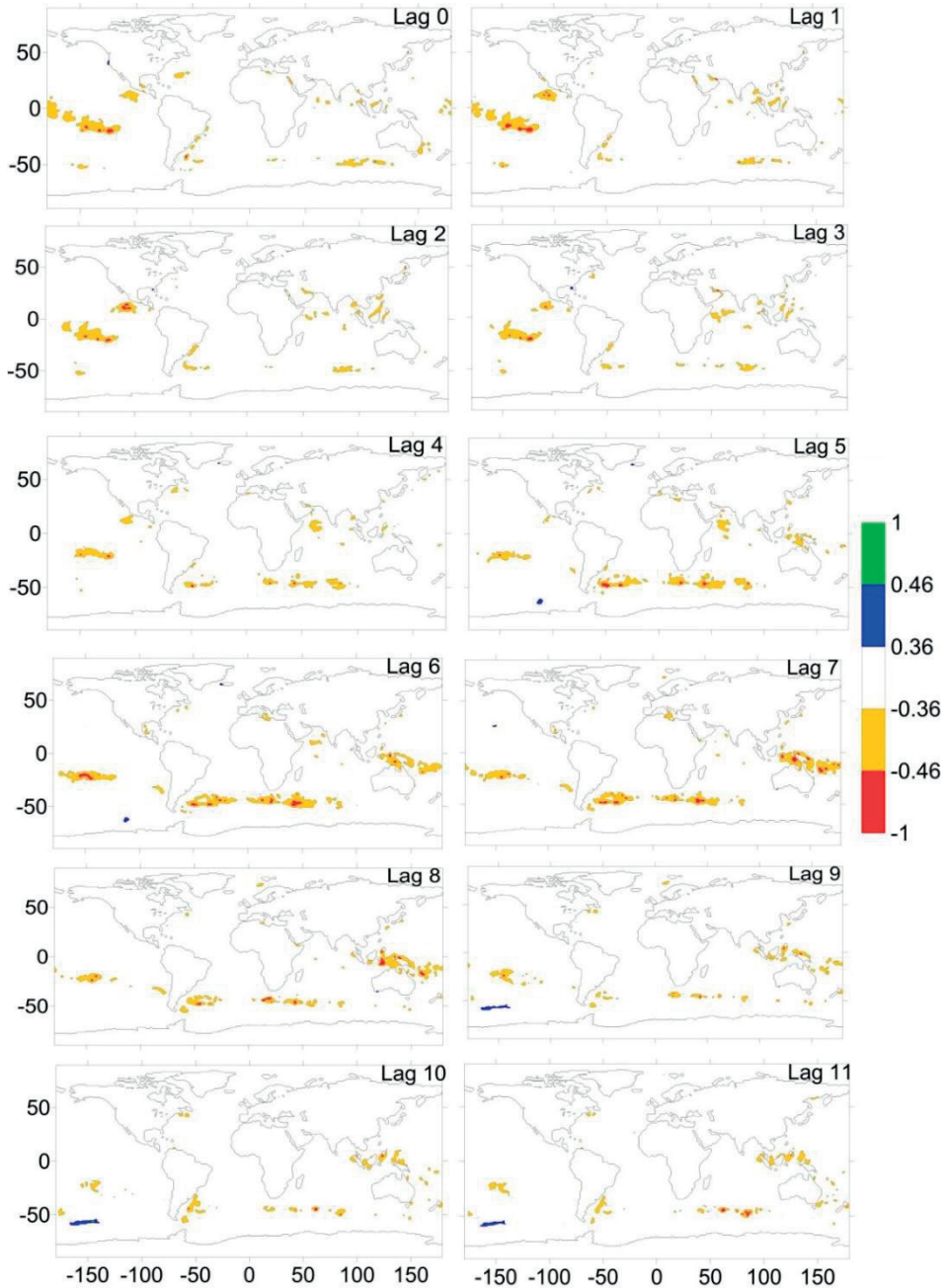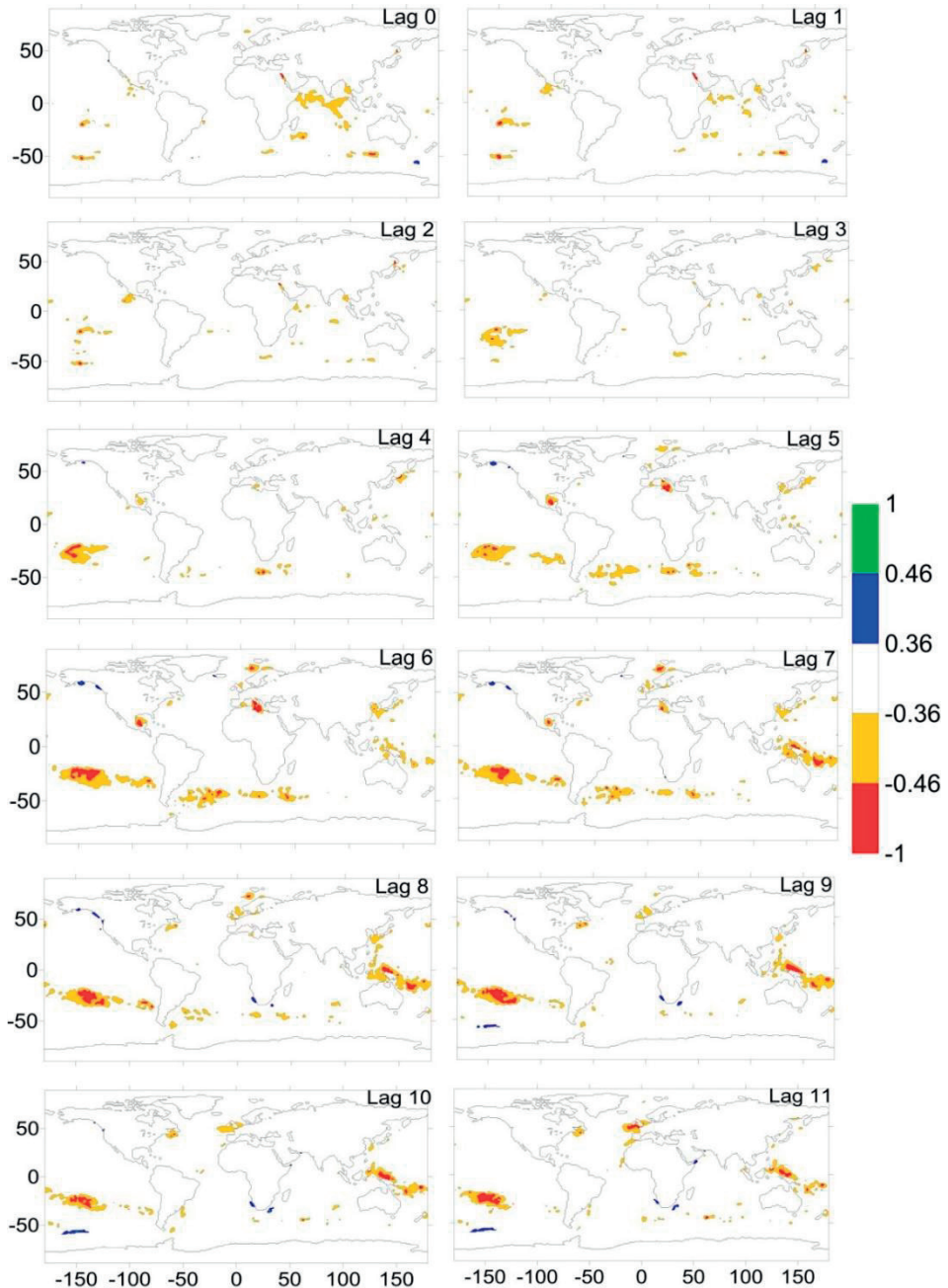
Figure 4.14 shows correlation between summer precipitation in zone 2 (central parts of source region of the Yellow River) and global SST. It has great similarity with the pattern for the whole region as shown in Fig. 4.12 but with more clear signals in the southern Indian and Atlantic Ocean, mainly due to the similar summer precipitation time series between the whole region and zone 2(Fig. 4.7). For short time lags of 0-4 month it is mainly central Pacific that explains rainfall. However, for lag 5-8 month it is southern Atlantic and Indian Ocean and western Pacific that is of importance. The clearest signials appeared at Lag 6 month and Lag 7 month for the southern Atlantic and India Ocean, and western Pacific, respectively.

Figure 4.15 shows correlation between summer precipitation in zone 3 (eastern parts of source region of the Yellow River) and global SST. Lag 0-3 month shows scattered and small areas. From lag 4 month the central Pacific emerges with strong correlation. When increasing the lag period western Pacific and the southern Atlantic also display strong correlation. Eventually, for the long lag periods of 6-11 month the central and western Pacific dominate the correlation.

It is clearly seen that SST has an influence on the summer precipitation in the source region of the Yellow River. The ENSO activity is typically monitored by observing the sea level pressures and SST in the equatorial Pacific. Thus, the Southern Oscillation Index was selected to further reveal the ENSO influence on summer precipitation in the source region of the Yellow River (**Paper II**). Table 4.9 shows the correlation coefficients between summer precipitation and SOI for different lags. Significant positive correlations were found for the 0-2 month lag for the entire region. In addition, zone 1 had a lag 4, 9-11 month significant positive correlations. Sustained negative values of the SOI often indicate El Nino episodes, and these negative values are usually accompanied by sustained warming of the central and eastern tropical Pacific Ocean, a decrease in the strength of the Pacific trade winds and a reduction in rainfall over China(Fu et al. 2013). The significant negative correlations with SST in equatorial Pacific Ocean and positive correlations with SOI for summer precipitation clearly shows the influence of ENSO activities on the source region of the Yellow River.

Table 4.9 Correlation coefficients between summer precipitation in the source region of the Yellow River and SOI with different lag month. The values in bold are statistical significance at the 0.05 level.

Precipitation	Lag 0	Lag 1	Lag 2	Lag 3	Lag 4	Lag 5	Lag 6	Lag 7	Lag 8	Lag 9	Lag 10	Lag 11
Whole area	**0.197**	**0.234**	**0.144**	0.070	0.043	0.004	-0.005	0.001	-0.035	-0.003	0.018	0.082
Zone 1	**0.153**	**0.169**	**0.140**	0.060	**0.136**	0.112	0.042	0.091	0.077	**0.150**	**0.140**	**0.190**
Zone2	**0.178**	**0.216**	**0.164**	0.065	0.026	0.026	0.033	0.004	-0.017	-0.026	0.014	0.055
Zone 3	**0.166**	**0.201**	0.083	0.055	-0.011	-0.070	-0.054	-0.051	-0.095	-0.070	-0.051	0.014

It is clear that ENSO events have an influence on the summer precipitation in the source region of the Yellow River. Fu et al. (2013) examined the trend and variability of extreme rainfall events in China and found that it is mainly influenced by ENSO, the magnitude of East Asian monsoon, global warming as well as wind circulations like the cyclonic and anti-cyclonic circulation anomalies dominating over Northwest and North China. Cuo et al. (2013) have shown that precipitation change in winter at northern Tibetan Plateau can be attributed to changes in the North Atlantic Oscillation, ENSO, the Arctic Oscillation and East Asian westerly jet, and in summer the changes in precipitation is only weakly related to these indices. Xu et al. (2013) defined an eastern Pacific southern oscillation index and a central Pacific southern oscillation index to measure the different responses of the atmospheric circulation to the two types of El Nino, and it showed that both indices exhibited positive correlations with rainfall anomalies in the upstream of the Yellow River. Zhang et al. (2013) found the warm phase of the North Atlantic SST is related to North Atlantic Oscillation that leads to less precipitation or more frequent droughts in the semi-arid subarea in the upper reaches of the Yellow River. Liu et al. (2012) investigated the variation of water discharge that is more likely to be correlated with large sale climatic process over the long time scales and is also influenced by both ENSO and human activities, and the ENSO impacts on the water discharge were exerted by influencing the precipitation through its effects on East Asian monsoon. Li et al. (2010) found that the recent warming of the tropics, especially the warming associated with the tropical interdecadal variability centred over the central and eastern Pacific is a primary cause for the weakening the EASM (East Asian Summer Monsoon) since the late 1970s. Two external sources of forcing, including Pacific and Indian Ocean SSTs and the snow cover in the Eurasia and the Tibetan Plateau, are believed to be primary contributing factors to physical processes and mechanisms related to the EASM (Ding and Chan 2005). The warming in the tropical Pacific and Indian Ocean leads to an abnormal Subtropical Pacific High that reduces water vapour transport to North China from South China Sea and thus contributes to precipitation decrease (Hu 1997). In view of the above it is clear that ENSO can exert an important impact on the Asian monsoon (Weng et al. 1999, Zhou et al. 2010).

4.3 Teleconnection pattern influence on precipitation

The precipitation for three identified homogeneous zones in the source region of the Yellow River was tested for relation against different climate indices using PCA and SVD (**Paper III**). Monthly precipitation and monthly climate indices for the same period from 1961 to 2010 were used for analysis. PCA revealed a close relationship that is direct or inverse between the precipitation for three zones and climate indices. The first two modes of PCA were analysed as they represent a major variance. Figure 4.16 gives the PCA biplot, and it is seen that the precipitation for the three zones is in general represented in the first PCA mode. It is positively related to NAO, WP and NINO3.4, and it is negatively related to POL. The PCA analysis shows strong evidences that the precipitation in different zones is closely related to different teleconnection patterns.
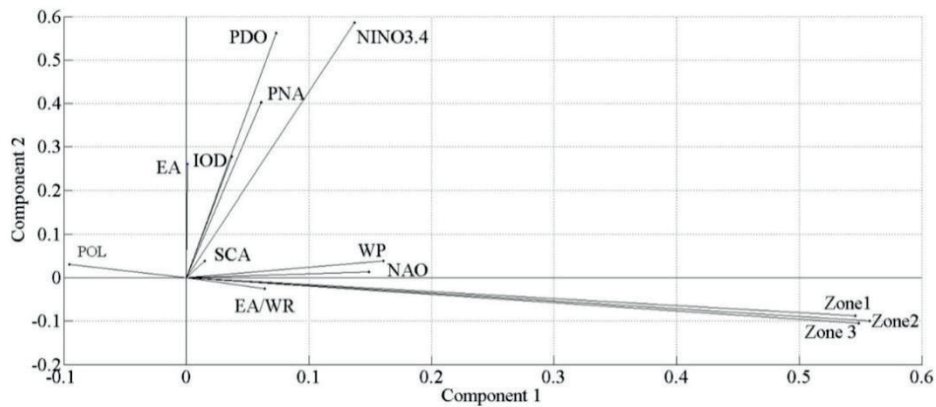
Fig. 4.16 Biplot from the first two modes of PCA

SVD was applied to the cross-variance matrix between monthly precipitation for the three zones and monthly climate indices for the same period from 1961 to 2010 in **Paper III**. Figure4.17 presents the time series of precipitation for the different zones and climate indices in the first mode of SVD with explained variance of 84.5%. A similar variation shows that precipitation for different zones is closely related to the teleconnection patterns. Table 4.10 shows the heterogeneous correlation for the different indices. It is noteworthy that the precipitation for the three zones is positively related to NAO, WP and NINO3.4, and negatively related to POL at 0.05 significance level. The result of SVD confirms the relationship from the PCA results between precipitation for the three zones and climate indices.

Table 4.10 Heterogeneous correlation table of summer precipitation and climatic indices

	Zone1	Zone 2	Zone3	NAO	EA	WP	PNA	EA/WR	SCA	POL	PDO	NINO3.4	IOD
Mode 1	**-0.25**	**-0.25**	**-0.23**	**-0.16**	0.01	**-0.17**	-0.05	-0.06	-0.02	**0.10**	-0.04	**-0.11**	-0.02
Mode 2	0.04	-0.01	-0.03	0.04	0.05	-0.04	0.00	0.05	**0.10**	0.05	0.01	0.02	0.02

Values in bold are statistically significant at the 0.05 level

The results in this study showed that ENSO, NAO, WP and POL events have an influence on the precipitation in the source region of the Yellow River. Xu et al. (2007) found that the La Nina phase corresponds to a relatively rainier season in the Yellow River basin. Fu et al. (2013) examined the trend and variability of extreme rainfall events in China and found that it is mainly influenced by ENSO and the magnitude of East Asian monsoon. Yuan et al. (2015b) examined the summer precipitation in the source region of the Yellow River teleconnections with global sea surface temperatures, and found that higher sea surface

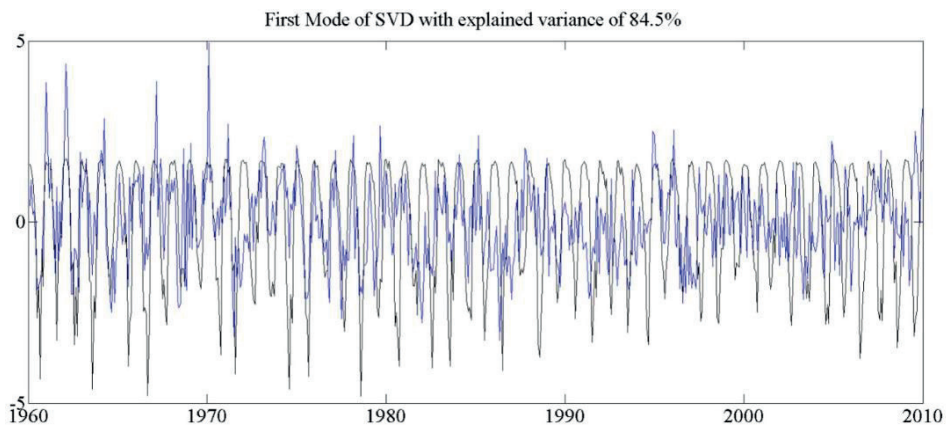First Mode of SVD with explained variance of 84.5%

Figure 4.17 Time series of predictor (monthly precipitation) and predictant (monthly climate indices) in the first mode of SVD.

temperature in equatorial Pacific areas corresponding to El Nino coincides with less summer precipitation. Cuo et al. (2012) showed that precipitation change in winter at northern Tibetan Plateau can be attributed to changes in the East Asian westerly jet, North Atlantic Oscillation and ENSO. Zhang et al. (2013) also examined that the warm phase of the North Atlantic SST is related to North Atlantic Oscillation that leads to less precipitation or more frequent droughts in the semi-arid subarea in the upper reaches of the Yellow River. Liu et al. (2015) found that NAO greatly controls the variability of summer precipitation between the north-eastern and the south-eastern Tibetan Plateau by modifying the atmospheric circulation over and around the Tibetan Plateau. During the positive phase of the NAO, warm moist air from the oceans around Asian is transported by the south-eastern flank of the anticyclone anomaly over East Asian to the north-eastern Tibetan Plateau, and this northward-moving warm moist air encounters cold air masses transported by the north-western flank of the cyclonic anomaly over the north-eastern Tibetan Plateau (Liu et al. 2015). This confluence of the cold and warm air masses subsequently strengthens cumulus convective activities and ultimately results in excessive precipitation over the north-eastern Tibetan Plateau. Research has showed that the strong positive and negative West Pacific patterns are related to the east-west and north-south movements of the East Asian jet stream, indicating that the change from cold to warm season results from the northward movement of the East Asian jet stream and thus affects aspects of the East Asian climate such as precipitation and temperature (Choi and Moon 2012, Barnston and Livezey 1987). Yan (2002) found that POL was positively associated with winter precipitation in China, indicating the significane of the winter monsoon in producing rainfall pattern. Lin (2014) showed that the POL has negative correlation with precipitation in North China.

4.4 Rainfall-runoff process

4.4.1 Summer precipitation prediction

Based on the revealed relationships between precipitation in the source region of the Yellow River and global teleconnection patterns (**Paper III**), a back propagation neural network was developed to predict the summer precipitation (June-September) using significantly correlated climate indices as input layer, including NAO, WP, POL and NINO3.4. One limitation of ANN analysis is that the model results vary depending on the random setting of the initial weights. Therefore, the neural network model run for one experiment was repeated ten times. The predicted summer precipitation refers to the most accurate results of ten model runs. Here, a 'trial and error' process was used to choose different nodes for the two hidden layers. Table 4.11 shows the Pearson correlation coefficients between observed and predicted summer precipitations for training and validation period. The correlation coefficients for the validation period are generally larger than 0.6. Figure 4.18 shows the observed and predicted summer precipitation for the validation period and the different zones and the whole area.
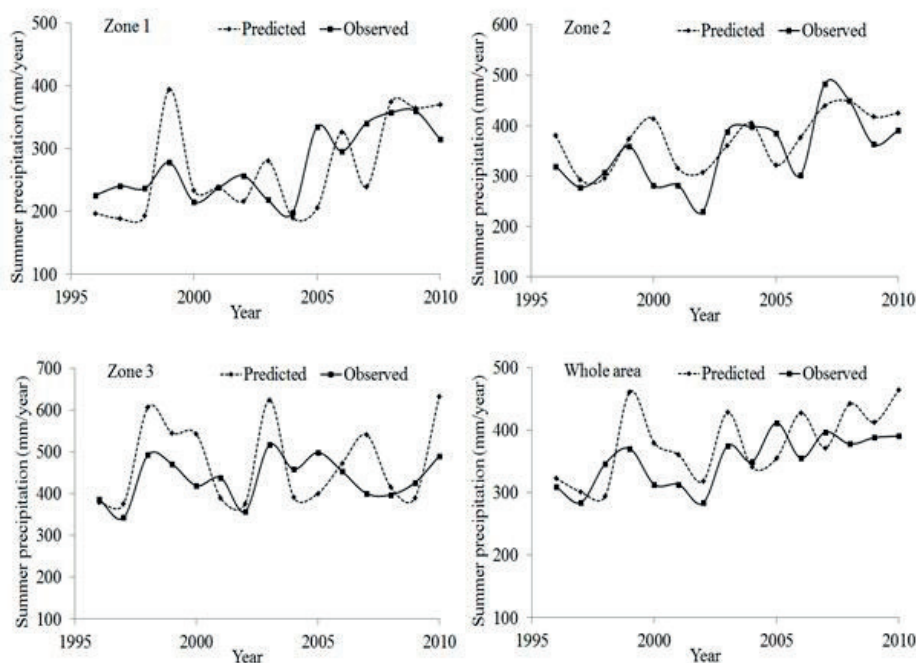
Fig. 4.18 The observed and predicted summer precipitation at the training period for different zones and the whole area

Table 4.11 ANN results for the three different zones

Period	Zone 1	Zone 2	Zone 3	Whole area
Training	0.90	0.82	0.97	0.86
Testing	0.60	0.68	0.62	0.61

4.4.2 Rainfall-runoff simulation using the Xinanjiang model

Interannual variability in streamflow mainly reflects catchment response to precipitation variability and is an important aspect of the hydrological regime for a catchment. Figure 4.19 shows the monthly precipitation and runoff depth in the source region of the Yellow River. It is seen that precipitation in the summer monsoon period (June-September) accounts for about 72% of the annual total. The monthly runoff depth shows dual peaks in July and September. Calibration and validation of the Xinanjiang model for the source region of the Yellow River were carried out using daily rainfall-runoff data. The Thiessen polygon method was used to calculate the daily mean areal precipitation and temperature over the experimental area. The daily discharge at Tangnaihai station was used to evaluate the model results since Tangnaihai station is the outlet of the source region of the Yellow River. The data from 1961 to 1995 were used for calibrating the model and the data from 1996 to 2009 was used for validation. Table 4.12 shows the results of the calibrated model parameters. According to the table all parameter values are in a reasonable range.
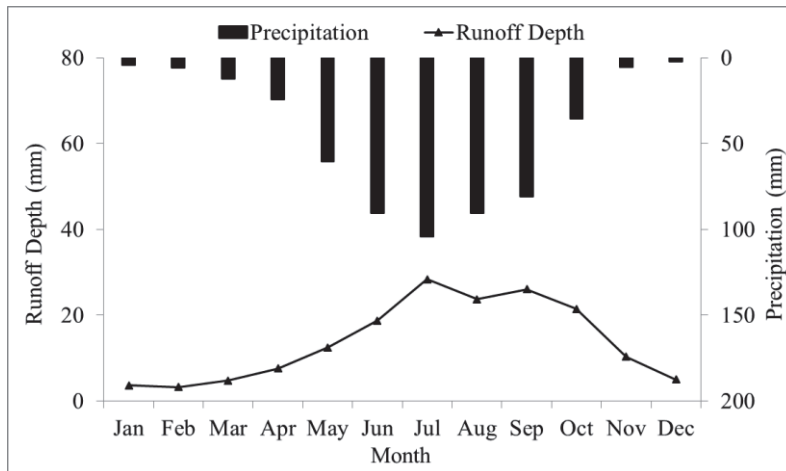
Fig. 4.19 Monthly precipitation and runoff depth in the source region of the Yellow River from 1961 to 2009

Figure 4.20 and 4.21 show the observed and simulated discharge for the catchment during calibration and validation period, respectively. It is seen that the Pearson correlation

coefficient for calibration period is 0.87 and 0.85 for validation period. Consequently, in general, the Xinanjiang model simulates the daily runoff series well.

Table 4.12 Calibrated model parameters.

Parameter	K	SM	CS	CI	CG	KG	KI	B	C	EX	IM	L	UM	LM	WM
Value	0.48	193	0.79	0.90	0.99	0.13	0.23	0.5	0.46	1.25	0.01	1	40	100	220
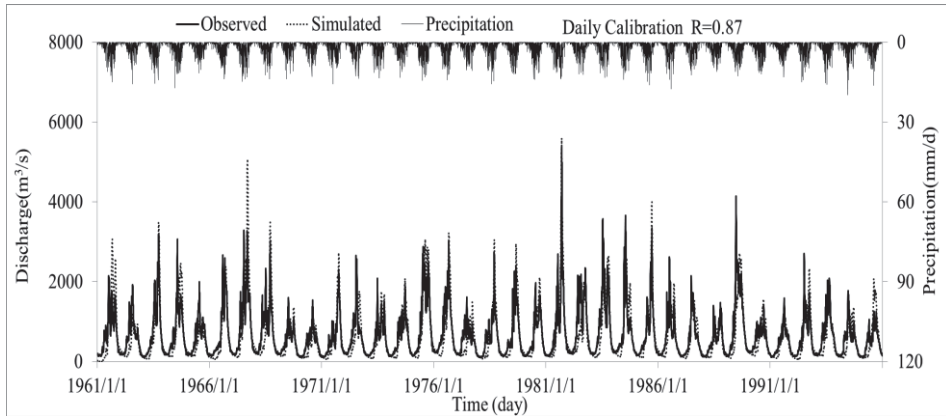
Fig. 4.20 Observed and simulated discharge for the source region of the Yellow River during calibration period.
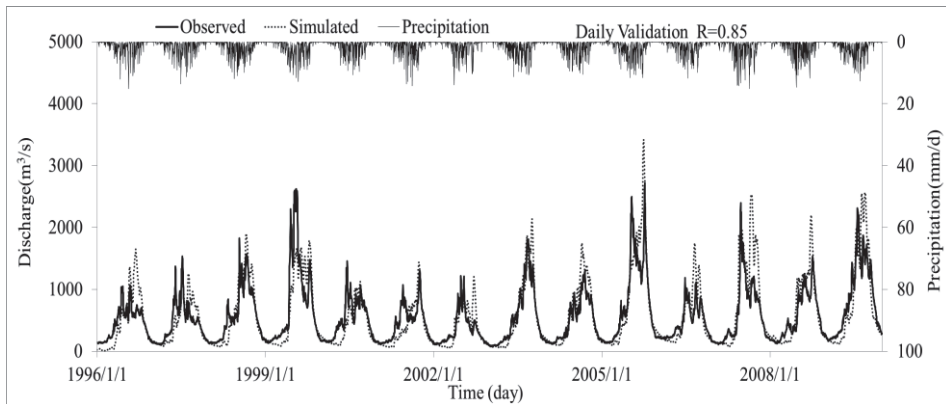
Fig. 4.21 Observed and simulated discharge for the source region of the Yellow River during the validation period.

5. CONCLUSIONS AND FUTURE STUDY

5.1 Conclusions

This study improved the physical understanding of hydroclimatic change in the source region of the Yellow River from the impacts of global sea surface temperature and teleconnection patterns, and promoted the application of hydrological modelling and forecasting techniques for water resources management. The trend and periodicity for temperature, precipitation, and streamflow from the early 1960s to 2010 for the Yellow River source region were investigated in **Paper I**. The analysis revealed a statistically significant increase in temperature for 9 out of 10 investigated stations. The temperature increased 1.5°C during the last 50-year period and had an accelerated increasing trend during last decade in the source region of the Yellow River. For precipitation the trend is less obvious. The mean annual precipitation decrease was about 30 mm over the entire 50-year period. In total 3 stations out of 10 displayed a statistically significant decreasing trend and one displayed increasing trend. The precipitation stations with significantly decreasing trends are all confined to the north-eastern parts of the catchment (Tongde, Zeku, and Maqu) and Maduo with increasing trend is located in the north-western part of the catchment. Thus, the varying trends depend on spatial location. The major part of annual rainfall comes from the monsoon, and the change in monsoon climate is likely to greatly affect the annual precipitation amount. There was a statistically significant decreasing trend for three out of four runoff stations during the period 1960-2009. The decadal mean discharge at Tangnaihai hydrologic station decreased significantly by about 28% from 1980s to 2000s. Significant change points were detected in 1998 for temperature and in 1990 for streamflow indicating a new hydrometeorological regime. The mean annual temperature was -0.58°C during 1961-1998, however, it increased to 0.43°C during 1999-2010. The mean annual runoff depth was 179.2mm during 1960-1990, and it decreased to 143.9mm during 1991-2009. Based on the streamflow change point analysis, seasonal analysis shows that the decreasing precipitation in the summer monsoon period is responsible for the annual precipitation decrease. Temperature increase is rather even throughout the year. The runoff depth decreased by 0.74 mm/year as an average for the entire study area. This change will have essential impact on the reservoir operation in the middle and down-stream areas of the Yellow River.

Wavelet analysis was used to identify and describe periodicity of runoff and hydro-climatic variables, and it gives us an insight in frequency and severity of drought and connections to the climate system. A statistically significant 2 to 4-year periodicity for mean areal precipitation and temperature could be seen during different periods over the area. An intense 8-year statistically significant periodicity for streamflow was revealed for the main discharge stations between the end of the 1960s to the beginning of the 1990s, and significant

change point in 1990 corroborated the time scale of strong 8-year periodicity. The annual periodicity of streamflow is partly overlapped by the statistically significant precipitation periodicity. Hydrological frequency analysis is examined to determine the magnitudes of mean annual precipitation and discharge corresponding to a given frequency or recurrence interval. The periodicity analysis examined the dynamical link between the streamflows and the climate variability in the source region of the Yellow River. Hydro-climatic trends and linkages at each sub-basin were investigated to further improve the understanding of observed streamflow changes. Precipitation in the Huangheyan and Jimai sub-basins showed increasing trend having an opposite trend with the whole basin. The significance of the correlations indicates that the streamflow is much more sensitive to precipitation and that the dependence increases from upstream to downstream. Both the increasing temperature and the decreasing precipitation are reasons for decrease in natural streamflow. The hydroclimatic change in the study area will have significant effects on the downstream water availability in the Yellow River.

The source region of the Yellow River was divided into three homogeneous zones based on precipitation variability, and its summer precipitation trends was explored (**Paper II**). The relationships between summer precipitation in the source region of the Yellow River and global SST and SOI were investigated in **Paper II**. The northwest part (zone 1) exhibited a non-significantly increasing trend during 1961 to 2010. The middle and southeast parts (zone 2 and 3) that receive the most precipitation displayed a statistically significant decreasing trend over the same period. This is due to a weakening of the summer monsoon and decreasing rainfall amounts during the summer months. The summer precipitation in the whole area shows statistically significant negative correlations with the central Pacific SST for 0-4 month lags and with the southern Indian and Atlantic Ocean SST for 5-8 month lags. The predominant negative correlations mean that lower SST in equatorial Pacific areas corresponding to La Nina coincides with more summer rainfall over the source region of the Yellow River. The summer precipitation in zone 1 is correlated with SST in mainly central and partly eastern Pacific. However, a small area with positive correlations appears in the central Pacific Ocean for a lag up to about 8 months. This explains that the precipitation in zone 1 had a non-significantly increasing trend during the last 50-year period. Zone 2 has similar influencing SST areas with the whole area but with a clearer signal. The precipitation in zone 3 is influenced by the central Pacific but also affected by southern Atlantic Oceans and western Pacific. SOI had significant positive correlations mainly for 0-2 month lag with summer precipitation in the source region of the Yellow River.

PCA and SVD were used to find relationships between the precipitation in the source region of the Yellow River and global teleconnecion patterns using climate indices in **Paper III**. The summer precipitation was predicted based on the revealed relationships using an ANN. The precipitation trend varies at different stations due to the temporal and spatial variation. The PCA analysis revealed relationships between some of these climate indices and precipitation. The first two modes of PCA were analysed since they can readily be associated to teleconnection patterns. The results showed that precipitation is positively

related to the North Atlantic Oscillation, West Pacific and El Nino Southern Oscillation and negatively related to the Polar Eurasian teleconnection. SVD was applied to the cross-covariance matrix between precipitation and climate indices. The results of SVD confirmed the relationship from the PCA. An ANN model was used to predict the summer precipitation in the source region of the Yellow River. The Pearson correlation coefficients between the predicted summer precipitation and observed summer precipitation are generally larger than 0.6. Thus, it is shown that significantly correlated climate indices can be used to predict the summer precipitation.

A partly modified Xinanjiang model was applied to the source region of the Yellow River for daily rainfall-runoff simulation in **Paper IV**. The magnitude and variation of evaporative losses is required for efficient water resources management. It is, however, difficult to select the most appropriate evaporation calculation method due to the wide range of data types needed in the various equations. The Blaney–Criddle method was chosen to calculate the potential evapotranspiration for the model input due to data scarcity of this area. The process of model calibration is normally performed either manually or by using computer-based automatic procedures. The process of manual calibration is generally tedious and time consuming. Hence, the Monte Carlo method was used for automatic calibration. The good fit showed that the Xinanjiang model can be used for daily runoff simulation and flood forecasting in the source region of the Yellow River.

This study improves the understanding of dynamics of hydrological cycle and leads to better hydrologic system modelling. The revealed results could be useful in improving steamflow forecast and operating the reservoirs for power generation, water supply and flood control in the middle and downstream of the Yellow River, and hence improving water resources management.

5.2 Future study

Global atmospheric general circulation models (GCMs) outputs are often used to investigate hydrological impacts of climate change. While GCMs demonstrate significant skill at the continental and hemispheric spatial scales and incorporate a large proportion of the complexity of the global system, however, the spatial resolution of GCMs is too coarse to represent regional climate variations at the scales required for water avaiability assessemtns, and they are inherently unable to represent local subgrid-scale features and dynamics (Wigley et al. 1990, Wilby et al. 2000, Sperna Weiland et al. 2010, Xu 1999). When considering the impacts of global climate change the focus is primarily on societal responses to the local and regional consequences of large- scale changes. The conflict between GCM performance at regional spatial scales and the needs of regional-scale impact assessment is largely related to model resolution in such a way that, while GCM accuracy decreases at increasingly finer spatial scales, the needs of impacts researchers conversely increase with higher resolution (Schulze 1997, Dibike and Coulibaly 2005) . Hence, statistical

downscaling approaches are necessary to convert the GCMs output into local meteorological variables required for reliable hydrological modelling.

Changes in global climate will have significant impact on local and regional hydrological regimes, which will in turn affect ecological, social and economic systems (Dibike and Coulibaly 2005).To further evaluate the streamflow variability in the source region of the Yellow River, future studies could focus on downscaling of large scale atmospheric variables from GCMs projections to climate variables at regional and local scale, which could be used as input for the Xinanjiang model in order to predict the future streamflow. The application of hydrological model and downscaling GCMs projections are essential to assess the potential effects of climate change on regional water resources.

REFERENCES

Barnston, A. G. and Livezey, R. E. 1987. Classification, Seasonality and Persistence of Low-Frequency Atmospheric Circulation Patterns. *Monthly Weather Review,* 115(6), 1083-1126.

Bonell, M. and Sumner, G. 1992. Autumn and Winter Daily Precipitation Areas in Wales, 1982-1983 to 1986-1987. *International Journal of Climatology,* 12(1), 77-102.

Bretherton, C. S., Smith, C. and Wallace, J. M. 1992. An Intercomparison of Methods for Finding Coupled Patterns in Climate Data. *Journal of Climate,* 5(6), 541-560.

Bueh, C. and Nakamura, H. 2007. Scandinavian pattern and its climatic impact. *Quarterly Journal of the Royal Meteorological Society,* 133(629), 2117-2131.

Burn, D. H. and Elnur, M. A. H. 2002. Detection of hydrologic trends and variability. *Journal of Hydrology,* 255(1-4), 107-122.

Cheng, C. T.*, et al.* 2006. Using genetic algorithm and TOPSIS for Xinanjiang model calibration with a single procedure. *Journal of Hydrology,* 316(1-4), 129-140.

Chiew, F. H. S.*, et al.* 1998. El Nino Southern Oscillation and Australian rainfall, streamflow and drought: Links and potential for forecasting. *Journal of Hydrology,* 204(1-4), 138-149.

Choi, K.-S. and Moon, I.-J. 2012. Influence of the Western Pacific teleconnection pattern on Western North Pacific tropical cyclone activity. *Dynamics of Atmospheres and Oceans,* 57(0), 1-16.

Collins, K., Hunt, W. and Hathaway, J. 2008. Hydrologic Comparison of Four Types of Permeable Pavement and Standard Asphalt in Eastern North Carolina. *Journal of Hydrologic Engineering,* 13(12), 1146-1157.

Costa, J. E. 1978. Holocene Stratigraphy in Flood Frequency-Analysis. *Water Resources Research,* 14(4), 626-632.

Coulibaly, P. and Burn, D. H. 2004. Wavelet analysis of variability in annual Canadian streamflows. *Water Resources Research,* 40(3).

CPC 2008. Northern Hemisphere Teleconnection Patterns. *http://www.cpc.ncep.noaa.gov/data/teledoc/teleintro.shtml*.

Cuo, L.*, et al.* 2012. Climate Change on the Northern Tibetan Plateau during 1957–2009: Spatial Patterns and Possible Mechanisms. *Journal of Climate,* 26(1), 85-109.

Cuo, L.*, et al.* 2013. Climate change on the northern Tibetan Plateau during 1957-2009: Spatial patterns and possible mechanisms. *Journal of Climate,* 26(1), 85-109.

Dibike, Y. B. and Coulibaly, P. 2005. Hydrologic impact of climate change in the Saguenay watershed: comparison of downscaling methods and hydrologic models. *Journal of Hydrology,* 307(1–4), 145-163.

Ding, Y. H. and Chan, J. C. L. 2005. The East Asian summer monsoon: an overview. *Meteorology and Atmospheric Physics,* 89(1-4), 117-142.

Fan, F. X., Mann, M. E. and Ammann, C. M. 2009. Understanding Changes in the Asian Summer Monsoon over the Past Millennium: Insights from a Long-Term Coupled Model Simulation. *Journal of Climate,* 22(7), 1736-1748.

Feng, J.*, et al.* 2011. Different impacts of El Nino and El Nino Modoki on China rainfall in the decaying phases. *International Journal of Climatology,* 31(14), 2091-2101.

Feng, J., Yu, L. and Hu, D. 2013. Influence of Indian Ocean subtropical dipole on spring rainfall over China. *International Journal of Climatology*, n/a-n/a.

Fischer, T.*, et al.* 2012. Change-points in climate extremes in the Zhujiang River Basin, South China, 1961–2007. *Climatic Change,* 110(3-4), 783-799.

Fovell, R. G. and Fovell, M.-Y. C. 1993. Climate Zones of the Conterminous United States Defined Using Cluster Analysis. *Journal of Climate,* 6(11), 2103-2135.

Fu, G.*, et al.* 2013. Temporal variation of extreme rainfall events in China, 1961–2009. *Journal of Hydrology,* 487(0), 48-59.

Giordano, M.*, et al.*, 2004. *Water management in the Yellow River Basin: background, current critical issues and future research needs.* IWMI.

Gong, X. F. and Richman, M. B. 1995. On the Application of Cluster-Analysis to Growing-Season Precipitation Data in North-America East of the Rockies. *Journal of Climate,* 8(4), 897-931.

Griffis, V. and Stedinger, J. 2007. Log-Pearson Type 3 Distribution and Its Application in Flood Frequency Analysis. I: Distribution Characteristics. *Journal of Hydrologic Engineering,* 12(5), 482-491.

Hartmann, H., Becker, S. and King, L. 2008. Predicting summer rainfall in the Yangtze River basin with neural networks. *International Journal of Climatology,* 28(7), 925-936.

Hu, Y. R.*, et al.* 2011. Streamflow trends and climate linkages in the source region of the Yellow River, China. *Hydrological Processes,* 25(22), 3399-3411.

Hu, Z. Z. 1997. Interdecadal variability of summer climate over East Asia and its association with 500 hPa height and global sea surface temperature. *Journal of Geophysical Research-Atmospheres,* 102(D16), 19403-19412.

Hurrell, J. W. 1995. Decadal Trends in the North-Atlantic Oscillation - Regional Temperatures and Precipitation. *Science,* 269(5224), 676-679.

Immerzeel, W. W., van Beek, L. P. H. and Bierkens, M. F. P. 2010. Climate Change Will Affect the Asian Water Towers. *Science,* 328(5984), 1382-1385.

IPCC 2007. Climate Change 2007: Synthesis Report.

IPCC, 2013. *Climate Change 2013: The Physical Science Basis.* IPCC.

Jayawardena, A. W. and Zhou, M. C. 2000. A modified spatial soil moisture storage capacity distribution curve for the Xinanjiang model. *Journal of Hydrology,* 227(1-4), 93-113.

Jiang, P.*, et al.* 2013. How well do the GCMs/RCMs capture the multi-scale temporal variability of precipitation in the Southwestern United States? *Journal of Hydrology,* 479, 75-85.

Kendall, M. G., 1975. *Rank Correlation Measures.* London: Charles Griffin.

Kingston, D. G., *et al.* 2011. Regional classification, variability, and trends of northern North Atlantic river flow. *Hydrological Processes,* 25(7), 1021-1033.

Kingston, D. G., *et al.* 2009. Uncertainty in the estimation of potential evapotranspiration under climate change. *Geophysical Research Letters,* 36(20), L20403.

Kodera, K. 2004. Solar influence on the Indian Ocean Monsoon through dynamical processes. *Geophysical Research Letters,* 31(24), L24209.

Labat, D., Ababou, R. and Mangin, A. 2000. Rainfall-runoff relations for karstic springs. Part II: continuous wavelet and discrete orthogonal multiresolution. *Journal of Hydrology,* 238(3-4), 149-178.

Lan, Y. C., *et al.* 2010. Response of runoff in the source region of the Yellow River to climate warming. *Quaternary International,* 226(1-2), 60-65.

Li, H., *et al.* 2010. Responses of East Asian summer monsoon to historical SST and atmospheric forcing during 1950–2000. *Climate Dynamics,* 34(4), 501-514.

Liang, S., *et al.* 2010. Can climate change cause the Yellow River to dry up? *Water Resources Research,* 46(2), n/a-n/a.

Lin, X. and Yu, S. 1993. El Nino and rainfall during the flood season(June-August) in China. *Acta Meteorologica Sinica,* 51, 434-441.

Lin, Z. 2014. Intercomparison of the impacts of four summer teleconnections over Eurasia on East Asian rainfall. *Advances in Atmospheric Sciences,* 31(6), 1366-1376.

Liu, C. and Xia, J. 2004. Water problems and hydrological research in the Yellow River and the Huai and Hai River basins of China. *Hydrological Processes,* 18(12), 2197-2210.

Liu, F., *et al.* 2012. Spatial and temporal variability of water discharge in the Yellow River Basin over the past 60 years. *Journal of Geographical Sciences,* 22(6), 1013-1033.

Liu, H., *et al.* 2015. Impact of the North Atlantic Oscillation on the Dipole Oscillation of summer precipitation over the central and eastern Tibetan Plateau. *International Journal of Climatology*, n/a-n/a.

Lloyd-Hughes, B. and Saunders, M. A. 2002. Seasonal prediction of European spring precipitation from El Niño–Southern Oscillation and Local sea-surface temperatures. *International Journal of Climatology,* 22(1), 1-14.

Lorenzo, M. N., Taboada, J. J. and Gimeno, L. 2008. Links between circulation weather types and teleconnection patterns and their influence on precipitation patterns in Galicia (NW Spain). *International Journal of Climatology,* 28(11), 1493-1505.

Mann, H. B. 1945. Nonparametric Tests Against Trend. *Econometrica,* 13(3), 245-259.

Mavromatis, T. and Stathis, D. 2011. Response of the water balance in Greece to temperature and precipitation trends. *Theoretical and Applied Climatology,* 104(1-2), 13-24.

Milly, P. C. D., Dunne, K. A. and Vecchia, A. V. 2005. Global pattern of trends in streamflow and water availability in a changing climate. *Nature,* 438(7066), 347-350.

Modarres, R. and Ouarda, T. B. M. J. 2013. Modeling rainfall–runoff relationship using multivariate GARCH model. *Journal of Hydrology,* 499(0), 1-18.

Parajka, J., *et al.* 2010. Seasonal characteristics of flood regimes across the Alpine–Carpathian range. *Journal of Hydrology,* 394(1–2), 78-89.

Qian, W., Kang, H. S. and Lee, D. K. 2002. Distribution of seasonal rainfall in the East Asian monsoon region. *Theoretical and Applied Climatology,* 73(3-4), 151-168.

Rana, A., *et al.* 2012. Trend analysis for rainfall in Delhi and Mumbai, India. *Climate Dynamics,* 38(1-2), 45-56.

Rayner, N. A., *et al.* 2003. Global analyses of sea surface temperature, sea ice, and night marine air temperature since the late nineteenth century. *Journal of Geophysical Research: Atmospheres,* 108(D14), 4407.

Redmond, K. T. and Koch, R. W. 1991. Surface Climate and Streamflow Variability in the Western United-States and Their Relationship to Large-Scale Circulation Indexes. *Water Resources Research,* 27(9), 2381-2399.

Sahai, A. K., *et al.* 2003. Teleconnections in recent time and prediction of Indian summer monsoon rainfall. *Meteorology and Atmospheric Physics,* 84(3-4), 217-227.

Saji, N. H., *et al.* 1999. A dipole mode in the tropical Indian Ocean. *Nature,* 401(6751), 360-363.

Schulze, R. E. 1997. Impacts of global climate change in a hydrologically vulnerable region: Challenges to South African hydrologists. *Progress in Physical Geography,* 21(1), 113-136.

SCO 2015. Global Patterns. *http://www.nc-climate.ncsu.edu/climate/patterns/PDO.html*.

Solomon, S., Change, I. P. o. C. and I., I. P. o. C. C. W. G., 2007. *Climate Change 2007 - The Physical Science Basis: Working Group I Contribution to the Fourth Assessment Report of the IPCC.* Cambridge University Press.

Sood, A. and Smakhtin, V. 2014. Global hydrological models: a review. *Hydrological Sciences Journal,* 60(4), 549-565.

Sperna Weiland, F. C., *et al.* 2012. Selecting the optimal method to calculate daily global reference potential evaporation from CFSR reanalysis data for application in a hydrological model study. *Hydrol. Earth Syst. Sci.,* 16(3), 983-1000.

Sperna Weiland, F. C., *et al.* 2010. The ability of a GCM-forced hydrological model to reproduce global discharge variability. *Hydrol. Earth Syst. Sci.,* 14(8), 1595-1621.

Tang, Q. H., *et al.* 2008. Hydrological cycles change in the Yellow River basin during the last half of the twentieth century. *Journal of Climate,* 21(8), 1790-1806.

Taylor, W. A., 2000. *Change-Point Analysis: A powerful new tool for detecting changes* [online]. Available from: http: //www.variation.com/cpa/tech/changepoint.html.

Tootle, G. A. and Piechota, T. C. 2006. Relationships between Pacific and Atlantic ocean sea surface temperatures and US streamflow variability. *Water Resources Research,* 42(7).

Torrence, C. and Compo, G. P. 1998. A practical guide to wavelet analysis. *Bulletin of the American Meteorological Society,* 79(1), 61-78.

Torrence, C. and Webster, P. J. 1999. Interdecadal changes in the ENSO-monsoon system. *Journal of Climate,* 12(8), 2679-2690.

Uvo, C. B. 2003. Analysis and regionalization of northern european winter precipitation based on its relationship with the North Atlantic oscillation. *International Journal of Climatology,* 23(10), 1185-1194.

Uvo, C. B.*, et al.* 1998. The relationships between tropical Pacific and Atlantic SST and northeast Brazil monthly precipitation. *Journal of Climate,* 11(4), 551-562.

Uvo, C. B., Tolle, U. and Berndtsson, R. 2000. Forecasting discharge in Amazonia using artificial neural networks. *International Journal of Climatology,* 20(12), 1495-1507.

Vogel, R. and Wilson, I. 1996. Probability Distribution of Annual Maximum, Mean, and Minimum Streamflows in the United States. *Journal of Hydrologic Engineering,* 1(2), 69-76.

Wallace, J. M., Smith, C. and Bretherton, C. S. 1992. Singular Value Decomposition of Wintertime Sea-Surface Temperature and 500-Mb Height Anomalies. *Journal of Climate,* 5(6), 561-576.

Wang, H. J.*, et al.* 2006. Interannual and seasonal variation of the Huanghe (Yellow River) water discharge over the past 50 years: Connections to impacts from ENSO events and dams. *Global and Planetary Change,* 50(3-4), 212-225.

Washington, R.*, et al.* 2000. Northern Hemisphere teleconnection indices and the mass balance of Svalbard glaciers. *International Journal of Climatology,* 20(5), 473-487.

Webster, P. J.*, et al.* 1998. Monsoons: Processes, predictability, and the prospects for prediction. *Journal of Geophysical Research: Oceans,* 103(C7), 14451-14510.

Weng, H. Y., Lau, K. M. and Xue, Y. K. 1999. Multi-scale summer rainfall variability over China and its long-term link to global sea surface temperature variability. *Journal of the Meteorological Society of Japan,* 77(4), 845-857.

Westmacott, J. R. and Burn, D. H. 1997. Climate change effects on the hydrologic regime within the Churchill-Nelson River Basin. *Journal of Hydrology,* 202(1-4), 263-279.

Wigley, T. M. L.*, et al.* 1990. Obtaining sub-grid-scale information from coarse-resolution general circulation model output. *Journal of Geophysical Research: Atmospheres,* 95(D2), 1943-1953.

Wilby, R. L.*, et al.* 2000. Hydrological responses to dynamically and statistically downscaled climate model output. *Geophysical Research Letters,* 27(8), 1199-1202.

Wilks, D. S., 2011. *Statistical methods in the atmospheric sciences.* 3rd ed. Amsterdam ; Boston: Elsevier/Academic Press.

Xu, C.-y. 1999. From GCMs to river flow: a review of downscaling methods and hydrologic modelling approaches. *Progress in Physical Geography,* 23(2), 229-249.

Xu, C. Y. and Singh, V. P. 2002. Cross Comparison of Empirical Equations for Calculating Potential Evapotranspiration with Data from Switzerland. *Water Resources Management,* 16(3), 197-219.

Xu, K., Zhu, C. and He, J. 2013. Two types of El Niño-related Southern Oscillation and their different impacts on global land precipitation. *Advances in Atmospheric Sciences,* 30(6), 1743-1757.

Xu, Z. X.*, et al.* 2007. Long-term trend of precipitation in China and its association with the El Nino-southern oscillation. *Hydrological Processes,* 21(1), 61-71.

Yan, Y. Y. 2002. Temporal and Spatial Patterns of Seasonal Precipitation Variability in China, 1951-1999. *Physical Geography,* 23(4), 281-301.

Yao, C.*, et al.* 2014. Improving the flood prediction capability of the Xinanjiang model in ungauged nested catchments by coupling it with the geomorphologic instantaneous unit hydrograph. *Journal of Hydrology,* 517, 1035-1048.

Yasuda, H.*, et al.* 2009. Prediction of Chinese Loess Plateau summer rainfall using Pacific Ocean spring sea surface temperature. *Hydrological Processes,* 23(5), 719-729.

Yihui, D. 1994. Monsoons over China. *Advances in Atmospheric Sciences,* 11(2), 252-252.

Yuan, F.*, et al.* 2015a. Hydro Climatic Trend and Periodicity for the Source Region of the Yellow River. *Journal of Hydrologic Engineering,* 0(0), 05015003.

Yuan, F.*, et al.* 2015b. Regional Sea Surface Temperatures Explain Spatial and Temporal Variation of Summer Precipitation in the Source Region of the Yellow River. *Hydrological Sciences Journal*.

Zhang, J.*, et al.* 2013. Decadal variability of droughts and floods in the Yellow River basin during the last five centuries and relations with the North Atlantic SST. *International Journal of Climatology,* 33(15), 3217-3228.

Zhao, R. J. 1992. The Xinanjiang Model Applied in China. *Journal of Hydrology,* 135(1-4), 371-381.

Zheng, H. X.*, et al.* 2007. Changes in stream flow regime in headwater catchments of the Yellow River basin since the 1950s. *Hydrological Processes,* 21(7), 886-893.

Zheng, H. X.*, et al.* 2009. Responses of streamflow to climate and land surface change in the headwaters of the Yellow River Basin. *Water Resources Research,* 45.

Zhou, H.*, et al.* 2005. Alpine grassland degradation and its control in the source region of the Yangtze and Yellow Rivers, China. *Grassland Science,* 51(3), 191-203.

Zhou, L.-T.*, et al.* 2010. Influence of South China Sea SST and the ENSO on winter rainfall over South China. *Advances in Atmospheric Sciences,* 27(4), 832-844.

Paper I

Case Study

Hydro Climatic Trend and Periodicity for the Source Region of the Yellow River

Feifei Yuan[1]; Ronny Berndtsson[2]; Linus Zhang[3]; Cintia Bertacchi Uvo[4]; Zhenchun Hao[5]; Xinping Wang[6]; and Hiroshi Yasuda[7]

Abstract: The hydrology of the Yellow River source region is expected to be affected by coming climate change. This will have repercussions for the 110 million basin inhabitants. Consequently, precipitation, temperature, and streamflow trends and periodicities during the last 50 years were investigated to identify significant changes in time and space over the study area. Results showed that mean annual temperature increased for all stations and it had an accelerated increasing trend during the last decade. Mean annual precipitation trends varied depending on the station; however, they were generally slightly decreasing. Annual streamflow decreased markedly, especially from the 1990s, but showed recovery during recent years. Statistically significant changes in trend occurred for temperature in 1998 and for streamflow in 1990. Based on the streamflow change point, seasonal analysis results showed that precipitation mainly decreased during the summer monsoon period (July–September) and temperature increased throughout the year. Corresponding to the weakened monsoon period the average runoff depth is decreasing by 0.74 mm/year over the whole area. Statistically significant 2- to 4-year periodicities for mean areal precipitation and temperature occurred over the area. For streamflow, an even stronger 8-year periodicity was revealed from the end of the 1960s to the beginning of the 1990s. Frequency analysis investigated the magnitudes of mean annual precipitation and discharge corresponding to a given frequency. Hydroclimatic trends and linkages at each subbasin were investigated to further improve the understanding of observed streamflow changes. The investigated results have important implications for future water availability in the Yellow River source region. **DOI: 10.1061/(ASCE)HE.1943-5584.0001182.** *© 2015 American Society of Civil Engineers.*

Author keywords: Climate change; Streamflow decrease; Yellow River source region.

Introduction

The Yellow River is of immense importance to China. It is 5,464 km long, has a basin area of 752,440 km^2, and is the main source of surface water in northwest and northern China (Tang et al. 2008a, b; Yang et al. 2008). The basin has more than 110 million inhabitants and 12.6 million ha cultivated land, representing approximately 8 and 13% of the national totals, respectively. The lower Yellow River has increasingly suffered from low-flow conditions and parts of the lower reaches have often been dry during the last 30 years. The situation has been exacerbated during recent

years (Liu and Zheng 2004; Sato et al. 2008; Tang et al. 2008a, b). The source region of the Yellow River contributes approximately 35% of the total water yield in the Yellow River basin (Lan et al. 2010). Consequently, it is an extremely important area in terms of water resources affecting agricultural productivity and municipal and industrial water supply for the whole basin.

Climate change will have major impacts on regional water resources (Yang et al. 2010). Many studies have shown that climate change has a strong impact on basin water resources through changes in temperature and hydrologic variables (Westmacott and Burn 1997). For example, the frequency and severity of drought events could increase as a result of changes in both precipitation and temperature. Changes in the hydrologic regime that do occur are expected to be spatially and temporally variable (Burn and Elnur 2002). The interannual periodicity in local hydroclimatic variables (temperature, precipitation, and streamflow) could be a reflection for low-frequency climatic fluctuations. For this reason, it is important to understand the underlying dynamics of the hydrological cycle for investigated basins (Coulibaly and Burn 2004). Thus, it becomes increasingly important to study trend and periodicity in temperature and hydrologic variables, which are essential for efficient integrated water resources planning and management.

Several studies have dealt with the issue of change in hydroclimatic variables in the source region of the Yellow River. Hu et al. (2011) investigated streamflow trends and climate linkages in the source region of the Yellow River during the last 50 years (1959–2008). Liu and Zheng (2004) attempted to detect trends associated with hydrological cycle components in the Yellow River basin using data from 1952 to 1997. Zheng et al. (2007) investigated changes in the streamflow regime of four headwater catchments using data from 1956 to 2000. Tang et al. (2008a, b) presented an analysis of changes in the spatial patterns of climatic variables

[1]Ph.D. Candidate, Dept. of Water Resources Engineering, Lund Univ., P.O. Box 118, SE-221 00 Lund, Sweden (corresponding author). E-mail: Feifei.yuan@tvrl.lth.se; ffei.yuan@gmail.com

[2]Professor, Dept. of Water Resources Engineering and Center for Middle Eastern Studies, Lund Univ., P.O. Box 118, SE-221 00 Lund, Sweden.

[3]Associate Professor, Dept. of Water Resources Engineering, Lund Univ., P.O. Box 118, SE-221 00 Lund, Sweden.

[4]Professor, Dept. of Water Resources Engineering, Lund Univ., P.O. Box 118, SE-221 00 Lund, Sweden.

[5]Professor, State Key Laboratory of Hydrology, Water Resources and Hydraulic Engineering, Hohai Univ., Nanjing 210098, P.R. China.

[6]Professor, Shapotou Desert Research and Experiment Station, Cold and Arid Regions Environmental and Engineering Research Institute, Chinese Academy of Sciences, 320, Donggang West Rd., Lanzhou, Gansu 730000, P.R. China.

[7]Associate Professor, Arid Land Research Center, Tottori Univ., 1390 Hamasaka, Tottori 680-0001, Japan.

in the Yellow River basin from 1960 to 2000. Cong et al. (2009) used a distributed hydrological model to analyze hydrological trends in the Yellow River basin. Several of these studies have reported dwindling streamflow in the Yellow River during the latest years. Zhang et al. (2013) reported substantially decreased annual flow of the Yellow River during recent years. The source area of the Yellow River is little influenced by human activities. Thus, it is important to separate this part from other parts of the Yellow River because the source region can be seen as an indicator of main climatic effects. Most of the trend analyses from previous studies have used hydrological and meteorological data up to about 2000. There are, however, indications that the hydrological regime may have changed significantly during the last decadal period. This change has not yet been quantified and analyzed in detail in relation to results from previous studies. Consequently, this paper investigates the trend for temperature, precipitation, and streamflow from 1960 to 2010. Change-point analysis was applied to identify the potential significant hydroclimatic changes in recent years. Based on the change-point results, seasonal analysis was examined indicating a new possible hydrometeorological regime. The hydroclimatic periodicity was investigated by wavelet analysis giving an insight in periodicity and severity of drought and connections to the climate system. Besides, hydrological frequency analysis was examined to determine the magnitudes of mean annual precipitation and discharge corresponding to a given frequency or recurrence interval. This study also explored the hydroclimatic trends and linkages at each subbasin to further improve the understanding of observed streamflow changes. Based on these analyses the paper is closed with a discussion on practical applications of the results.

Experimental Area and Methods

Experimental Area and Data

The source region of the Yellow River is located on the northeast Qinghai-Tibet Plateau between 32°12′–35°48′N and 95°50′–103°28′ E and includes the area upstream of the Tangnaihai runoff observation station. The area is 12.2×10^4 km^2, occupying approximately 16% of the Yellow River Basin, and it has a great elevation change from 2,670 m in the east to 6,253 m in the west. Grassland covers 80% of the catchment and it includes typical alpine swamp, steppe, and shrub meadows. In recent years, the alpine grasslands in this area have suffered from severe degradation (Zhou et al. 2005). The grassland degradation is thought to be a joint effect of long-term overgrazing and climate warming. The area of lakes

and swamps is approximately 2,000 km^2. There is a permanent snowpack and glaciers in the southern Animaqing, Bayankala, and northern Qilian mountains. The area has a comparably low population density and a total of approximately half a million inhabitants. The area is therefore regarded as relatively unaffected by human activities (Hu et al. 2011; Zheng et al. 2009). Neither large irrigation projects nor large dams exist in the area even though the population increase of humans and domestic livestock is increasingly affecting the grass cover and soil erosion.

Climatologically the area belongs to the semihumid region of the Tibetan Plateau subfrigid zone and 75–90% of the annual precipitation in this area falls during the wet summer season (June–September) due to the southwest monsoon from the Bay of Bengal (Hu et al. 2011). Thus, the climate of the source region of the Yellow River is greatly influenced by the southwest monsoon and the East Asian summer monsoon (Ding and Chan 2005). The earliest onset of the East Asian summer monsoon occurs in the central and southern Indochina Peninsula. It displays a distinct stepwise northward and northeastward movement and then finally penetrates in to the upper Yellow River from the south of China (Ding and Chan 2005). The effects of atmospheric circulation are in general different for the upper and lower Yellow River. The monsoon rain belt in the upper part is caused by southeasterly flow, while the corresponding monsoon rain belt in the lower parts is influenced by southwesterly flow (Qian et al. 2002). This causes differences in spatial distribution of summer precipitation between the two parts of the Yellow River. The upper part of the Yellow River is characterized by low temperatures, sharp day–night temperature contrasts, long cold and short warm seasons, and intense sunlight (Liang et al. 2010). Annual average temperature varies between −4 and 2°C from southeast to northwest. The precipitation in this region is generally of low intensity (<50 mm/day), long duration (10–30 days), and covers a large area (>100,000 km^2) (Hu et al. 2011; Zheng et al. 2007). Snowfall is concentrated from November to March, when more than 78% of the total precipitation falls in the form of snow. However, the total amount of annual snowfall accounts for less than 10% of the annual precipitation (Hu et al. 2011). The potential evaporation is 1,300–1,400 mm/year (Liang et al. 2010).

Daily precipitation and temperature observations from 1961 to 2010 collected from 10 meteorological stations (Fig. 1)—Xinghai, Tongde, Zeku, Henan, Maduo, Dari, Jiuzhi, Maqu, Ruoergai, and Hongyuan—were obtained from the China Meteorological Administration. Daily streamflow data from 1960 to 2009 at four runoff observation stations, including Huangheyan, Jimai, Maqu, and Tangnaihai, were obtained from the Yellow River Conservancy
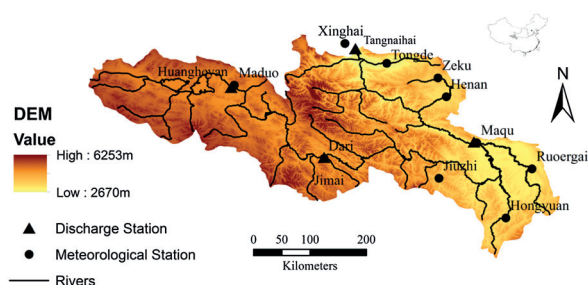

Fig. 1. Yellow River source region topography, river network, and hydroclimatic stations (data from Consortium for Spatial Information 2013)

Table 1. Observation Stations for Precipitation and Temperature

Station	Altitude (m)	Longitude (°E)	Latitude (°N)	Mean annual precipitation (mm/year)	Mean annual temperature (°C)	Minimum annual precipitation (mm/year)	Maximum annual precipitation (mm/year)	Minimum annual temperature (°C)	Maximum annual temperature (°C)
Xinghai	3,323	99.98	35.58	365.3	1.44	214.1	530.9	0.2	2.9
Tongde	3,289	100.39	35.16	411.2	0.67	199.0	598.7	−0.5	3.4
Zeku	3,663	101.28	35.02	418.1	−2.16	214.6	651.8	−3.7	2.7
Henan	3,500	101.36	34.44	562.9	−0.23	384.1	835.3	−1.7	1.0
Maduo	4,272	98.13	34.55	318.5	−3.63	184.0	485.6	−5.5	−2.0
Dari	3,967	99.65	33.75	551.8	−0.78	413.1	698.7	−2.2	0.8
Jiuzhi	3,629	101.48	33.43	744.7	0.71	562.6	1,030.8	−0.5	2.3
Maqu	3,471	102.08	34.00	589.2	1.58	448.4	924.7	0.5	3.4
Ruoergai	3,440	102.97	33.58	649.7	1.20	464.8	862.9	0.1	2.8
Hongyuan	3,492	102.55	32.80	747.1	1.52	508.1	996.3	0.5	2.8

Commission. Runoff data from 1968 to 1975 at the Huangheyan station were not available. The missing data were interpolated based on the linear regression with the Jimai station because the Jimai station has the highest correlation with the Huangheyan station. The precipitation and runoff data have previously been quality checked (Chen 1996). The shuttle radar topography mission (SRTM) 90-m digital elevation data were downloaded from the Consortium for Spatial Information (CGIAR-CSI). Tables 1 and 2 show a summary of these data.

Methods

Mann-Kendall trends in precipitation, temperature, and streamflow time series were examined by the nonparametric Mann-Kendall test. The Kendall statistic was originally devised as a nonparametric test for trend by Mann (1945). Later Kendall (1975) derived the exact distribution of the test statistic. The method has been widely used in hydroclimatic time series analysis for identifying trend (Burn and Elnur 2002; Rana et al. 2012; Westmacott and Burn 1997). The Mann-Kendall test is independent of the statistical distribution of the data. Statistical significance of the trend was evaluated at the 0.05 level of significance against the null hypothesis that there is no trend for the data series. A detailed procedure for this statistical test can be found in Burn and Elnur (2002).

Change-Point Analyzer was used to investigate the potential abrupt hydroclimatic changes in the source region of the Yellow River (Taylor 2000) and to detect the change points. Change-Point Analyzer is a software package for analyzing time-ordered data to determine whether a change has taken place, and it detects multiple changes and provides confidence levels for each change. It iteratively uses a combination of time-varying cumulative sum charts (cusums) and bootstrapping to detect changes (Taylor 2000). It has been widely used for detecting change points in hydroclimatic areas (Collins et al. 2008; Fischer et al. 2012; Mavromatis and Stathis 2011).

Wavelet Analysis

Wavelet analysis is a common tool for signal processing. It is an effective method to identify the dominant modes of periodicity by decomposing time series into time-frequency space

(Coulibaly and Burn 2004; Jiang et al. 2013). The wavelet power spectrum is defined as the absolute value squared by the wavelet transform and gives a measure of the time series variance at each scale and at each time and there is no need for a predetermined scale that might limit the frequency range (Coulibaly and Burn 2004; Torrence and Webster 1999). For a more detailed description of wavelet analysis in hydrology, see Torrence and Compo (1998). The method applied here was the Morlet wavelet, which consists of a complex exponential Gaussian modulation

$$\Psi_0(\eta) = \pi^{-1/4} e^{iw_0\eta} e^{-\eta^2/2} \tag{1}$$

where w_0 = nondimensional frequency, here taken to be 6. To reduce wraparound effects each time series was padded with zeros. The cone of influence is the region of the wavelet spectrum in which edge effects become important. The background spectrum was chosen as red noise, which means that power increases with decreasing frequency.

Frequency Analysis

Hydrological frequency analysis is examined to determine the magnitudes of mean annual precipitation and discharge corresponding to a given frequency or recurrence interval. The log-Pearson Type III distribution is a statistical technique for fitting frequency distribution data to predict the design flood that has been widely used in hydrology (Griffis and Stedinger 2007; Vogel and Wilson 1996). It is a three-parameter distribution; the parameters are the mean, standard deviation, and skew coefficient (Costa 1978). A detailed procedure for this statistical technique can be found in Griffis and Stedinger (2007).

Results

Annual Trend Analysis

Fig. 2 shows the spatial variation of mean annual precipitation over the Yellow River source region. The mean areal precipitation over the catchment is 515.1 mm/year. There is a strongly increasing gradient from the northwest parts with approximately

Table 2. Observation Stations for Streamflow

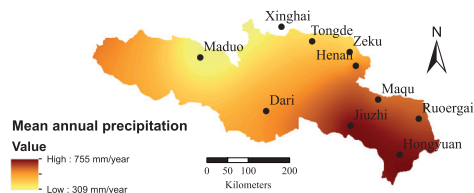| Station	Altitude (m)	Longitude (°E)	Latitude (°N)	Mean discharge (m³/s)	Minimum discharge (m³/s)	Maximum discharge (m³/s)	Drainage area (km²)
Huangheyan	4,221	98.17	34.88	23.4	0.6	78.2	20,930
Jimai	3,969	99.65	33.77	130.2	62.0	263.0	45,019
Maqu	3,471	102.08	33.97	456.3	228.3	707.0	86,048
Tangnaihai	2,546	100.15	35.50	641.1	335.4	1,040.0	121,972

Fig. 2. Spatial variation of mean annual precipitation over the Yellow River source region (data from Consortium for Spatial Information 2013)

309–755 mm/year in the southeast. The topographical gradient of rainfall and the annual rainfall variability are greatly influenced by the southeasterly summer monsoon flow. This makes annual precipitation amounts decline with altitude as a general pattern in the region from the southeast to the northwest as seen from Figs. 1 and 2. The Maduo station receives 319 mm annual mean precipitation only in spite of its high location (4,272 m). The reason is partly rain shadow effects due to the high mountain peaks in the central parts of the catchment and partly effects of the spatial extension of the summer monsoon.

Fig. 3 shows the mean areal precipitation and temperature depending on time for the study area. The Thiessen polygon method was used to calculate the mean areal precipitation and temperature over the experimental area. The area as a whole has a slight decreasing nonsignificant trend in precipitation and a significant increasing trend in temperature. The mean annual precipitation decrease is approximately 0.6 mm/year (30 mm for the entire 50-year period) and the mean annual temperature increase is approximately 0.03°C/year (1.5°C for the entire 50-year period). Both temperature and precipitation have displayed above-average annual values during the last 10-year period.

Fig. 4 shows linear trends for mean annual precipitation and temperature at each observation station. The trend is quantified in Table 3 and as noted 9 out of 10 stations show statistically significant increasing trend for temperature. For precipitation the trend is less clear. Seven precipitation stations display a decreasing trend while three show an increasing trend. All decreasing stations are located in the eastern and northeastern part of the Yellow River source area. Because this area is much affected by the summer monsoon it is rather clear that the declining rainfall is related to weakening of the monsoon rainfall.
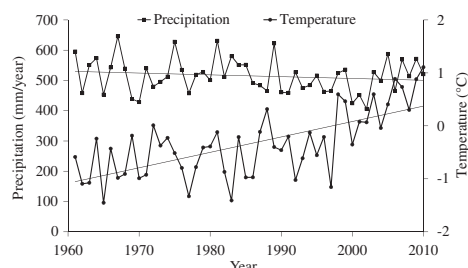

Fig. 3. Mean areal annual precipitation and temperature trend in the Yellow River source region

The linear trend results are corroborated by the Mann-Kendall test in Table 3. Standard deviation (SD) and coefficient of variation (COV) are calculated to examine the variation. The coefficient of variation for precipitation ranges from 0.13 to 0.27. It is seen that four stations display a statistically significant trend. The precipitation stations Tongde, Zeku, and Maqu exhibit a significantly decreasing trend at the 0.05 significance level, while the Maduo station shows an increasing trend at the 0.05 significance level. The precipitation stations with significantly decreasing trends are all confined to the northeastern parts of the catchment (Tongde, Zeku, and Maqu) and Maduo with an increasing trend is located in the northwestern part of the catchment. There is, thus, a geographical dependence for the trend and annual data.

Fig. 5 shows the corresponding streamflow at the four runoff stations during 1960–2009. When comparing decadal streamflow at the four investigated runoff stations, the last two decades' streamflow has been significantly lower than corresponding streamflow during 1960–1990 [Fig. 5(b)]. The decadal mean streamflow at the Tangnaihai station decreased by approximately 28% from 1980 to 2000s. Consequently, there is a clear decreasing trend for streamflow considering the entire 50-year investigated period (Table 4). According to Fig. 5(a), there is also a pronounced periodicity in annual streamflow that decreases towards the end of the 1990s. The streamflow showed an increasing trend during the last 10-year period. The decreasing linear trend is statistically significant for three of the four runoff stations as seen from Table 4. The coefficient of variation for the Huangheyan station is highest, followed in order by Jimai, Tangnaihai, and Maqu.

Seasonal Trend Analysis

Change-Point Analyzer was applied to annual precipitation, temperature, and streamflow data series to further explore the potential abrupt hydroclimatic change points in the source region of the Yellow River. The analysis results are summarized in Table 5. No change point was detected for precipitation. Temperature change occurred in 1998 with 99% confidence level, and streamflow change occurred in 1990 with 96% confidence level. The mean annual temperature was −0.58°C during 1961–1998, and it increased to 0.43°C during 1999–2010. The mean annual runoff depth was 179.2 mm during 1960–1990 and it decreased to 143.9 mm during 1991–2009. Hydrological systems act as spatial and temporal integrators of precipitation and temperature over certain watersheds and streamflow observations can serve as a pertinent index of interannual hydroclimatic variability at the regional scale, hence the two periods before and after 1990 were divided to further investigate the change.

The seasonal analysis corroborates the preceding annual trend and change-point analysis. Fig. 6 shows the monthly change for precipitation, temperature, and runoff by comparing the periods 1960–1990 and 1991–2010. As seen from the comparison in Fig. 6, temperature has increased rather evenly throughout the year and all months except for January. Regarding precipitation it is mainly the monsoon period (July–September) that has displayed a decrease. In general, the monsoon period (June–September) accounts for approximately 62% of the annual total precipitation. September is the month with largest relative decrease in precipitation. The streamflow displays the largest decrease from July to October as a result from decreasing monsoon rainfall, and there is also a general smaller decrease for the rest of the months.

The increasing temperature causes more glacier and snow melt, and it increases the proportion of snowmelt runoff to the total runoff. However, the clear decrease in streamflow as seen from Fig. 6 indicates that the melt water has only limited impact on the total
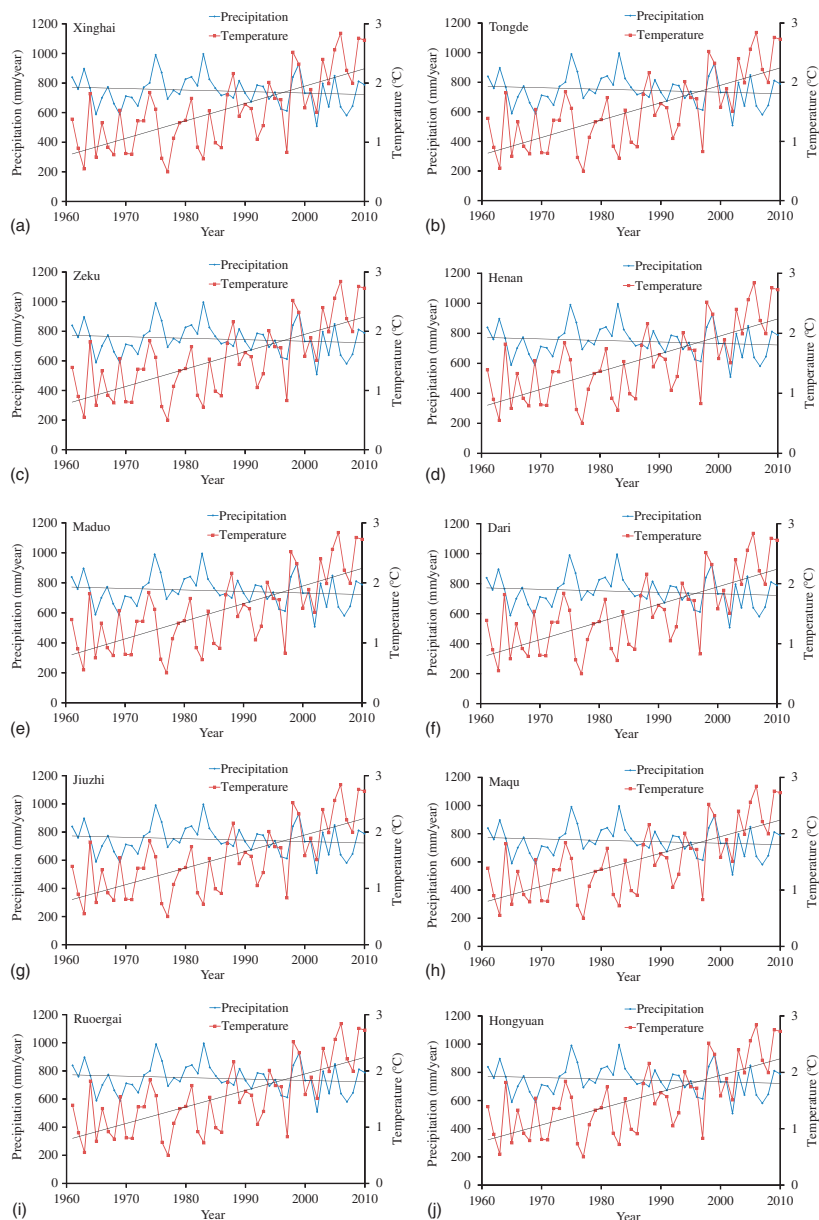
Fig. 4. Precipitation and temperature trends depending on station: (a) Xinghai; (b) Tongde; (c) Zeku; (d) Henan; (e) Maduo; (f) Dari; (g) Jiuzhi; (h) Maqu; (i) Ruoergai; (j) Hongyuan

Table 3. Precipitation and Temperature Linear Trends and Mann-Kendall Statistics (Z)

Station	Precipitation trend (mm/year)	Temperature trend (°C/year)	Precipitation standard deviation	Temperature standard deviation	Precipitation coefficient of variation	Precipitation Z	Precipitation P	Temperature Z	Temperature P
Xinghai	1.13	0.034	69.6	0.66	0.19	1.56	0.120	**5.68**	1.35×10^{-08}
Tongde	−1.74	0.037	88.4	0.78	0.21	**−1.99**	0.047	**5.17**	2.35×10^{-07}
Zeku	−3.28	0.018	114.9	1.00	0.27	**−2.94**	0.003	1.68	0.093
Henan	−0.04	0.015	93.8	0.88	0.16	−1.47	0.141	**2.53**	0.011
Maduo	1.32	0.039	65.1	0.89	0.20	**2.27**	0.023	**4.88**	1.08×10^{-06}
Dari	0.36	0.032	71.8	0.74	0.13	0.67	0.503	**4.90**	9.50×10^{-07}
Jiuzhi	−1.56	0.040	99.3	0.72	0.13	−1.44	0.150	**6.35**	2.17×10^{-10}
Maqu	−3.36	0.034	111.0	0.68	0.18	**−2.44**	0.015	**5.21**	1.88×10^{-07}
Ruoergai	−1.21	0.033	98.4	0.66	0.15	−1.49	0.137	**5.47**	4.48×10^{-08}
Hongyuan	−1.01	0.029	101.5	0.62	0.14	−0.75	0.452	**5.05**	4.36×10^{-07}

Note: Values in bold are statistically significant at the 0.05 level.

Fig. 5. (a) Annual and (b) decadal mean discharge at the four discharge stations

Table 4. Streamflow Linear Trends and Mann-Kendall Statistics (Z)

Station	Streamflow trend (m³/s/year)	Mann-Kendall Z	P	SD	COV
Huangheyan	−0.75	**−2.19**	0.028	20.5	0.96
Jimai	−0.18	−1.47	0.239	49.1	0.38
Maqu	−2.15	**−2.40**	0.017	115.2	0.25
Tangnaihai	−2.95	**−2.31**	0.021	169.8	0.26

Note: Values in bold are statistically significant at the 0.05 level.

Table 5. Results and Confidence Levels of Change Point Analysis

Hydroclimatic variables	Change point	Confidence (%)
Precipitation	None	—
Temperature	1998	99
Streamflow	1990	96

streamflow. The decreasing trend in monsoon precipitation is the major reason for the reduced streamflow in the 1990s and 2000s, but also increasing evapotranspiration due to increasing temperature for other parts of the year is a significant factor. Zheng et al. (2009) reported that the land use change played a more important role than the climate in reducing streamflow in the 1990s. Due to the complexity of temperature influence, topography, land use change, and precipitation variability, further investigations are necessary to gain a deeper understanding of the linkages among hydroclimatic variables and land use for the area.

Periodicity Analysis

To further investigate the observed annual periodicity in streamflow according to Fig. 5, a wavelet analysis was performed on annual

areal precipitation, temperature, and streamflow. The results are shown in Figs. 7 and 8. From Fig. 7 it can be seen that there are statistically significant 2- to 4-year periodicities, especially for precipitation in the beginning of the experimental period (1960–1980). For temperature there are significant 2- to 4-year periodicities during 1961–1970 and 1980–2010, and an intense 8-year periodicity was found during 1975–1990. The precipitation also showed an intense 8-year periodicity during 1965–1985. Dominant periodicities for the annual streamflow at each station are shown in Fig. 8. As seen from the figure there is a strong statistically significant 8-year periodicity for all stations from the ends of the 1960s to the beginning of the 1990s. The significant change point for streamflow in 1990 (Table 5) confirmed the time scale of strong 8-year periodicity. Less strong but still significant is also the 4-year periodicity for mainly Jimai, Maqu, and Tangnaihai stations. When comparing Figs. 7 and 8 it can be noted that the annual periodicity of precipitation and streamflow overlap, especially for the 8-year periodicity during the early part of the experimental period. However, the wavelet power spectrum of 8-year periodicity for the streamflow is much stronger than that for the precipitation and temperature during the same period.Frequency analysis for mean annual precipitation and discharge in the source region of the Yellow River were analyzed using log-Pearson Type III probability distribution as seen in Fig. 9. It is seen that log-Pearson Type III probability distribution is a suitable pattern due to the general good fitting. The probabilities for mean annual precipitation at 1, 5, 10, and 20% correspond to 670, 616, 590, and 561 mm,
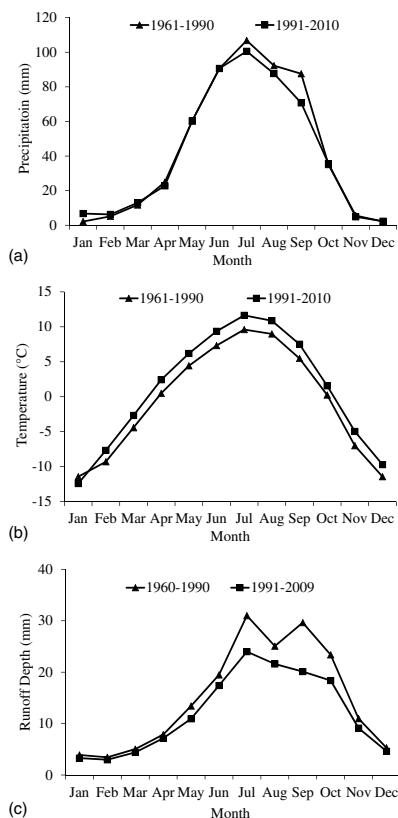
(a)

(b)

(c)

Fig. 6. Decadal change of monthly: (a) precipitation; (b) temperature; (c) runoff depth in the source region of the Yellow River

(a)

(b)

Fig. 7. Wavelet power spectrum for annual areal (a) precipitation and (b) temperature; power units are mm^2 and °C^2; the black line shows statistical significance at the 0.05 level

(a)

(b)

(c)

(d)

Fig. 8. Wavelet power spectrum of annual streamflow for each station; power unit is mm^2; the black line shows statistical significance at the 0.05 level: (a) Huangheyan station; (b) Jimai station; (c) Maqu station; (d) Tangnaihai station

respectively. The probabilities for mean annual discharge at 1, 5, 10, and 20% correspond to 1,250, 982, 872, and 763 m^3/s, respectively.

Water Balances

The streamflow in the Yellow River source region is greatly affected by the changing climate. Due to the vast area and spatial variation in the source region of the Yellow River, water balances were first analyzed at the subbasin level. Annual areal precipitation and temperature trend analysis for each subbasin is shown in Table 6. Temperature significantly increased corresponding to the station analysis, and precipitation in the Huangheyan and Jimai subbasins also showed increasing trend having an opposite trend with the whole basin. Correlations between annual streamflow at the four discharge stations and annual areal precipitation and temperature for each subbasin are shown in Table 7. Streamflow at all four hydrologic stations are positively correlated with precipitation and negatively correlated with temperature. The significance of the
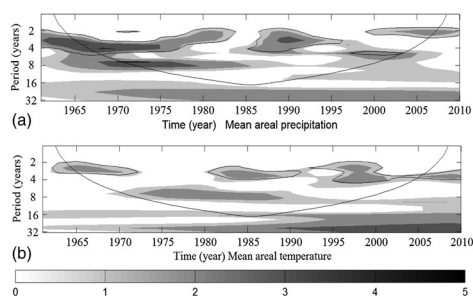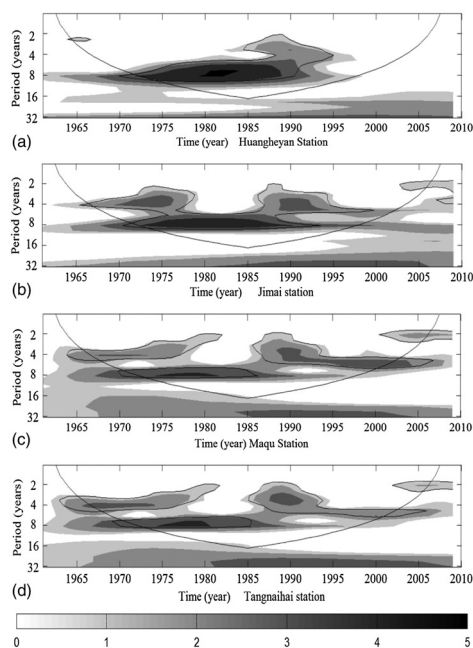
correlations indicates that the streamflow is much more sensitive to precipitation and that the dependence increases from upstream to downstream. Similarly, the highest correlation between temperature and streamflow is for the most upstream station (Huangheyan).
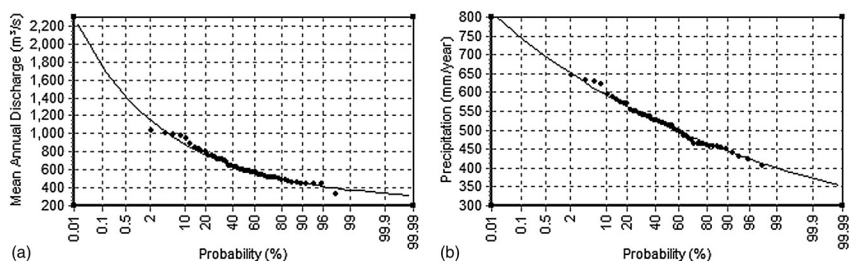
© ASCE

05015003-7

J. Hydrol. Eng.

Fig. 9. Frequency analysis for mean annual precipitation and discharge in the source region of the Yellow River

Table 6. Annual Areal Precipitation and Temperature for Each Subbasin's Mann-Kendall Statistics (Z)

Station	Huangheyan		Jimai		Maqu		Tangnaihai	
	Z	P	Z	P	Z	P	Z	P
Precipitation	**2.27**	0.023	1.34	0.182	−0.54	0.581	−0.97	0.332
Temperature	**4.88**	1.08×10^{-06}	**4.58**	4.71×10^{-06}	**5.20**	2.02×10^{-07}	**4.87**	1.13×10^{-06}

Note: Values in bold are statistically significant at the 0.05 level.

Table 7. Correlation Coefficients between Annual Streamflow and Annual Areal Precipitation and Temperature for Each Subbasin

Station	Huangheyan	Jimai	Maqu	Tangnaihai
Precipitation	**0.343**	**0.576**	**0.821**	**0.849**
Temperature	−0.286	−0.066	−0.178	−0.190

Note: Values in bold are statistically significant at the 0.05 level.

Table 8. Summary for Multivariate Linear Regression

Variable	Coefficients	Standard error	t stat	P-value
Intercept	−177.1	28.7	−6.17	1.63×10^{-07}
P	0.66	0.055	11.9	1.29×10^{-15}
T	−15.1	5.23	−2.89	0.0059

Thus, it suggested that temperature effects on runoff are more important for upstream stations due to glacier melting.

To assess the relative contribution of precipitation and temperature to streamflow, a multivariate linear regression analysis is investigated here: $R = 0.66P - 15.1T - 177.1$, where R represents annual runoff depth in the Yellow River source region and P and T represent mean annual areal precipitation and temperature, respectively. The R^2 is equal to 0.76. The bias was insignificant with a value of -2.5×10^{-13}, and the root-mean-square error is 21.9 mm. All coefficients were statistically tested for significance at the 0.05 level (Table 8). Both the increasing temperature and the decreasing precipitation are reasons for decrease in natural streamflow. The globally averaged surface temperature showed a warming of 0.85 (0.65–1.06)°C over the period 1880–2012, and 1983–2012 was likely the warmest 30-year period of the last 1,400 years [Intergovernmental Panel on Climate Change (IPCC) 2013]. The temperature change for the source region of the Yellow River for the last 50 years is even larger based on this paper's analysis. It is estimated that the global mean surface temperature change for the period 2016–2035 relative to 1986–2005 will likely be in the range of 0.3–0.7°C (IPCC 2013). Immerzeel et al. (2010) predicted that the rainfall in the Yellow River upstream will increase approximately 14% over the period 2046–2065. However, regional precipitation predictions should be treated with caution because most climate models experience difficulties in simulating mean monsoon and interannual precipitation variation. The changing climate will have significant effects on the downstream water availability in the Yellow River.

Discussion and Conclusions

The present study investigated trend and periodicity for temperature, precipitation, and streamflow from the early 1960s to 2010 for the Yellow River source region. The analysis revealed a statistically significant increase in temperature for 9 out of 10 investigated stations. The temperature increased 1.5°C during the last 50-year period and had an accelerated increasing trend during the last decade in the source region of the Yellow River. For precipitation the trend is less obvious. The mean annual precipitation decrease was approximately 30 mm over the entire 50-year period. In total 3 stations out of 10 displayed a statistically significant decreasing trend and one displayed an increasing trend. The precipitation stations with significantly decreasing trends are all confined to the northeastern parts of the catchment (Tongde, Zeku, and Maqu), and Maduo with increasing trend is located in the northwestern part of the catchment. Thus, the varying trends depend on spatial location. The major part of annual rainfall comes from the monsoon, and the change in monsoon climate is likely to greatly affect the annual precipitation amount. Ding and Chan (2005) suggested that the Pacific and Indian Ocean Sea surface temperature and the internal variability of the atmospheric circulation are main factors affecting the Asian summer monsoon. However, the duration of dry and wet seasons caused by the monsoon could be different, depending on the geographical location. There was a statistically significant decreasing trend for three out of four runoff stations during the period 1960–2009. The decadal mean discharge at Tangnaihai hydrologic station decreased significantly by approximately 28% from 1980 to 2000s. Significant change points were detected in 1998 for temperature and in 1990 for streamflow,

indicating a new hydrometeorological regime. The mean annual temperature was −0.58°C during 1961–1998, however, it increased to 0.43°C during 1999–2010. The mean annual runoff depth was 179.2 mm during 1960–1990, and it decreased to 143.9 mm during 1991–2009. Based on the streamflow change-point analysis, seasonal analysis shows that the decreasing precipitation in the summer monsoon period is responsible for the annual precipitation decrease. Temperature increase is rather even throughout the year. The runoff depth decreased by 0.74 mm/year as an average for the entire study area. This change will have an essential impact on the reservoir operation in the middle and downstream areas of the Yellow River.

Wavelet analysis was used to identify and describe periodicity of runoff and hydroclimatic variables, and it gives an insight in frequency and severity of drought and connections to the climate system. A statistically significant 2- to 4-year periodicity for mean areal precipitation and temperature could be seen during different periods over the area. An intense 8-year statistically significant periodicity for streamflow was revealed for the main discharge stations from the end of the 1960s to the beginning of the 1990s, and a significant change point in 1990 corroborated the time scale of strong 8-year periodicity. The annual periodicity of streamflow is partly overlapped by the statistically significant precipitation periodicity. Hydrological frequency analysis is examined to determine the magnitudes of mean annual precipitation and discharge corresponding to a given frequency or recurrence interval. The periodicity analysis examined the dynamic link between the streamflows and the climate variability in the source region of the Yellow River. It improves the understanding of dynamics of hydrological cycle and leads to better hydrologic system modeling. The revealed results could be useful in improving steamflow forecast and operating the reservoirs for power generation, water supply, and flood control in the middle and downstream of the Yellow River, hence improving water resources management. Hydroclimatic trends and linkages at each subbasin were investigated to further improve the understanding of observed streamflow changes. Precipitation in the Huangheyan and Jimai subbasins showed increasing trends, having an opposite trend from the whole basin. The significance of the correlations indicates that the streamflow is much more sensitive to precipitation and that the dependence increases from upstream to downstream. Both the increasing temperature and the decreasing precipitation are reasons for decrease in natural streamflow. The hydroclimatic change in the study area will have significant effects on the downstream water availability in the Yellow River.

Acknowledgments

References

Burn, D. H., and Elnur, M. A. H. (2002). "Detection of hydrologic trends and variability." *J. Hydrol.*, 255(1–4), 107–122.

CGIAR-CSI (Consortium for Spatial Information). (2008). "SRTM 90 m digital elevation database V4.1." ⟨http://www.cgiar-csi.org/data/srtm-90 m-digital-elevation-database-v4-1⟩ (Mar. 2, 2013).

Chen, X. D. (1996). *Hydrology of the Yellow River*, Yellow River Water Conservancy Press, Zhengzhou, China (in Chinese).

Collins, K., Hunt, W., and Hathaway, J. (2008). "Hydrologic comparison of four types of permeable pavement and standard asphalt in eastern North Carolina." *J. Hydrol. Eng.*, 10.1061/(ASCE)1084-0699(2008)13:12 (1146), 1146–1157.

Cong, Z. T., Yang, D. W., Gao, B., Yang, H. B., and Hu, H. P. (2009). "Hydrological trend analysis in the Yellow River basin using a distributed hydrological model." *Water Resour. Res.*, 45(7), W00A13.

Costa, J. E. (1978). "Holocene stratigraphy in flood frequency-analysis." *Water Resour. Res.*, 14(4), 626–632.

Coulibaly, P., and Burn, D. H. (2004). "Wavelet analysis of variability in annual Canadian streamflows." *Water Resour. Res.*, 40(3), W03105.

Ding, Y. H., and Chan, J. C. L. (2005). "The east Asian summer monsoon: An overview." *Meteorol. Atmos. Phys.*, 89(1–4), 117–142.

Fischer, T., Gemmer, M., Liu, L., and Su, B. (2012). "Change-points in climate extremes in the Zhujiang River basin, south China, 1961–2007." *Clim. Change*, 110(3–4), 783–799.

Griffis, V., and Stedinger, J. (2007). "Log-Pearson Type 3 distribution and its application in flood frequency analysis. I: Distribution characteristics." *J. Hydrol. Eng.*, 10.1061/(ASCE)1084-0699(2007)12:5(482), 482–491.

Hu, Y. R., Maskey, S., Uhlenbrook, S., and Zhao, H. L. (2011). "Streamflow trends and climate linkages in the source region of the Yellow River, China." *Hydrol. Processes*, 25(22), 3399–3411.

Immerzeel, W. W., van Beek, L. P. H., and Bierkens, M. F. P. (2010). "Climate change will affect the Asian water towers." *Science*, 328(5984), 1382–1385.

IPCC (Intergovernmental Panel on Climate Change). (2013). "Climate change 2013: The physical science basis." *Summary for Policymakers of the Working Group I*, Cambridge University Press, Cambridge, U.K.

Jiang, P., Gautam, M. R., Zhu, J. T., and Yu, Z. B. (2013). "How well do the GCMs/RCMs capture the multi-scale temporal variability of precipitation in the southwestern United States?" *J. Hydrol.*, 479, 75–85.

Kendall, M. G. (1975). *Rank correlation measures*, Charles Griffin, London.

Lan, Y. C., Zhao, G. H., Zhang, Y. N., Wen, J., Liu, J. Q., and Hu, X. L. (2010). "Response of runoff in the source region of the Yellow River to climate warming." *Quat. Int.*, 226(1–2), 60–65.

Liang, S., Ge, S., Wan, L., and Zhang, J. (2010). "Can climate change cause the Yellow River to dry up?" *Water Resour. Res.*, 46(2), W02505.

Liu, C. M., and Zheng, H. X. (2004). "Changes in components of the hydrological cycle in the Yellow River basin during the second half of the 20th century." *Hydrol. Processes*, 18(12), 2337–2345.

Mann, H. B. (1945). "Nonparametric tests against trend." *Econometrica*, 13(3), 245–259.

Mavromatis, T., and Stathis, D. (2011). "Response of the water balance in Greece to temperature and precipitation trends." *Theor. Appl. Climatol.*, 104(1–2), 13–24.

Qian, W., Kang, H. S., and Lee, D. K. (2002). "Distribution of seasonal rainfall in the east Asian monsoon region." *Theor. Appl. Climatol.*, 73(3–4), 151–168.

Rana, A., Uvo, C. B., Bengtsson, L., and Sarthi, P. P. (2012). "Trend analysis for rainfall in Delhi and Mumbai, India." *Clim. Dyn.*, 38(1–2), 45–56.

Sato, Y., et al. (2008). "Analysis of long-term water balance in the source area of the Yellow River basin." *Hydrol. Processes*, 22(11), 1618–1629.

Tang, Q., Oki, T., Kanae, S., and Hu, H. (2008a). "A spatial analysis of hydro-climatic and vegetation condition trends in the Yellow River basin." *Hydrol. Processes*, 22(3), 451–458.

Tang, Q. H., Oki, T., Kanae, S., and Hu, H. P. (2008b). "Hydrological cycles change in the Yellow River basin during the last half of the twentieth century." *J. Clim.*, 21(8), 1790–1806.

Taylor, W. A. (2000). "Change-point analysis: A powerful new tool for detecting changes." ⟨http://www.variation.com/cpa/tech/changepoint.html⟩ (Oct. 7, 2014).

Torrence, C., and Compo, G. P. (1998). "A practical guide to wavelet analysis." *Bull. Am. Meteorol. Soc.*, 79(1), 61–78.

Torrence, C., and Webster, P. J. (1999). "Interdecadal changes in the ENSO-monsoon system." *J. Clim.*, 12(8), 2679–2690.

Vogel, R., and Wilson, I. (1996). "Probability distribution of annual maximum, mean, and minimum streamflows in the United States." *J. Hydrol. Eng.*, 10.1061/(ASCE)1084-0699(1996)1:2(69), 69–76.

Westmacott, J. R., and Burn, D. H. (1997). "Climate change effects on the hydrologic regime within the Churchill-Nelson River basin." *J. Hydrol.*, 202(1–4), 263–279.

Yang, T., et al. (2010). "Regional frequency analysis and spatio-temporal pattern characterization of rainfall extremes in the Pearl River basin, China." *J. Hydrol.*, 380(3–4), 386–405.

Yang, T., Zhang, Q., Chen, Y. D., Tao, X., Xu, C.-Y., and Chen, X. (2008). "A spatial assessment of hydrologic alteration caused by dam construction in the middle and lower Yellow River, China." *Hydrol. Processes*, 22(18), 3829–3843.

Zhang, Q., Singh, V. P., and Li, J. F. (2013). "Eco-hydrological requirements in arid and semiarid regions: Case study of the Yellow River in China." *J. Hydrol. Eng.*, 10.1061/(ASCE)HE.1943-5584.0000653, 689–697.

Zheng, H. X., Zhang, L., Liu, C. M., Shao, Q. X., and Fukushima, Y. (2007). "Changes in stream flow regime in headwater catchments of the Yellow River basin since the 1950s." *Hydrol. Processes*, 21(7), 886–893.

Zheng, H. X., Zhang, L., Zhu, R. R., Liu, C. M., Sato, Y., and Fukushima, Y. (2009). "Responses of streamflow to climate and land surface change in the headwaters of the Yellow River basin." *Water Resour. Res.*, 45(7), W00A19.

Zhou, H., Zhao, X., Tang, Y., Gu, S., and Zhou, L. (2005). "Alpine grassland degradation and its control in the source region of the Yangtze and Yellow Rivers, China." *Grassland Sci.*, 51(3), 191–203.

Paper II

Hydrological Sciences Journal

Regional sea surface temperatures explain spatial and temporal variation of summer precipitation in the source region of the Yellow River

Feifei Yuan[a], Hiroshi Yasuda[b], Ronny Berndtsson[c], Cintia Bertacchi Uvo[a], Linus Zhang[a], Zhenchun Hao[d] & Xinping Wang[e]

[a] Department of Water Resources Engineering, Lund University, Lund, Sweden

[b] Arid Land Research Center, Tottori University, Hamasaka, Japan

[c] Department of Water Resources Engineering and Center for Middle Eastern Studies, Lund University, Lund, Sweden

[d] State Key Laboratory of Hydrology, Water Resources and Hydraulic Engineering, Hohai University, Nanjing, P.R. China

[e] Shapotou Desert Research and Experiment Station, Cold and Arid Regions Environmental and Engineering Research Institute, Chinese Academy of Sciences, Lanzhou, P.R. China
Accepted author version posted online: 02 Apr 2015.

PLEASE SCROLL DOWN FOR ARTICLE

Regional sea surface temperatures explain spatial and temporal variation of summer precipitation in the source region of the Yellow River

Feifei Yuan[1], Hiroshi Yasuda[2], Ronny Berndtsson[3], Cintia Bertacchi Uvo[1], Linus Zhang[1], Zhenchun Hao[4] and Xinping Wang[5]

[1]*Department of Water Resources Engineering, Lund University, Box 118, SE-221 00 Lund, Sweden*

Feifei.yuan@tvrl.lth.se

[2]*Arid Land Research Center, Tottori University, 1390 Hamasaka Tottori, 680-0001 Japan*

[3]*Department of Water Resources Engineering and Center for Middle Eastern Studies, Lund University,*

Box 201, SE-221 00 Lund, Sweden

[4] *State Key Laboratory of Hydrology, Water Resources and Hydraulic Engineering, Hohai University,*

210098, Nanjing, P.R. China

[5]*Shapotou Desert Research and Experiment Station, Cold and Arid Regions Environmental and*

Engineering Research Institute, Chinese Academy of Sciences, 320, Donggang West Road 730000,

Lanzhou, Gansu, P.R. China.

Abstract The summer precipitation (June-September) in the source region of the Yellow River accounts for about 70% of the annual total, playing an important role in water availability. This study divided the source region of the Yellow River into homogeneous zones based on precipitation variability using cluster analysis. Summer precipitation trends and teleconnections with global sea surface temperatures (SST) and Southern Oscillation Index (SOI) from 1961 to 2010 were investigated by Mann-Kendall test and Pearson product-moment correlation analysis. The results show that the northwest part (zone 1) had a non-significantly increasing trend, and the middle and southeast parts (zones 2 and 3) that receive the most precipitation displayed a statistically significant decreasing trend for summer precipitation. The summer precipitation in the whole region shows statistically significant negative correlations with the central Pacific SST for 0-4 month lags and with the southern Indian and Atlantic Ocean SST for 5-8 month lags. Analyses of sub-regions reveal intricate and complex correlations with different SST areas that further explain the summer precipitation variability. The SOI had significant positive correlations mainly for 0-2 month lag with summer precipitation in the source region of the Yellow River. It is seen that El Niño Southern Oscillation (ENSO) events have an influence on the summer precipitation, and the predominant negative correlations indicate that higher SST in equatorial Pacific areas corresponding to El Niño coincides with less summer precipitation in the source region of the Yellow River.

1 INTRODUCTION

The Yellow River is of immense importance to China since it supplies fresh water for 107 million people and 13% of China´s totally irrigated farming lands in 2006 (Wang et al. 2006, Yang et al. 2008). The river basin population is expected to increase by about 20 million people until 2030, and consequently water availability has a major relevance for food security for the growing population (Marx 2012). The source region of the Yellow River contributes about 35% of the basin's total streamflow playing an important role in meeting downstream water resources requirements (Zheng *et al.* 2007). The last 50 years have witnessed decreasing trends in annual precipitation and streamflow for the Yellow River source region, mainly due to a weakening of the summer monsoon rainfall (Yuan et al. 2015). Corresponding to the weakened monsoon rainfall the average runoff depth has been decreasing by 0.74 mm/year over the entire study area (Yuan et al. 2015). The precipitation and streamflow decrease may cause further water shortage problems in the downstream of the Yellow River.

It has been shown that sea surface temperature (SST) can provide important predictive information about hydrologic variability in many regions of the world (Tootle and Piechota 2006, Yasuda et al. 2009). For example, ENSO events are closely linked to patterns of flood and drought in different areas as they strongly affect local and regional scale climates through teleconnections between the coupled ocean-atmosphere and land systems (Wang et al. 2006, Jiang et al. 2013). Thus, it is essential to improve the knowledge regarding the relationship between summer (June to September) precipitation

in the source region of the Yellow River and global SST. This would have important implications for water resources management.

Research in recent decades has tried to link global atmospheric circulation with more localized hydrological response (Tootle and Piechota 2006, Uvo et al. 1998, Yasuda et al. 2009, Peng et al. 2013). Several studies have shown teleconnections between SST and the hydroclimatology of certain areas in China during the recent years. Fu *et al.* (2007) examined the precipitation variability between EI Nino and La Nina years in the Yellow River basin, and found that the average annual precipitation in La Nina years is 18.8% higher than the one in El Nino years. Lau and Weng (2001) studied the influence of SST variability across the globe on the flood and drought occurrences over China in the summers of 1997 and 1998 using coherent modes of rainfall and SST. They found that the severe flood in south China in 1998 was associated with biennial tendency of basin-scale SST anomaly during the transition from El Nino to La Nina in 1997-1998. Lü *et al.* (2011) explored the rainfall-ENSO relationship using Southern Oscillation Index for the source region of the Yellow River. Xu *et al.* (2007) studied the long-term trend of precipitation in China and its association with ENSO and found that drought in the Yellow River basin may easily occur during El Nino episodes . Wang et al. (2000) found that ENSO events can affect the East Asian climate through a Pacific-East Asian teleconnection, with an anomalous anti-cyclone east of the Philippines during El Nino events often observed over West-Pacific and the southward shift of the seasonal rain belt. To the authors´ knowledge, there are still no studies regarding the precipitation variability in the source region of the Yellow River and summer precipitation teleconnections with global SST. It is important to quantify the above relationship for the source region of the Yellow River and develop the possible quantitative summer

precipitation prediction techniques. In this study, cluster analysis was used to separate the precipitation stations in the source region of the Yellow River into homogeneous zones. Linear regression and Mann-Kendall test for each zone revealed the spatial variability of summer precipitation. Correlation analysis examined the links between summer precipitation in the source region of the Yellow River and global SST and Southern Oscillation Index (SOI). The significantly correlated SST areas identified the influence of climate patterns on summer precipitation variability in the source region of the Yellow River.

2 STUDY AREA, DATA AND METHODS

2.1 Study area and data

The source region of the Yellow River is located on the northeast Qinghai-Tibet Plateau between 32º12´-35º48´N and 95º50´-103º28´E and includes the area above the Tangnaihai hydrologic station. The area is 12.2×10^4 km^2 occupying about 16% of the Yellow River Basin and it has a great elevation change from 6253 m in the west to 2670 m in the east (Fig. 1). The climate in the source region of the Yellow River is greatly influenced by the southwest monsoon and the East Asian summer monsoon (Ding and Chan 2005, Qian et al. 2002). The earliest onset of the East Asian summer monsoon occurs in the central and southern Indochina Peninsula. It displays a distinct stepwise northward and northeastward movement and then finally penetrates into the upper Yellow River from the south of China (Ding and Chan 2005, Qian et al. 2002). The effects of atmospheric circulation are in general different for the upper and lower Yellow River. The monsoon rain belt in the upper part is caused by southeasterly flow while the

corresponding monsoon rain belt in the lower parts is influenced by southwesterly flow (Qian *et al.* 2002). This causes differences in spatial distribution of summer precipitation between the two parts of the Yellow River. The precipitation is generally of low intensity (<50 mm/d), long duration (10-30 d), and covers a large area (>100, 000 km^2) (Hu *et al.* 2011, Zheng *et al.* 2007).

Monthly precipitation observations from 1961 to 2010 collected from ten meteorological stations (Fig. 1) were obtained from the Chinese Meteorological Administration (CMA), and data quality has been checked by CMA. Monthly global sea surface temperature (1×1º) version HadISST 1.1 from 1960 to 2010 obtained from courtesy of the British Atmospheric Data Centre was used here (Rayner et al. 2003). The monthly Southern Oscillation Index (SOI) data from 1960 to 2010 was from the Climate Prediction Centre (CPC, NOAA) (http://www.cpc.ncep.noaa.gov/data/indices/soi). The Shuttle Radar Topographic Mission (SRTM) 90 m digital elevation data were downloaded from the Consortium for Spatial Information (CGIAR-CSI).

Figure 1

2.2 Methods

2.2.1 Cluster analysis

Due to the large and diverse topography of the area and marked spatial variability of precipitation, a division into homogeneous precipitation areas was done by cluster analysis using monthly precipitation data. The results were used to investigate the spatial dependence and influence of different SST areas on the summer precipitation within the source region. Cluster analysis is primarily an exploratory data analysis tool to separate data into groups whose identities are not known in advance (Wilks 2011). The number of

groups is defined by the degree of similarity and difference between individual observations (Wilks 2011). The cluster analysis is a widely used pre-analysis technique in hydrological and meteorological areas (Gong and Richman 1995, Uvo 2003). A correlation matrix was calculated to discern the levels of dependence among the precipitation stations. This method produces a dendrogram in which the correlations between all precipitation stations are shown as a tree-like hierarchical diagram.

In our case, we have an n×p data matrix X, where n is the number of variables and p is the number of precipitation stations. Preprocessing of the variables before calculation of the distance measures is necessary since different variables may be measured on different scales and may also contain irrelevant or redundant information(Fovell and Fovell 1993, Parajka et al. 2010, Kingston et al. 2011). The means of the variables have been removed, and then the data matrix is standardized. Principal component analysis was applied to create new variables composed of mutually orthogonal linear combinations of the original variables, each accounting for a specific fraction of the original total variance as indicated by the size of its associated eigenvalue. Retention of only the most significant components presenting more than 90% of the total variance accomplishes variable reduction. These created new variables were used to generate component scores that were clustered in place of the raw precipitation data for cluster analysis. Euclidean distance is used here for measuring similarity between pairs of ten precipitation stations. Ward method is chosen as a clustering technique, which is based on mutually exclusive subsets of the data set and does not assume normality (Bonell and Sumner 1992).

2.2.2 Mann-Kendall Test

To investigate summer precipitation trend and variability in the source region of the Yellow River, annual summer precipitation time series from 1961 to 2010 at different zones were examined by the non-parametric Mann-Kendall test, which is independent of the statistical distribution of the data. Statistical significance of the trend was evaluated at the 0.05 level of significance against the null hypothesis that there is no trend for the data series. A detailed procedure for this statistical test can be found in Burn and Elnur (2002).

2.2.3 Correlation analysis

To identify potential teleconnections or covariabilities between global SST and the summer precipitation (June, July, August, and September) in the source region of the Yellow River, 0-11 month lagged Pearson product-moment correlation coefficients r between monthly SST and precipitation were calculated. The summer precipitation normal distribution was tested by Kolmogorov-Smirnov test in Matlab, and SST data followed the normal distribution that could be seen here (Rayner et al. 2003, Kodera 2004, Yasuda et al. 2009). Statistical significance was assessed using the Student's *t*-test against the null hypothesis of no correlation(Lloyd-Hughes and Saunders 2002). Correlations $| r | > 0.36$ and $| r | > 0.46$ correspond to a statistical significance level of 0.01 and 0.001, respectively.

The Southern Oscillation Index (SOI) was used to further reveal the correlated SST influence on summer precipitation in the source region of the Yellow River. The 0-11 month lagged Pearson product-moment correlation coefficients r between monthly SOI and precipitation were calculated. The statistical significance was assessed at the 0.05 level.

3 RESULTS

3.1 Summer precipitation trend and variability

Fig. 2 shows the outcome of the cluster analysis that the precipitation stations in this region can be divided into three homogeneous zones, namely, 1: Xinghai, Tongde, and Maduo; 2: Zeku, Henan, and Dari, and 3: Jiuzhi, Maqu, Ruoergai, and Hongyuan. Fig. 3 shows the corresponding mean annual precipitation over the Yellow River source region. As seen from the figure, there is a strongly increasing gradient from the northwest parts with about 309 mm/year to about 755 mm/year in the southeast due to the influence of the summer monsoon from the southeast. Consequently, there is a general inverse relationship between annual precipitation and topography. The summer monsoon rainfall in China is concentrated in about four months from June to September, and the monsoon rain belt in the upper Yellow River is caused by southeasterly flow (Qian *et al.* 2002). Prevailing southeasterlies converge along the east edge of the Tibetan Plateau causing rainfall to generally decrease with topography. Thus, the cluster analysis results are mainly characterized by different average annual precipitation amount. The mean annual precipitation totals are 365, 517.9, and 692.4 mm/year for zone 1, zone 2, and zone 3, respectively.

Figure 2

Figure 3

Summer precipitation trends for the whole region and three identified homogeneous zones were investigated. As can be seen in Table 1 and Fig. 4, the summer precipitation for the whole region had a decreasing trend for the period 1961–2010. Zone 1 had a non-significantly increasing trend during 1961 to 2010. On the contrary, both

zone 2 and 3 had significantly decreasing summer precipitation. The decrease is 1.33 and 1.60 mm/year for zone 2 and zone 3, respectively. Dividing the region into homogeneous zones displays clear differences in summer precipitation and a clearer picture of the spatially dependent trend. The trend is the strongest for the wettest area of the Yellow River source region and gradually decreases with decreasing annual precipitation. The trend analysis indicates that the summer monsoon is gradually becoming weaker resulting in less summer rainfall. Table 1 also shows the contribution of the wet season precipitation to the annual total for the different zones. June to September precipitation represents 68-75% of annual total. There is a general increase in the contribution of summer monsoon rainfall to the total annual amount as the climate becomes dryer (Fig. 3 and Table 1). This was also noted in the middle stream of the Yellow River by Yasuda et al. (2009). Fig. 5 shows the monthly average precipitation for different zones in the source region of the Yellow River. The general monthly distribution pattern is similar for all three zones. Precipitation in July represents the maximum.

Table 1

Figure 4

Figure 5

3.2 Correlation analysis

Figure 6 shows the 0-11 month lagged cross-correlation between global SST and the summer precipitation (June to September) for the source region of the Yellow River as a whole. The figure shows statistically significant negative correlations with different SST areas of various lags. During lag 0-4 month it is the large area in the central Pacific that is dominating. However, with increasing lag new areas in the southern Indian and

Atlantic Ocean become a dominant influence. The predominant negative correlations mean that lower SST in these areas coincides with more summer rainfall over the source region of the Yellow River. El Nino events occur in the eastern Pacific Pattern and the central Pacific pattern according to the location of the onset of warm SST anomalies (Lin and Yu 1993, Feng et al. 2011). The results also suggest significant relationships with southern Indian and Atlantic Ocean especially for lags between 5 to 8 months. Feng et al. (2013) examined that the SST anomalies over the southern Indian Ocean could induce consistent atmosphere circulation and precipitation anomalies over China, and the warm SST anomalies could decrease the rainfall that is generally in agreement with the negative correlations we found above.

Figure 6

Figure 7 shows correlation between summer precipitation in zone 1 and global SST. Different correlated SST areas emerge when dividing the Yellow River source region into homogeneous precipitation areas. Zone 1 rainfall is correlated with SST in mainly central and only partly eastern Pacific. Significant negative correlation remains for a lagged period up to 9 months in this area. It is also seen that a small area with positive correlations (blue area in Fig. 7) appears in the central Pacific Ocean for a lag up to about 8 months. The significant positive correlation corroborates with non-significantly increasing summer precipitation trend in zone 1 during the last 50-year period. It is quite clear that rainfall in zone 1 (western and northwestern parts of the source region of the Yellow River) is mainly governed by central and eastern Pacific SST.

Figure 7

Figure 8 shows correlation between summer precipitation in zone 2 (central parts of source region of the Yellow River) and global SST. It has great similarity with the pattern for the whole region as shown in Fig. 6 but with more clear signals in the southern Indian and Atlantic Ocean, mainly due to the similar summer precipitation time series between the whole region and zone 2 (Fig. 4) . For short time lags of 0-4 month it is mainly central Pacific that explains summer precipitation. However, for lag 5-8 month it is southern Atlantic and Indian Ocean and western Pacific that is of importance. The clearest signals appeared at Lag 6 month and Lag 7 month for the southern Atlantic and India Ocean, and western Pacific, respectively.

Figure 8

Figure 9 shows correlation between summer precipitation in zone 3 (eastern parts of source region of the Yellow River) and global SST. Lag 0-3 month shows scattered and small areas. From lag 4 month the central Pacific emerges with strong correlation. When increasing the lag period western Pacific and the southern Atlantic also display strong correlation. Eventually, for the long lag periods of 6-11 month the central and western Pacific dominate the correlation.

Figure 9

It is clearly seen that SST has an influence on the summer precipitation in the source region of the Yellow River. The ENSO activity is typically monitored by observing the sea level pressures and SST in the equatorial Pacific. Thus, the Southern Oscillation Index (SOI) was selected to further reveal the ENSO influence on summer precipitation in the source region of the Yellow River. Table 2 shows the correlation coefficients between summer precipitation and SOI for different lags. Significant positive correlations were found for the 0-2 month lag for the entire region. In addition, zone 1 had lag 4, 9-11 month

significant positive correlations. Sustained negative values of the SOI often indicate El Nino episodes, and these negative values are usually accompanied by sustained warming of the central and eastern tropical Pacific Ocean, a decrease in the strength of the Pacific trade winds and a reduction in rainfall over China(Fu et al. 2013). The significant negative correlations with SST in equatorial Pacific Ocean and positive correlations with SOI for summer precipitation clearly shows the influence of ENSO activities on the source region of the Yellow River.

Table 2

4 DISCUSSION AND CONCLUSION

This study divided the source region of the Yellow River into three homogeneous zones based on precipitation variability and investigated the summer precipitation trends. The relationships between summer precipitation in the source region of the Yellow River and global SST and SOI were investigated. The northwest part (zone 1) exhibited a non-significantly increasing trend during 1961 to 2010. The middle and southeast parts (zone 2 and 3) that receive the most precipitation displayed a statistically significant decreasing trend over the same period. This is due to a weakening of the summer monsoon and decreasing rainfall amounts during the summer months. The summer precipitation in the whole area shows statistically significant negative correlations with the central Pacific SST during 0-4 month lags and with the southern Indian and Atlantic Ocean SST during 5-8 month lags. The predominant negative correlations mean that lower SST in equatorial Pacific areas corresponding to La Nina coincides with more summer rainfall over the source region of the Yellow River. The summer precipitation in zone 1 is correlated with SST in mainly central and partly eastern Pacific. However, a small area

with positive correlations appears in the central Pacific Ocean for a lag up to about 8 months. This explains that the precipitation in zone 1 had a non-significantly increasing trend during the last 50-year period. Zone 2 has similar influencing SST areas with the whole area but with a clearer signal. The precipitation in zone 3 is influenced by the central Pacific but also affected by southern Atlantic Oceans and western Pacific. SOI had significant positive correlations mainly during 0-2 month lag with summer precipitation in the source region of the Yellow River.

It is clear to see that ENSO events have an influence on the summer precipitation in the source region of the Yellow River. Xu et al. (2007) found that the La Nina phase (lower SST of the eastern tropical Pacific Ocean) corresponds to a relatively rainier season in the Yellow River basin. The results here reveal the correlated SST areas and confirm the importance of ENSO events for the summer precipitation in the source region of the Yellow River. Fu et al. (2013) examined the trend and variability of extreme rainfall events in China and found that it is mainly influenced by ENSO, the magnitude of East Asian monsoon, global warming as well as wind circulations like the cyclonic and anti-cyclonic circulation anomalies dominating over Northwest and North China. Cuo et al. (2013) have shown that precipitation change in winter at northern Tibetan Plateau can be attributed to changes in the North Atlantic Oscillation, ENSO, the Arctic Oscillation and East Asian westerly jet, and in summer the changes in precipitation is only weakly related to these indices. Xu et al. (2013) defined an eastern Pacific southern oscillation index and a central Pacific southern oscillation index to measure the different responses of the atmospheric circulation to the two types of El Nino, and it showed that both indices exhibited positive correlations with rainfall anomalies in the upstream of the Yellow River. Zhang et al. (2013) examined that the

warm phase of the North Atlantic SST is related to North Atlantic Oscillation that leads to less precipitation or more frequent droughts in the semi-arid subarea in the upper reaches of the Yellow River. Liu et al. (2012) investigated the variation of water discharge that is more likely to be correlated with large sale climatic process over the long time scales and is also influenced by both ENSO and human activities, and the ENSO impacts on the water discharge were exerted by influencing the precipitation through its effects on East Asian monsoon.

The precipitation in the source region of the Yellow River is greatly influenced by the southwest monsoon and the East Asian summer monsoon. The Asian monsoon region assumes the most distinct variation of the annual cycle and the alternation of dry and wet seasons which is in concert with the seasonal reversal of the monsoon circulation features (Webster et al. 1998). However, the different parts of the Asian monsoon region, the durations of dry and wet seasons may be different, depending on their climate regions and the degree of effects of the Asian monsoon (Ding and Chan 2005). The monsoon variability greatly affects the precipitation in the source region of the Yellow River (Feng et al. 2011). Li et al. (2010) found that the recent warming of the tropics, especially the warming associated with the tropical interdecadal variability centered over the central and eastern Pacific is a primary cause for the weakening the East Asian Summer Monsoon (EASM) since the late 1970s. Two external sources of forcing, including Pacific and Indian Ocean SSTs and the snow cover in the Eurasia and the Tibetan Plateau, are believed to be primary contributing factors to physical processes and mechanisms related to the EASM (Ding and Chan 2005). The warming in the tropical Pacific and Indian Ocean leads to an abnormal Subtropical Pacific High that reduces water vapor transport to North China from South China Sea and thus contributes

to precipitation decrease (Hu 1997). In view of the above it is clear that ENSO can exert an important impact on the Asian monsoon (Weng et al. 1999, Zhou et al. 2010). This study examined the relationship between summer precipitation in the source region of the Yellow River and global SST. The summer precipitation in the source region of the Yellow River is closely related to ENSO phenomenon of which the SSTs in the equatorial Pacific are a major component. The significant lagged correlations can be used for precipitation forecasting.

The summer precipitation in the source region of the Yellow River is of importance for food production and water supply in the middle and downstream of the river basin. This study is an essential part of the development of optimal reservoir planning and operation policies for power generation, water supply, irrigation, and flood control for the mid and down-stream areas of the Yellow River.

REFERENCES

Bonell, M. and Sumner, G. 1992. Autumn and Winter Daily Precipitation Areas in Wales, 1982-1983 to 1986-1987. *International Journal of Climatology,* 12(1), 77-102.

Burn, D. H. and Elnur, M. A. H. 2002. Detection of hydrologic trends and variability. *Journal of Hydrology,* 255(1-4), 107-122.

Cuo, L*., et al.* 2013. Climate change on the northern Tibetan Plateau during 1957-2009: Spatial patterns and possible mechanisms. *Journal of Climate,* 26(1), 85-109.

Ding, Y. H. and Chan, J. C. L. 2005. The East Asian summer monsoon: an overview. *Meteorology and Atmospheric Physics,* 89(1-4), 117-142.

Feng, J*., et al.* 2011. Different impacts of El Nino and El Nino Modoki on China rainfall in the decaying phases. *International Journal of Climatology,* 31(14), 2091-2101.

Feng, J., Yu, L. and Hu, D. 2013. Influence of Indian Ocean subtropical dipole on spring rainfall over China. *International Journal of Climatology*, n/a-n/a.

Fovell, R. G. and Fovell, M.-Y. C. 1993. Climate Zones of the Conterminous United States Defined Using Cluster Analysis. *Journal of Climate,* 6(11), 2103-2135.

Fu, G*., et al.* 2007. Impacts of climate variability on stream-flow in the Yellow River. *Hydrological Processes,* 21(25), 3431-3439.

Fu, G*., et al.* 2013. Temporal variation of extreme rainfall events in China, 1961–2009. *Journal of Hydrology,* 487(0), 48-59.

Gong, X. F. and Richman, M. B. 1995. On the Application of Cluster-Analysis to Growing-Season Precipitation Data in North-America East of the Rockies. *Journal of Climate,* 8(4), 897-931.

Hu, Y. R*., et al.* 2011. Streamflow trends and climate linkages in the source region of the Yellow River, China. *Hydrological Processes,* 25(22), 3399-3411.

Hu, Z. Z. 1997. Interdecadal variability of summer climate over East Asia and its association with 500 hPa height and global sea surface temperature. *Journal of Geophysical Research-Atmospheres,* 102(D16), 19403-19412.

Jiang, P*., et al.* 2013. How well do the GCMs/RCMs capture the multi-scale temporal variability of precipitation in the Southwestern United States? *Journal of Hydrology,* 479, 75-85.

Kingston, D. G*., et al.* 2011. Regional classification, variability, and trends of northern North Atlantic river flow. *Hydrological Processes,* 25(7), 1021-1033.

Kodera, K. 2004. Solar influence on the Indian Ocean Monsoon through dynamical processes. *Geophysical Research Letters,* 31(24), L24209.

Lü, A*., et al.* 2011. El Niño-Southern Oscillation and water resources in the headwaters region of the Yellow River: links and potential for forecasting. *Hydrol. Earth Syst. Sci.,* 15(4), 1273-1281.

Lau, K. M. and Weng, H. 2001. Coherent Modes of Global SST and Summer Rainfall over China: An Assessment of the Regional Impacts of the 1997–98 El Niño. *Journal of Climate,* 14(6), 1294-1308.

Li, H*., et al.* 2010. Responses of East Asian summer monsoon to historical SST and atmospheric forcing during 1950–2000. *Climate Dynamics,* 34(4), 501-514.

Lin, X. and Yu, S. 1993. El Nino and rainfall during the flood season(June-August) in China. *Acta Meteorologica Sinica,* 51, 434-441.

Liu, F*., et al.* 2012. Spatial and temporal variability of water discharge in the Yellow River Basin over the past 60 years. *Journal of Geographical Sciences,* 22(6), 1013-1033.

Lloyd-Hughes, B. and Saunders, M. A. 2002. Seasonal prediction of European spring precipitation from El Niño–Southern Oscillation and Local sea-surface temperatures. *International Journal of Climatology,* 22(1), 1-14.

Marx, S. 2012. Chinese river basins, Yellow River, Huai, Interior Basins, Preliminary Results of the GCI II Survey. *River Basins and Water-Energy-Food Security Nexus, IISD – GWSP Conference on the Water-Energy-Food Security Nexus,* (GWSP IPO).

Parajka, J*., et al.* 2010. Seasonal characteristics of flood regimes across the Alpine–Carpathian range. *Journal of Hydrology,* 394(1–2), 78-89.

Peng, J., Yu, Z. and Gautam, M. R. 2013. Pacific and Atlantic Ocean influence on the spatiotemporal variability of heavy precipitation in the western United States. *Global and Planetary Change,* 109(0), 38-45.

Qian, W., Kang, H. S. and Lee, D. K. 2002. Distribution of seasonal rainfall in the East Asian monsoon region. *Theoretical and Applied Climatology,* 73(3-4), 151-168.

Rayner, N. A*., et al.* 2003. Global analyses of sea surface temperature, sea ice, and night marine air temperature since the late nineteenth century. *Journal of Geophysical Research: Atmospheres,* 108(D14), 4407.

Tootle, G. A. and Piechota, T. C. 2006. Relationships between Pacific and Atlantic ocean sea surface temperatures and US streamflow variability. *Water Resources Research,* 42(7).

Uvo, C. B. 2003. Analysis and regionalization of northern european winter precipitation based on its relationship with the North Atlantic oscillation. *International Journal of Climatology,* 23(10), 1185-1194.

Uvo, C. B*., et al.* 1998. The relationships between tropical Pacific and Atlantic SST and northeast Brazil monthly precipitation. *Journal of Climate,* 11(4), 551-562.

Wang, B., Wu, R. G. and Fu, X. H. 2000. Pacific-East Asian teleconnection: how does ENSO affect East Asian climate? *Journal of Climate,* 13(9), 1517-1536.

Wang, H. J*., et al.* 2006. Interannual and seasonal variation of the Huanghe (Yellow River) water discharge over the past 50 years: Connections to impacts from ENSO events and dams. *Global and Planetary Change,* 50(3-4), 212-225.

Webster, P. J*., et al.* 1998. Monsoons: Processes, predictability, and the prospects for prediction. *Journal of Geophysical Research: Oceans,* 103(C7), 14451-14510.

Weng, H. Y., Lau, K. M. and Xue, Y. K. 1999. Multi-scale summer rainfall variability over China and its long-term link to global sea surface temperature variability. *Journal of the Meteorological Society of Japan,* 77(4), 845-857.

Wilks, D. S., 2011. *Statistical methods in the atmospheric sciences.* 3rd ed. Amsterdam ; Boston: Elsevier/Academic Press.

Xu, K., Zhu, C. and He, J. 2013. Two types of El Niño-related Southern Oscillation and their different impacts on global land precipitation. *Advances in Atmospheric Sciences,* 30(6), 1743-1757.

Xu, Z. X*., et al.* 2007. Long-term trend of precipitation in China and its association with the El Nino-southern oscillation. *Hydrological Processes,* 21(1), 61-71.

Yang, T*., et al.* 2008. A spatial assessment of hydrologic alteration caused by dam construction in the middle and lower Yellow River, China. *Hydrological Processes,* 22(18), 3829-3843.

Yasuda, H*., et al.* 2009. Prediction of Chinese Loess Plateau summer rainfall using Pacific Ocean spring sea surface temperature. *Hydrological Processes,* 23(5), 719-729.

Yuan, F*., et al.* 2015. Hydro Climatic Trend and Periodicity for the Source Region of the Yellow River. *Journal of Hydrologic Engineering,* 0(0), 05015003.

Zhang, J., *et al.* 2013. Decadal variability of droughts and floods in the Yellow River basin during the last five centuries and relations with the North Atlantic SST. *International Journal of Climatology,* 33(15), 3217-3228.

Zheng, H. X., *et al.* 2007. Changes in stream flow regime in headwater catchments of the Yellow River basin since the 1950s. *Hydrological Processes,* 21(7), 886-893.

Zhou, L.-T., *et al.* 2010. Influence of South China Sea SST and the ENSO on winter rainfall over South China. *Advances in Atmospheric Sciences,* 27(4), 832-844.

Table 1 Summer precipitation (SP) from June to September linear trends and Mann-Kendall statistics (Z); NS: no significant trend; * is statistical significance at the 0.05 level.

Area	Mean annual SP (mm/year)	Min. annual SP (mm/year)	Max. annual SP (mm/year)	Linear Trend (mm/year)	Mann-Kendall Trend	Contribution of SP to annual total (%)
Whole region	372.7	281.4	492.9	-0.84	NS	72
Zone 1	273.4	184.9	395.4	0.40	NS	75
Zone 2	375.9	229.2	551.2	-1.33	*	73
Zone 3	468.7	343.4	636.6	-1.60	*	68

Table 2 The Pearson product-moment correlation coefficients between summer precipitation in the source region of the Yellow River and SOI with different time lags (months). The values in bold are statistical significance at the 0.05 level.

Precipitation	Lag 0	Lag 1	Lag 2	Lag 3	Lag 4	Lag 5	Lag 6	Lag 7	Lag 8	Lag 9	Lag 10	Lag 11
Whole region	**0.197**	**0.234**	**0.144**	0.070	0.043	0.004	-0.005	0.001	-0.035	-0.003	0.018	0.082
Zone 1	**0.153**	**0.169**	**0.140**	0.060	**0.136**	0.112	0.042	0.091	0.077	**0.150**	**0.140**	**0.190**
Zone2	**0.178**	**0.216**	**0.164**	0.065	0.026	0.026	0.033	0.004	-0.017	-0.026	0.014	0.055
Zone 3	**0.166**	**0.201**	0.083	0.055	-0.011	-0.070	-0.054	-0.051	-0.095	-0.070	-0.051	0.014

FIGURE CAPTIONS

Fig. 1 Topography, river network and precipitation stations in the source region of the Yellow River.
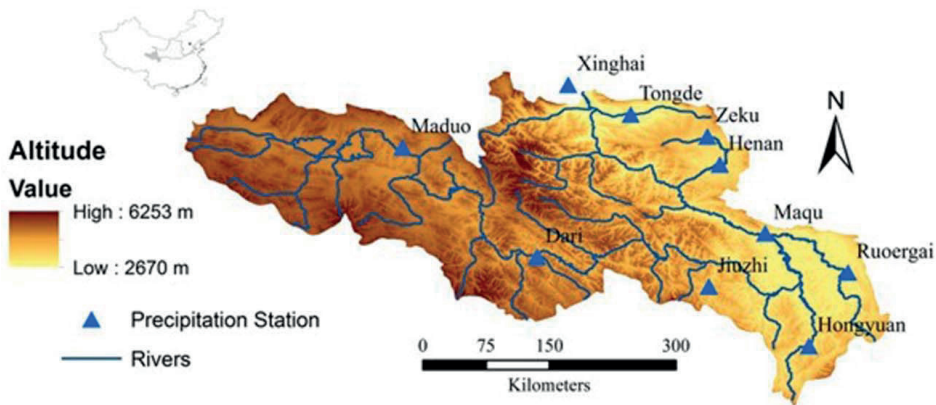
Fig. 2 Results from cluster analysis using monthly precipitation from 1961 to 2010 in the source region of the Yellow River.
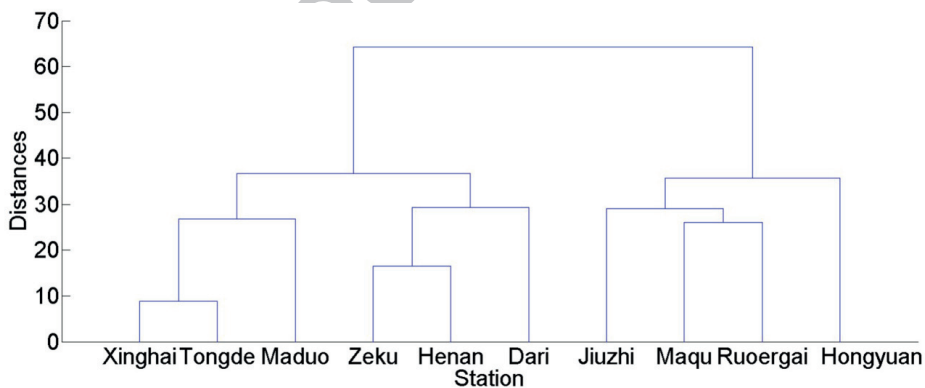
Fig. 3 Mean annual precipitation over the source region of the Yellow River for the period 1961–2010.
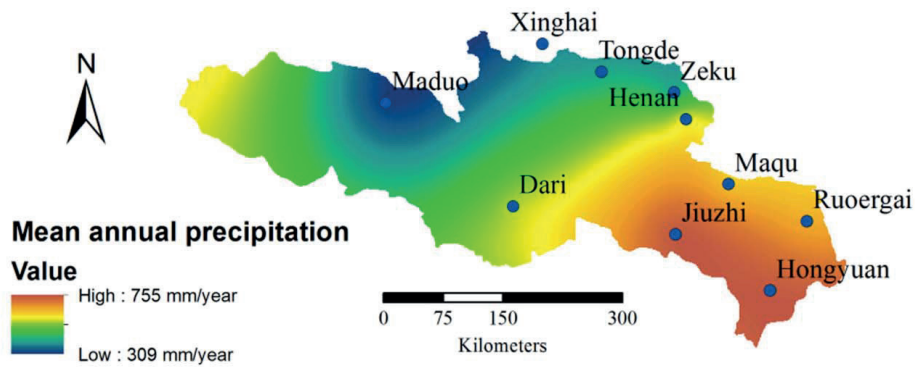
Fig. 4 Annual summer precipitation for the whole region and zones 1–3 from 1961 to 2010 in the source region of the Yellow River.
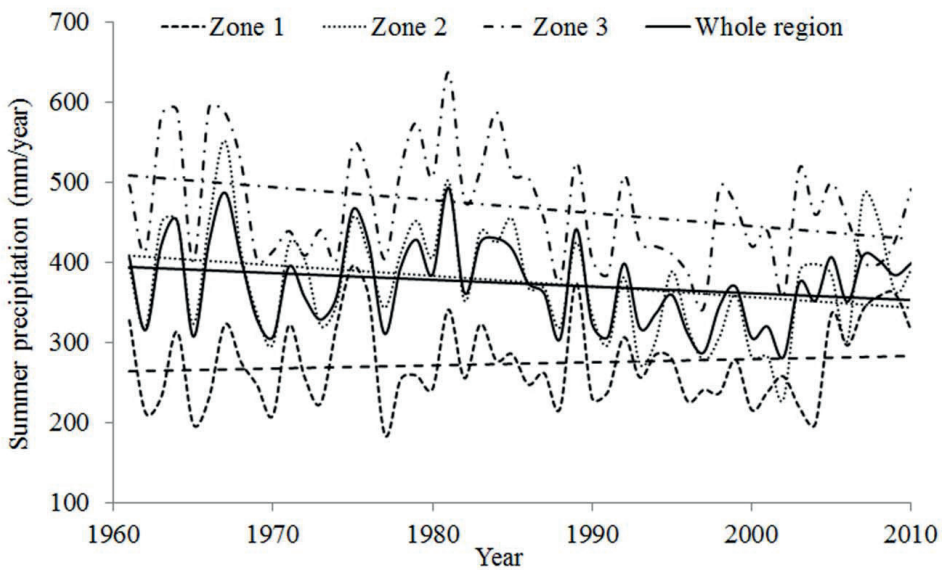
Fig. 5 Monthly average precipitation for zones 1–3 for 1961–2010 in the source region of the Yellow River.
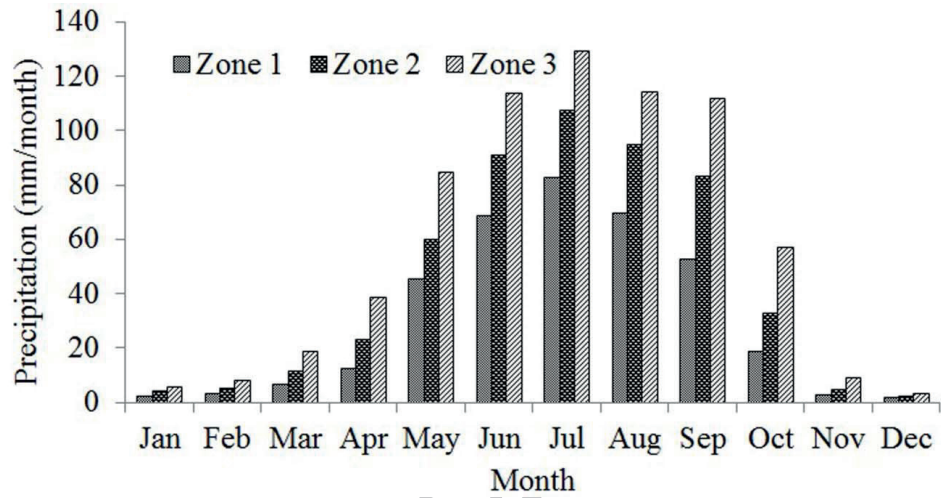
Fig. 6 Correlation between summer precipitation in the Yellow River source region and global SST for the period 1961–2010 ($|r| > 0.36$ and $|r| > 0.46$ correspond to a statistical significance level of 0.01 and 0.001, respectively).
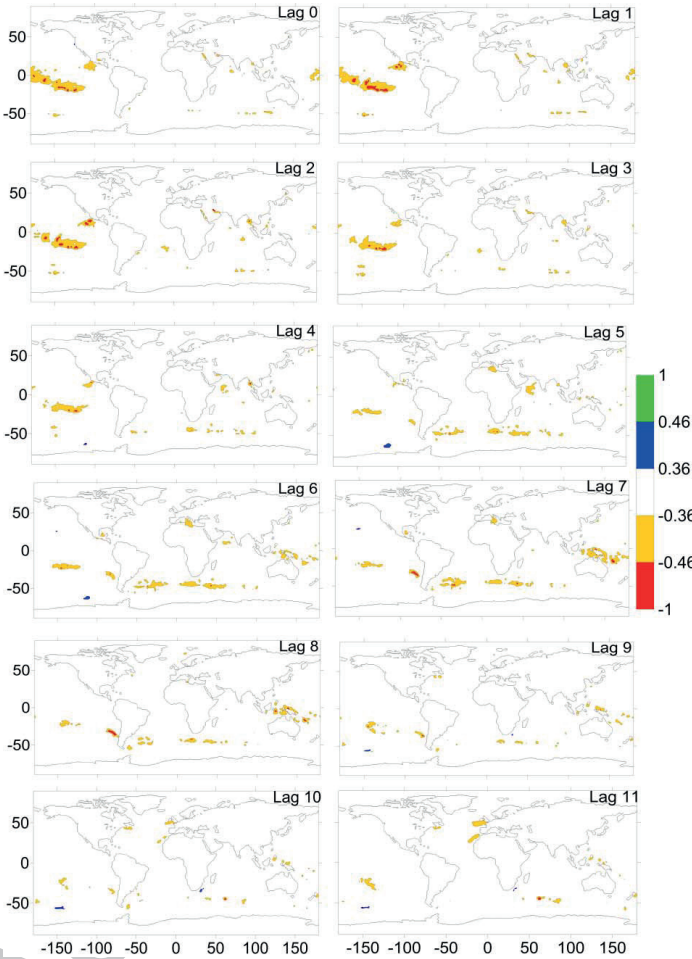
Fig. 7 Correlation between summer precipitation in Zone 1 and global SST, 1961–2010 (see Fig. 6).
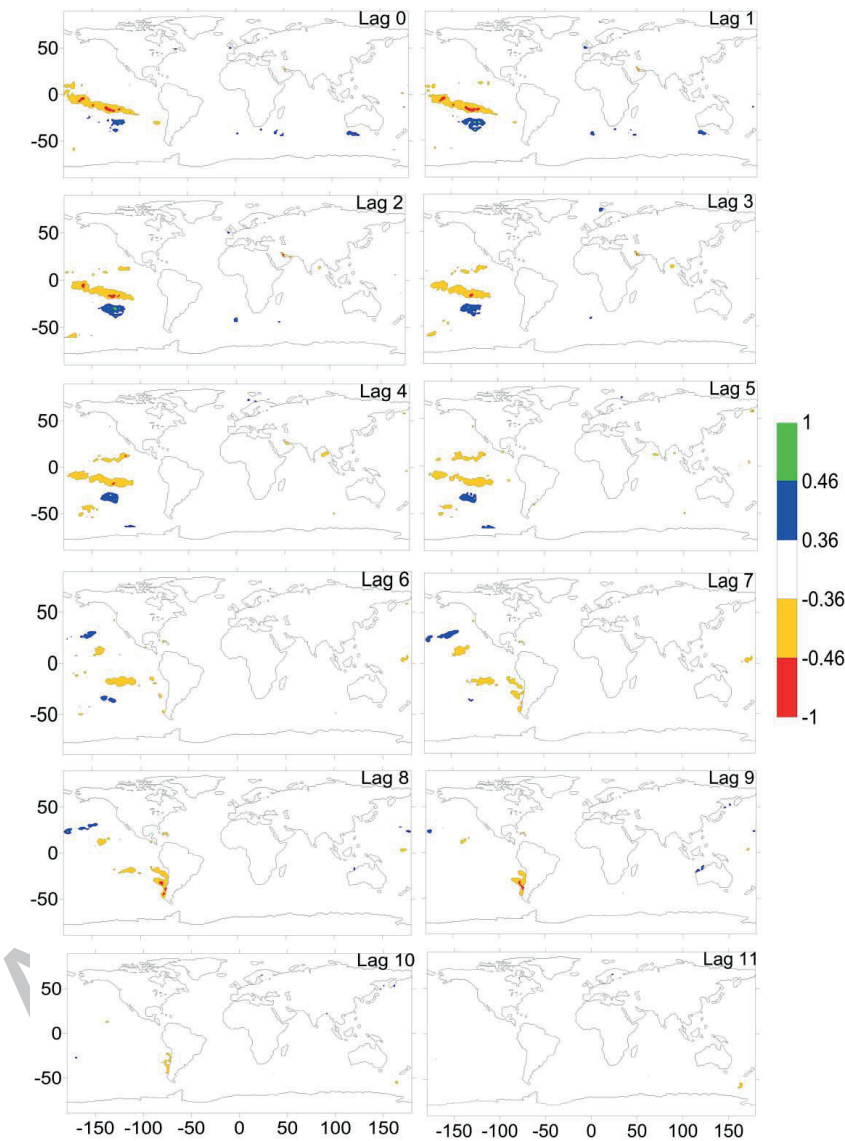
Fig. 8 Correlation between summer precipitation in Zone 2 and global SST, 1961–2010
(see Fig. 6).
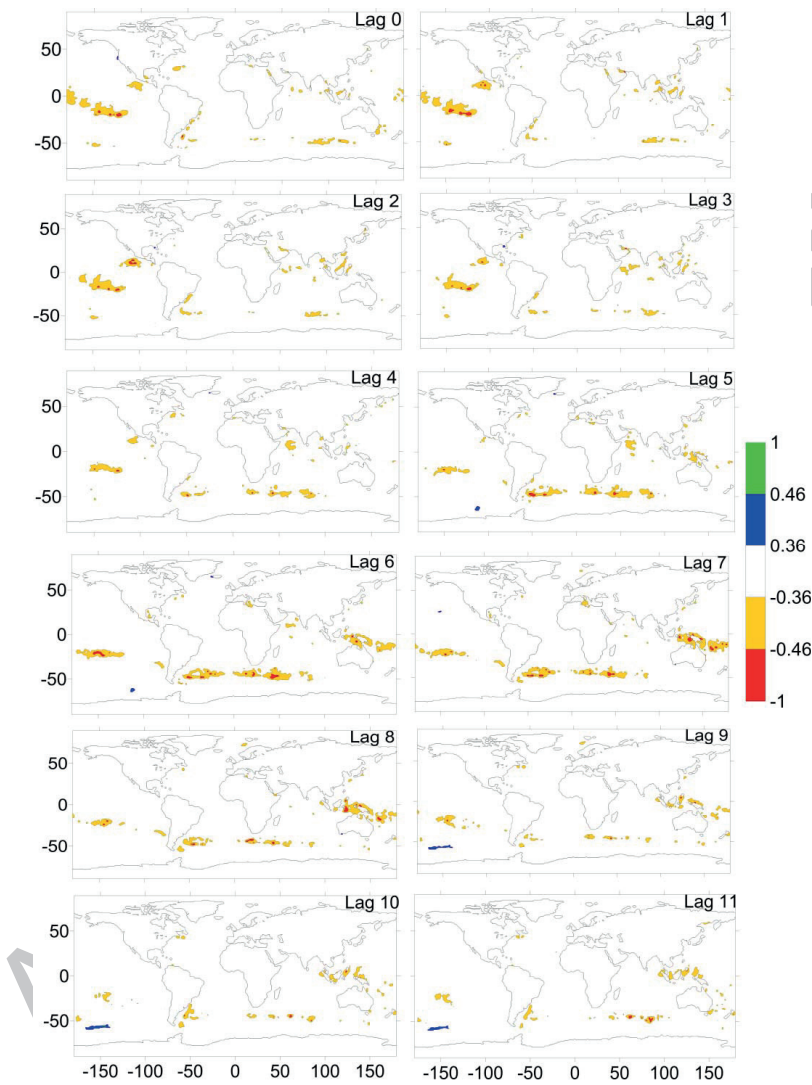
Fig. 9 Correlation between summer precipitation in Zone 3 and global SST, 1961–2010 (see Fig. 6).
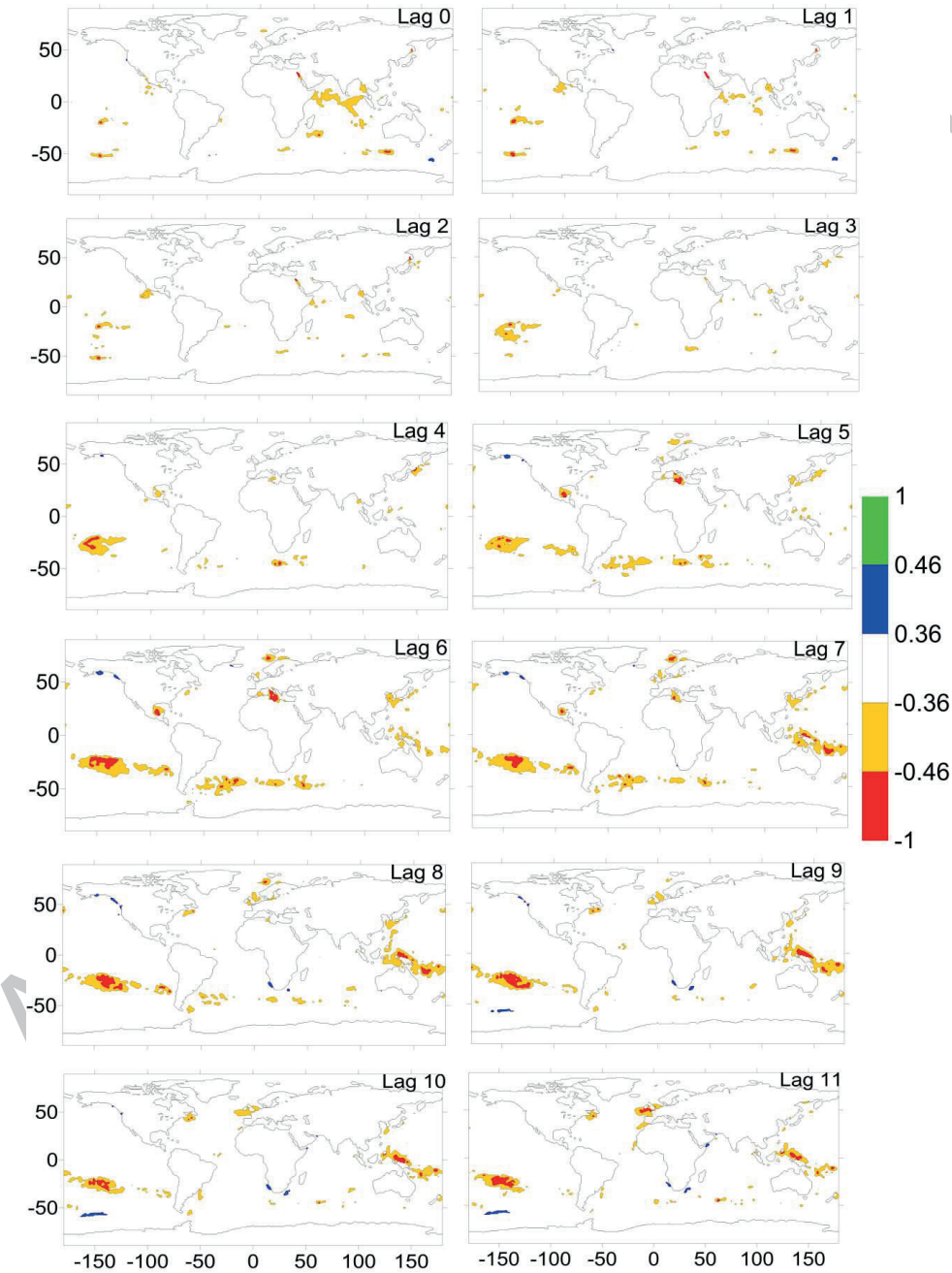
Paper III

1 **Summer precipitation prediction in the source region of the Yellow River using climate**

2 **indices**

3 Feifei Yuan[1], Ronny Berndtsson[2], Cintia Bertacchi Uvo[1], Linus Zhang[1] and Peng Jiang[3]

4 *[1]Department of Water Resources Engineering, Lund University, P.O. Box 118, SE-221 00*

5 *Lund, Sweden*

6 *Feifei.yuan@tvrl.lth.se Tel: +46-736456805   Fax: +46-46 222 44352*

7 *[2]Department of Water Resources Engineering and Center for Middle Eastern Studies, Lund*

8 *University, P.O. Box 118, SE-221 00 Lund, Sweden*

9 *[3]Division of Hydrologic Sciences, Desert Research Institute, Las Vegas, NV 89119, USA*

10 **Abstract:** The source region of the Yellow River contributes about 35% of the total water

11 yield in the Yellow River basin playing an important role in meeting downstream water

12 resources requirements. The summer precipitation from June to September in the source

13 region of the Yellow River accounts for about 70% of the annual total, and its decrease would

14 cause further water shortage problems. Consequently, the objectives of this study are to

15 improve the understanding of the linkages between the precipitation in the source region of

16 the Yellow River and global teleconnection patterns, and to predict the summer precipitation

17 based on revealed teleconnections. Spatial variability of precipitation was investigated based

18 on three homogeneous sub-regions. Principal component analysis and singular value

19 decomposition were used to find significant relations between the precipitation in the source

20 region of the Yellow River and global teleconnection patterns using climate indices. A back-

21 propagation neural network was developed to predict the summer precipitation using

22 significantly correlated climate indices. It was found that precipitation in the study area is

23 positively related to North Atlantic Oscillation, West Pacific Pattern and El Nino Southern

24 Oscillation, and inversely related to Polar Eurasian pattern. Summer precipitation was overall

well predicted using these significantly correlated climate indices, and the Pearson correlation

coefficient between predicted and observed summer precipitation was in general larger than

0.6. The results are useful for integrated water resources management in the Yellow River

basin.

Keywords: summer precipitation prediction, teleconnection pattern, the source region of the

Yellow River

INTRODUCTION

The Yellow River is extremely important to China since it supplies fresh water for 110

million people and 13% of China´s totally irrigated farming lands (Wang et al. 2006). The

source region of the Yellow River contributes about 35% of the basin's total streamflow

playing an important role in meeting downstream water resources requirements (Zheng et al.

2007). Consequently, it is an important area affecting agricultural productivity, municipal,

and industrial water supply for the whole basin. The last 50 years have witnessed a general

increasing trend in temperature and decreasing trends in annual precipitation and streamflow

for the Yellow River source region. Decreasing precipitation during the monsoon

period(June-September) is much responsible for the annual precipitation decrease (Yuan et al.

2015a). Continued precipitation and streamflow decrease may cause further water shortage

problems in the downstream of the Yellow River.

Climate variability is closely linked to patterns of flood and drought in different areas of

the world and strongly affecting local and regional scale climate through teleconnections.

Teleconnections are statistical associations among climate variables separated by large

distances, and they are a consequence of the large-scale dynamics of the ocean and

atmosphere linking disparate regional climates into one unified, global climatic system

(Leathers et al. 1991, Jiang et al. 2013). Numerous studies have shown that climate variability

has strong impact on basin water resources through changes in hydrologic variables (Lorenzo

et al. 2008, Uvo 2003, Rana et al. 2012, Peng et al. 2013). The interannual variability in local hydroclimatic variables (temperature, precipitation, and streamflow) could be a reflection of low-frequency climatic fluctuations. Understanding this linkage between local precipitation and global teleconnection patterns is essential for water resources management, and it could also improve the ability to predict the local precipitation based on physical reasoning (Redmond and Koch 1991, Hartmann et al. 2008).

Much research has been devoted to the issue of precipitation change in the source region of the Yellow River (Cong et al. 2009, Tang et al. 2008, Hu et al. 2012). Research during recent decades have also tried to link global atmospheric circulation (e.g. ENSO and global SST) with more localized hydrological response in the Yellow River basin (Yasuda et al. 2009, Fu et al. 2007, Lau and Weng 2001, Xu et al. 2007). Wang et al. (2000) found that ENSO events can affect the East Asian climate through a Pacific-East Asian teleconnection, with an anomalous anti-cyclone east of the Philippines during El Nino events. Lü et al. (2011) explored the rainfall-ENSO relationship using Southern Oscillation Index for the source region of the Yellow River. Feng et al. (2013) investigated the influence of Indian Ocean subtropical dipole on spring rainfall over China, and found that it has a significant correlation with the boreal spring rainfall over the Yellow River valley. Lorenzo et al. (2008) examined the links between circulation weather types and teleconnection patterns and their influence on precipitation patterns in Galicia. Hartmann et al. (2008) predicted summer precipitation in the Yangtze River basin with neural networks using climate indices. Chan and Shi (1999) predicted the summer monsoon rainfall over south China using climate indices. The Indian summer monsoon rainfall was shown to be well predicted by neural networks using different climate indices (Venkatesan et al. 1997, Sahai et al. 2003). In view of the above, the summer precipitation in the source region of the Yellow River could be predicted by exploring its relationship with global teleconnection patterns.

Thus, in this paper we aim at improving the knowledge by investigating the relationships between precipitation in the source region of the Yellow River and global atmospheric fluctuations, and possibly predicting the summer precipitation using related climate indices. It is important to quantify the above relationships for the source region of the Yellow River and to develop quantitative prediction techniques. The objectives of this paper were thus to identify the linkages between precipitation in the source region of the Yellow River and global teleconnection patterns and predict the summer precipitation using an artificial neural network (ANN). Establishing such links would improve the physical understanding of rainfall variability with important implications for water resources management. Also, the predicted precipitation is of utmost importance for food production and flood mitigation.

STUDY AREA AND METHODS

Study Area and Data

The source region of the Yellow River is located on the northeast Qinghai-Tibet Plateau between 32º12´-35º48´N and 95º50´-103º28´E and includes the area above the Tangnaihai runoff observation station. The area is 12.2×10^4 km^2 accounting for 16% of the Yellow River basin, and it has a great elevation change from 2,670 m in the east to 6,253 m in the west (Fig. 1). Grassland covers 80% of the catchment and it includes typical alpine swamp, steppe, and shrub meadows. The area of lakes and swamps is about 2,000 km^2. There is a permanent snowpack and glaciers in the southern Animaqing, Bayankala, and Northern Qilian mountains. The area has a comparably low population density with a total of about half a million inhabitants. The region is therefore regarded as relatively unaffected by human activities (Hu et al. 2011, Zheng et al. 2009). Neither large irrigation projects nor large dams exist in the area even though the population increase of humans and domestic livestock is increasingly affecting the grass cover and soil erosion.

4

100   Figure 1

101   Climatologically the area belongs to the semi-humid region of the Tibetan Plateau

102   subfrigid zone and around 70% of the annual precipitation in this area fall during the wet

103   summer season (June-September) due to the southwest monsoon from the Bay of Bengal (Hu

104   et al. 2011). Thus, the climate of the source region of the Yellow River is greatly influenced

105   by the southwest monsoon and the East Asian summer monsoon (Ding and Chan 2005). The

106   earliest onset of the East Asian summer monsoon occurs in the central and southern

107   Indochina Peninsula. It displays a distinct stepwise northward and northeastward movement

108   and then finally penetrates in to the upper Yellow River from the south of China (Ding and

109   Chan 2005). The effects of atmospheric circulation are in general different for the upper and

110   lower Yellow River. The monsoon rain belt in the upper part is caused by southeasterly flow

111   while the corresponding monsoon rain belt in the lower parts is influenced by southwesterly

112   flow (Qian et al. 2002). This causes differences in spatial distribution of summer precipitation

113   between the two parts of the Yellow River. The upper part is characterized by low-

114   temperatures, sharp day-night temperature contrasts, long-cold and short-warm seasons, and

115   intense sunlight (Liang et al. 2010). The precipitation in the region is generally of low

116   intensity (<50 mm/day), long duration (10-30 days), and covers a large area (>100 000 km^2)

117   (Hu et al. 2011, Zheng et al. 2007). Snowfall is concentrated from November to March, when

118   more than 78% of the total precipitation falls as snow. However, total amount of annual

119   snowfall accounts for less than 10% of the annual (Hu et al. 2011). The potential evaporation

120   is 1300-1400 mm/year (Liang et al. 2010) .

121   Monthly precipitation data from 1961 to 2010 collected from ten meteorological stations

122   (Fig. 1); Xinghai, Tongde, Zeku, Henan, Maduo, Dari, Jiuzhi, Maqu, Ruoergai, and

123   Hongyuan, were obtained from the China Meteorological Administration (CMA). The data

124   quality has previously been checked by the CMA. The Shuttle Radar Topography Mission

(SRTM) 90 m digital elevation data were downloaded from the Consortium for Spatial Information (CGIAR-CSI). Global monthly climate indices data representing teleconnection patterns, including North Atlantic Oscillation (NAO), East Atlantic Pattern (EA), West Pacific Pattern (WP), Pacific/North American Pattern (PNA), East Atlantic/West Russia Pattern (EA/WR), India Ocean Dipole (IOD), EL Nino-Southern Oscillation (NINO3.4), Scandinavia Pattern (SCA), Polar/Eurasia Pattern (POL) and Pacific Decadal Oscillation (PDO), were obtained from the National Weather Service, Climate Prediction Centre (NOAA). Further explanation of each teleconnection pattern is described here (Washington et al. 2000, Barnston and Livezey 1987).

Methods

Principal component analysis (PCA) and singular value decomposition (SVD) were used to find relationships between precipitation in the source region of the Yellow River and teleconnection patterns using climate indices. PCA is a multivariate data analysis tool that offers a way to present complex data in a simplified way to identify relations between different parameters. It maximizes variance explained by weighted sum of elements in two or more fields and identifies linear transformations of the dataset that concentrate as much of the variance as possible into a small number of variables (Rana et al. 2012, Uvo 2003). The PCA biplot is used to visualize the magnitude and sign of each variable's contribution to the first two principal components, and how each observation is represented in terms of those components.

SVD is performed on the cross-covariance matrix of fields of two datasets and isolates the combinations of variables with the fields that tend to be linearly related to one another by maximizing the covariance between them (Rana et al. 2012, Wallace et al. 1992). Here, SVD was conducted on the cross-covariance matrix of the climate indices and precipitation data sets for three homogenous precipitation zones. The SVD of the cross-covariance matrix of

150　two fields yields two matrices of singular vectors and one set of singular values. A singular

151　vector pair describes spatial patterns for each field which have overall covariance given by

152　the corresponding singular value (Uvo et al. 1998). Heterogeneous correlation maps of the

153　left and right fields from SVD show correlation coefficients between the values of one field

154　and the singular vector of the other field (Uvo et al. 1998). In our case, the patterns shown by

155　the heterogeneous correlation maps for the kth SVD expansion mode indicate how well the

156　pattern of the precipitation anomalies relate to the kth singular vector of climate indices. The

157　correlation coefficients are a good indication of strength of the relationship between the two

158　fields. A detailed procedure for this statistical test can be found here (Bretherton et al. 1992,

159　Wallace et al. 1992).

160　　A back propagation neural network was applied for predicting summer precipitation in

161　the source region of the Yellow River using the significantly correlated global climate indices.

162　ANN is a powerful tool for prediction of meteorological phenomena involving many complex

163　and nonlinear physical processes (Hartmann et al. 2008, Sahai et al. 2003, Uvo et al. 2000,

164　Yasuda et al. 2009). The significantly correlated global climate indices were used as input

165　variables, and the summer precipitation (June-September) in the source region of the Yellow

166　River will be used as output variable in the ANN. The architecture of the neural network is

167　determined by a 'trial and error' approach. Two hidden layers were placed between the input

168　and output layers. The function 'tansig' in Matlab was used for this purpose. The four-layer

169　ANN was connected by weights. A training period (1961-1995) and a validation period

170　(1996-2010) were selected for optimization of the weights.

RESULTS

172 **Precipitation characteristics**

173 Due to the large and diverse topography of the area, the precipitation in the source region of

174 the Yellow River shows great spatial and temporal variability. It has a strongly increasing

175 gradient from the northwest part with approximately 309 to 755 mm/year in the southeast,

176 and the topographical gradient of rainfall and the annual rainfall variability are greatly

177 influenced by the southeasterly summer monsoon flow (Yuan et al. 2015a). In order to

178 identify the precipitation spatial variability in the source region of the Yellow River, cluster

179 analysis was performed to separate the precipitation stations into homogeneous regions using

180 monthly precipitation data from 1961 to 2010 (Yuan et al. 2015b). Fig. 2 shows the outcome

181 of this analysis and that the region can be divided into three homogeneous areas. The

182 precipitation stations were thus divided into three zones, namely, 1: Xinghai, Tongde, and

183 Maduo; 2: Zeku, Henan, and Dari, and 3: Jiuzhi, Maqu, Ruoergai, and Hongyuan.

184   Figure 2

185   The linear trends for annual precipitation were quantified using the Mann-Kendall test

186 (Table 1, Fig. 3). As seen from Table 1 and Fig. 3, mean annual precipitations for the three

187 different zones are 365, 517.9, and 692.4 mm/year for zone 1, zone 2, and zone 3,

188 respectively. Zone 1 had a non-significantly increasing trend with 0.24 mm/year during 1961

189 to 2010. On the contrary, both zone 2 and 3 had significantly decreasing annual precipitation.

190 The decrease was 1.49 and 1.79 mm/year for zone 2 and zone 3, respectively. The mean

191 annual precipitation decrease for the whole area is approximately 0.6 mm/year. Previous

192 studies have indicated a small but a statistically non-significant trend for precipitation in the

193 source region of the Yellow River (Liu and Zheng 2004, Tang et al. 2008, Zheng et al. 2007).

194 However, dividing the area into homogeneous zones displays clear differences in

195 precipitation characteristics and a clearer picture of the spatially dependent trend. This trend

196   is the strongest for the wettest area of the source region and then gradually decreases with

197   decreasing annual precipitation.

198   Table 1

199   Figure 3

200   **Relationships between precipitation and teleconnection patterns**

201   The precipitation for three identified homogeneous zones in the source region of the Yellow

202   River was tested for relation against different climate indices using PCA and SVD. Monthly

203   precipitation and monthly climate indices for the same period from 1961 to 2010 were used

204   for analysis. PCA revealed a close relationship that is direct or inverse between the

205   precipitation for three zones and climate indices. The first two modes of PCA were analysed

206   as they represent a major variance. Fig. 4 gives the PCA biplot, and it is seen that the

207   precipitation for the three zones is in general represented in the first PCA mode. It is

208   positively related to NAO, WP and NINO3.4, and it is negatively related to POL. The PCA

209   analysis shows strong evidences that the precipitation in different zones is closely related to

210   different teleconnection patterns.

211   Figure 4

212   SVD was applied to the cross-variance matrix between monthly precipitation for the

213   three zones and monthly climate indices for the same period from 1961 to 2010. Fig.5

214   presents the time series of precipitation for the different zones and climate indices in the first

215   mode of SVD with explained variance of 84.5%. A similar variation shows that precipitation

216   for different zones is closely related to the teleconnection patterns. Table 2 shows the

217   heterogeneous correlation for the different indices. It is noteworthy that the precipitation for

218   the three zones is positively related to NAO, WP and NINO3.4, and negatively related to

9

219 POL at 0.05 significance level. The result of SVD confirms the relationship from the PCA

220 results between precipitation for the three zones and climate indices.

221   Table 2

222   Figure 5

223 **Summer precipitation prediction**

224 Based on the revealed relationships between precipitation in the source region of the Yellow

225 River and global teleconnection patterns, a back propagation neural network was developed

226 to predict the summer precipitation (June-September) using significantly correlated climate

227 indices as input layer, including NAO, WP, POL and NINO3.4. One limitation of ANN

228 analysis is that the model results vary depending on the random setting of the initial weights.

229 Therefore, the neural network model run for one experiment was repeated ten times. The

230 predicted summer precipitation refers to the most accurate results of ten model runs. Here, a

231 'trial and error' process was used to choose different nodes for the two hidden layers. Table 3

232 shows the Pearson correlation coefficients between observed and predicted summer

233 precipitations for training and validation period. The correlation coefficients for the

234 validation period are generally larger than 0.6. Fig.6 shows the observed and predicted

235 summer precipitation for the validation period and the different zones and the whole area.

236   Table 3

237   Figure 6

238 **DISCUSSION AND CONCLUSIONS**

239 In this study, the spatial variability of precipitation was investigated based on the results from

240 cluster analysis using monthly precipitation data from 1961 to 2010. Subdivision of the

241 source region of the Yellow River into three homogeneous zones was made to investigate

spatial variability of trends. PCA and SVD were used to find relationships between the precipitation in the source region of the Yellow River and global teleconnection patterns using climate indices. The summer precipitation was predicted based on the revealed relationships using an ANN. The precipitation trend varies at different stations due to the temporal and spatial variation. The PCA analysis revealed relationships between some of these climate indices and precipitation. The first two modes of PCA were analysed since they can readily be associated to teleconnection patterns. The results showed that precipitation is positively related to the North Atlantic Oscillation, West Pacific and El Nino Southern Oscillation and negatively related to the Polar Eurasian teleconnection. SVD was applied to the cross-covariance matrix between precipitation and climate indices. The results of SVD confirmed the relationship from the PCA. An ANN model was used to predict the summer precipitation in the source region of the Yellow River. The Pearson correlation coefficients between the predicted summer precipitation and observed summer precipitation are generally larger than 0.6. Thus, it is shown that significantly correlated climate indices can be used to predict the summer precipitation.

The revealed results in this study showed that ENSO, NAO, WP and POL events have an influence on the precipitation in the source region of the Yellow River. Xu et al. (2007) found that the La Nina phase corresponds to a relatively rainier season in the Yellow River basin. Fu et al. (2013) examined the trend and variability of extreme rainfall events in China and found that it is mainly influenced by ENSO and the magnitude of East Asian monsoon. Yuan et al. (2015b) examined the summer precipitation in the source region of the Yellow River teleconnections with global sea surface temperatures, and found that higher sea surface temperature in equatorial Pacific areas corresponding to El Nino coincides with less summer precipitation. Cuo et al. (2012) showed that precipitation change in winter at northern Tibetan Plateau can be attributed to changes in the East Asian westerly jet, North Atlantic Oscillation

11

and ENSO. Zhang et al. (2013) also examined that the warm phase of the North Atlantic SST is related to North Atlantic Oscillation that leads to less precipitation or more frequent droughts in the semi-arid subarea in the upper reaches of the Yellow River. Liu et al. (2015) found that NAO greatly controls the variability of summer precipitation between the northeastern and the southeastern Tibetan Plateau by modifying the atmospheric circulation over and around the Tibetan Plateau. During the positive phase of the NAO, warm moist air from the oceans around Asian is transported by the southeastern flank of the anticyclone anomaly over East Asian to the northeastern Tibetan Plateau, and this northward-moving warm moist air encounters cold air masses transported by the northwestern flank of the cyclonic anomaly over the northeastern Tibetan Plateau (Liu et al. 2015). This confluence of the cold and warm air masses subsequently strengthens cumulus convective activities and ultimately results in excessive precipitation over the northeastern Tibetan Plateau. Research showed that the strong positive and negative West Pacific patterns are related to the east-west and north-south movements of the East Asian jet stream, indicating that the change from cold to warm season results from the northward movement of the East Asian jet stream and thus affects aspects of the East Asian climate such as precipitation and temperature (Choi and Moon 2012, Barnston and Livezey 1987). Yan (2002) found that POL was positively associated with winter precipitation in China, indicating the significane of the winter monsoon in producing rainfall pattern. Lin (2014) showed that the POL has negative correlation with precipitation in North China.

Improving the knowledge regarding the relationship between precipitation in the source region of the Yellow River and global teleconnection patterns have important implications for water management. We also conclude that there is sufficient evidence to support the suitability of significantly correlated climate indices as predictors of summer precipitation in

the source region of the Yellow River. The results are useful for integrated water resources management in the Yellow River basin.

REFERENCES

Barnston, A. G. and Livezey, R. E. 1987. Classification, Seasonality and Persistence of Low-Frequency Atmospheric Circulation Patterns. *Monthly Weather Review,* 115(6), 1083-1126.

Bretherton, C. S., Smith, C. and Wallace, J. M. 1992. An Intercomparison of Methods for Finding Coupled Patterns in Climate Data. *Journal of Climate,* 5(6), 541-560.

Chan, J. C. L. and Shi, J. E. 1999. Prediction of the summer monsoon rainfall over South China. *International Journal of Climatology,* 19(11), 1255-1265.

Choi, K.-S. and Moon, I.-J. 2012. Influence of the Western Pacific teleconnection pattern on Western North Pacific tropical cyclone activity. *Dynamics of Atmospheres and Oceans,* 57(0), 1-16.

Cong, Z. T*., et al.* 2009. Hydrological trend analysis in the Yellow River basin using a distributed hydrological model. *Water Resources Research,* 45.

Cuo, L*., et al.* 2012. Climate Change on the Northern Tibetan Plateau during 1957–2009: Spatial Patterns and Possible Mechanisms. *Journal of Climate,* 26(1), 85-109.

Ding, Y. H. and Chan, J. C. L. 2005. The East Asian summer monsoon: an overview. *Meteorology and Atmospheric Physics,* 89(1-4), 117-142.

Feng, J., Yu, L. and Hu, D. 2013. Influence of Indian Ocean subtropical dipole on spring rainfall over China. *International Journal of Climatology*, n/a-n/a.

315   Fu, G*., et al.* 2007. Impacts of climate variability on stream-flow in the Yellow River.
316   *Hydrological Processes,* 21(25), 3431-3439.

317   Fu, G*., et al.* 2013. Temporal variation of extreme rainfall events in China, 1961–2009.
318   *Journal of Hydrology,* 487(0), 48-59.

319   Hartmann, H., Becker, S. and King, L. 2008. Predicting summer rainfall in the Yangtze River
320   basin with neural networks. *International Journal of Climatology,* 28(7), 925-936.

321   Hu, Y. R., Maskey, S. and Uhlenbrook, S. 2012. Trends in temperature and rainfall extremes
322   in the Yellow River source region, China. *Climatic Change,* 110(1-2), 403-429.

323   Hu, Y. R*., et al.* 2011. Streamflow trends and climate linkages in the source region of the
324   Yellow River, China. *Hydrological Processes,* 25(22), 3399-3411.

325   Jiang, P*., et al.* 2013. How well do the GCMs/RCMs capture the multi-scale temporal
326   variability of precipitation in the Southwestern United States? *Journal of Hydrology,*
327   479, 75-85.

328   Lü, A*., et al.* 2011. El Niño-Southern Oscillation and water resources in the headwaters
329   region of the Yellow River: links and potential for forecasting. *Hydrol. Earth Syst.*
330   *Sci.,* 15(4), 1273-1281.

331   Lau, K. M. and Weng, H. 2001. Coherent Modes of Global SST and Summer Rainfall over
332   China: An Assessment of the Regional Impacts of the 1997–98 El Niño. *Journal of*
333   *Climate,* 14(6), 1294-1308.

334   Leathers, D. J., Yarnal, B. and Palecki, M. A. 1991. The Pacific North-American
335   Teleconnection Pattern and United-States Climate .1. Regional Temperature and
336   Precipitation Associations. *Journal of Climate,* 4(5), 517-528.

337   Liang, S*., et al.* 2010. Can climate change cause the Yellow River to dry up? *Water*
338   *Resources Research,* 46(2), n/a-n/a.

339   Lin, Z. 2014. Intercomparison of the impacts of four summer teleconnections over Eurasia on

340   East Asian rainfall. *Advances in Atmospheric Sciences,* 31(6), 1366-1376.

341   Liu, C. M. and Zheng, H. X. 2004. Changes in components of the hydrological cycle in the

342   Yellow River basin during the second half of the 20th century. *Hydrological*

343   *Processes,* 18(12), 2337-2345.

344   Liu, H.*, et al.* 2015. Impact of the North Atlantic Oscillation on the Dipole Oscillation of

345   summer precipitation over the central and eastern Tibetan Plateau. *International*

346   *Journal of Climatology*, n/a-n/a.

347   Lorenzo, M. N., Taboada, J. J. and Gimeno, L. 2008. Links between circulation weather types

348   and teleconnection patterns and their influence on precipitation patterns in Galicia

349   (NW Spain). *International Journal of Climatology,* 28(11), 1493-1505.

350   Peng, J., Yu, Z. and Gautam, M. R. 2013. Pacific and Atlantic Ocean influence on the

351   spatiotemporal variability of heavy precipitation in the western United States. *Global*

352   *and Planetary Change,* 109(0), 38-45.

353   Qian, W., Kang, H. S. and Lee, D. K. 2002. Distribution of seasonal rainfall in the East Asian

354   monsoon region. *Theoretical and Applied Climatology,* 73(3-4), 151-168.

355   Rana, A.*, et al.* 2012. Trend analysis for rainfall in Delhi and Mumbai, India. *Climate*

356   *Dynamics,* 38(1-2), 45-56.

357   Redmond, K. T. and Koch, R. W. 1991. Surface Climate and Streamflow Variability in the

358   Western United-States and Their Relationship to Large-Scale Circulation Indexes.

359   *Water Resources Research,* 27(9), 2381-2399.

360   Sahai, A. K.*, et al.* 2003. Teleconnections in recent time and prediction of Indian summer

361   monsoon rainfall. *Meteorology and Atmospheric Physics,* 84(3-4), 217-227.

362   Tang, Q. H.*, et al.* 2008. Hydrological cycles change in the Yellow River basin during the last

363   half of the twentieth century. *Journal of Climate,* 21(8), 1790-1806.

364   Uvo, C. B. 2003. Analysis and regionalization of northern european winter precipitation

365   based on its relationship with the North Atlantic oscillation. *International Journal of*

366   *Climatology,* 23(10), 1185-1194.

367   Uvo, C. B*., et al.* 1998. The relationships between tropical Pacific and Atlantic SST and

368   northeast Brazil monthly precipitation. *Journal of Climate,* 11(4), 551-562.

369   Uvo, C. B., Tolle, U. and Berndtsson, R. 2000. Forecasting discharge in Amazonia using

370   artificial neural networks. *International Journal of Climatology,* 20(12), 1495-1507.

371   Venkatesan, C*., et al.* 1997. Prediction of all India summer monsoon rainfall using error-

372   back-propagation neural networks. *Meteorology and Atmospheric Physics,* 62(3-4),

373   225-240.

374   Wallace, J. M., Smith, C. and Bretherton, C. S. 1992. Singular Value Decomposition of

375   Wintertime Sea-Surface Temperature and 500-Mb Height Anomalies. *Journal of*

376   *Climate,* 5(6), 561-576.

377   Wang, B., Wu, R. G. and Fu, X. H. 2000. Pacific-East Asian teleconnection: how does ENSO

378   affect East Asian climate? *Journal of Climate,* 13(9), 1517-1536.

379   Wang, H. J*., et al.* 2006. Interannual and seasonal variation of the Huanghe (Yellow River)

380   water discharge over the past 50 years: Connections to impacts from ENSO events

381   and dams. *Global and Planetary Change,* 50(3-4), 212-225.

382   Washington, R*., et al.* 2000. Northern Hemisphere teleconnection indices and the mass

383   balance of Svalbard glaciers. *International Journal of Climatology,* 20(5), 473-487.

384   Xu, Z. X*., et al.* 2007. Long-term trend of precipitation in China and its association with the

385   El Nino-southern oscillation. *Hydrological Processes,* 21(1), 61-71.

386   Yan, Y. Y. 2002. Temporal and Spatial Patterns of Seasonal Precipitation Variability in

387   China, 1951-1999. *Physical Geography,* 23(4), 281-301.

388   Yasuda, H., *et al.* 2009. Prediction of Chinese Loess Plateau summer rainfall using Pacific
389   Ocean spring sea surface temperature. *Hydrological Processes,* 23(5), 719-729.

390   Yuan, F., *et al.* 2015a. Hydro Climatic Trend and Periodicity for the Source Region of the
391   Yellow River. *Journal of Hydrologic Engineering,* 0(0), 05015003.

392   Yuan, F., *et al.* 2015b. Regional Sea Surface Temperatures Explain Spatial and Temporal
393   Variation of Summer Precipitation in the Source Region of the Yellow River.
394   *Hydrological Sciences Journal*.

395   Zhang, J., *et al.* 2013. Decadal variability of droughts and floods in the Yellow River basin
396   during the last five centuries and relations with the North Atlantic SST. *International*
397   *Journal of Climatology,* 33(15), 3217-3228.

398   Zheng, H. X., *et al.* 2007. Changes in stream flow regime in headwater catchments of the
399   Yellow River basin since the 1950s. *Hydrological Processes,* 21(7), 886-893.

400   Zheng, H. X., *et al.* 2009. Responses of streamflow to climate and land surface change in the
401   headwaters of the Yellow River Basin. *Water Resources Research,* 45.

402

403

404

405

406

407

408

409   Table 1: Linear precipitation trends and Mann-Kendall statistics (Z); NS: no significant trend;

410   * is statistical significance at the 0.05 level.

Region	Mean annual precipitation (mm/year)	Min. annual precipitation (mm/year)	Max. annual precipitation (mm/year)	Linear trend (mm/year)	Mann-Kendall trend
Zone 1	365.0	247.9	522.5	0.24	NS
Zone 2	517.9	337.3	738.5	-1.49	*
Zone 3	692.4	533.9	860.5	-1.79	*
Whole area	515.3	406.0	645.8	-0.60	NS

411

412

413   Table 2 Heterogeneous correlation between precipitation and climate indices

	Zone1	Zone 2	Zone3	NAO	EA	WP	PNA	EA/WR	SCA	POL	PDO	NINO3.4	IOD
Mode 1	**-0.25**	**-0.25**	**-0.23**	**-0.16**	0.01	**-0.17**	-0.05	-0.06	-0.02	**0.10**	-0.04	**-0.11**	-0.02
Mode 2	0.04	-0.01	-0.03	0.04	0.05	-0.04	0.00	0.05	**0.10**	0.05	0.01	0.02	0.02

414   Values in bold are statistically significant at the 0.05 level

415

416   Table 3 ANN results for different areas

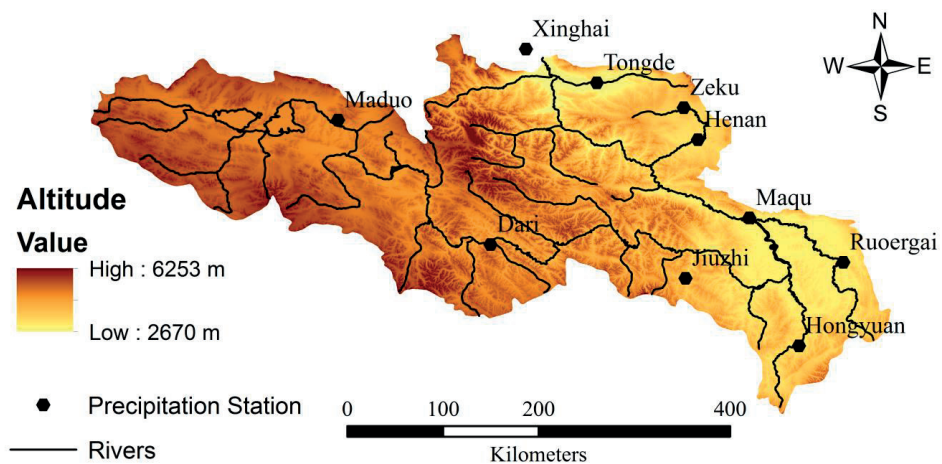| Period	Zone 1	Zone 2	Zone 3	Whole area
Training	0.90	0.82	0.97	0.86
Validation	0.60	0.68	0.62	0.61

417

418

419   Fig. 1. The Yellow River source region topography, river network and precipitation stations.
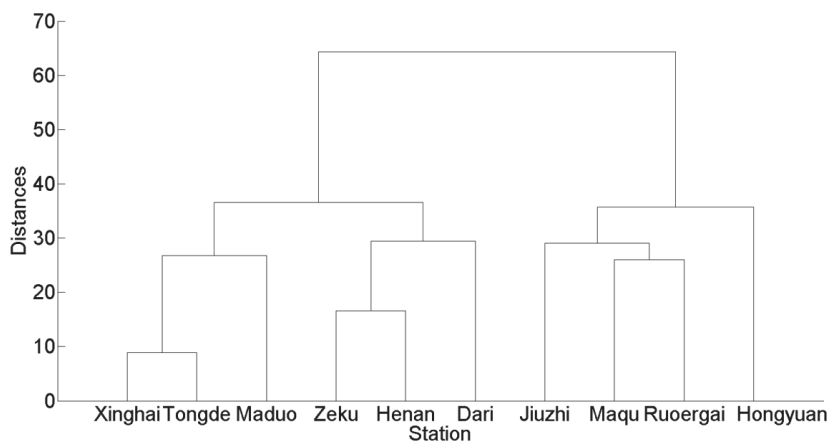
420

421

422   Fig. 2 Results from cluster analysis in the source region of the Yellow River(Yuan et al.
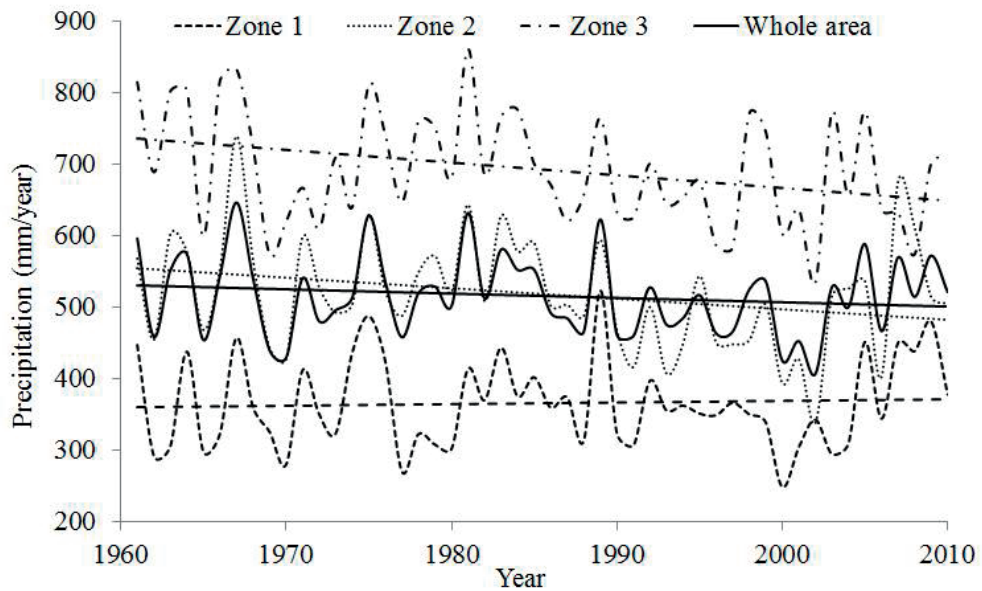
423   2015b).

424

425

Fig. 3 Annual precipitation from 1961 to 2010 for the three different zones and the whole
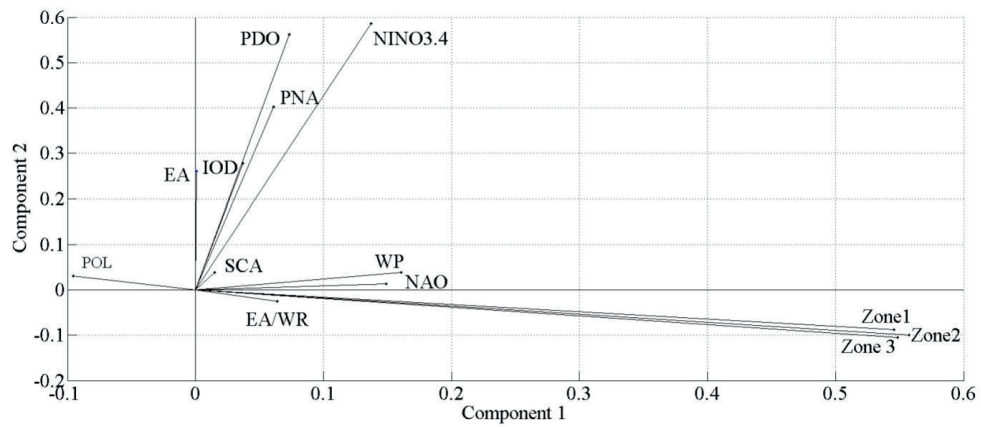
area in the source region of the Yellow River

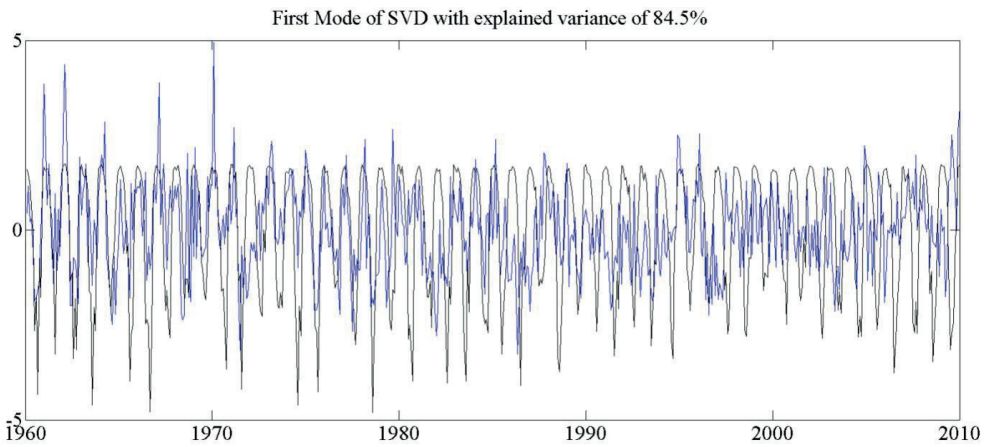428

429

430   Fig. 4 Biplot from the first two modes of PCA

431

First Mode of SVD with explained variance of 84.5%

432

433   Fig. 5 Time series of predictor (monthly precipitation) and predictant (monthly climate

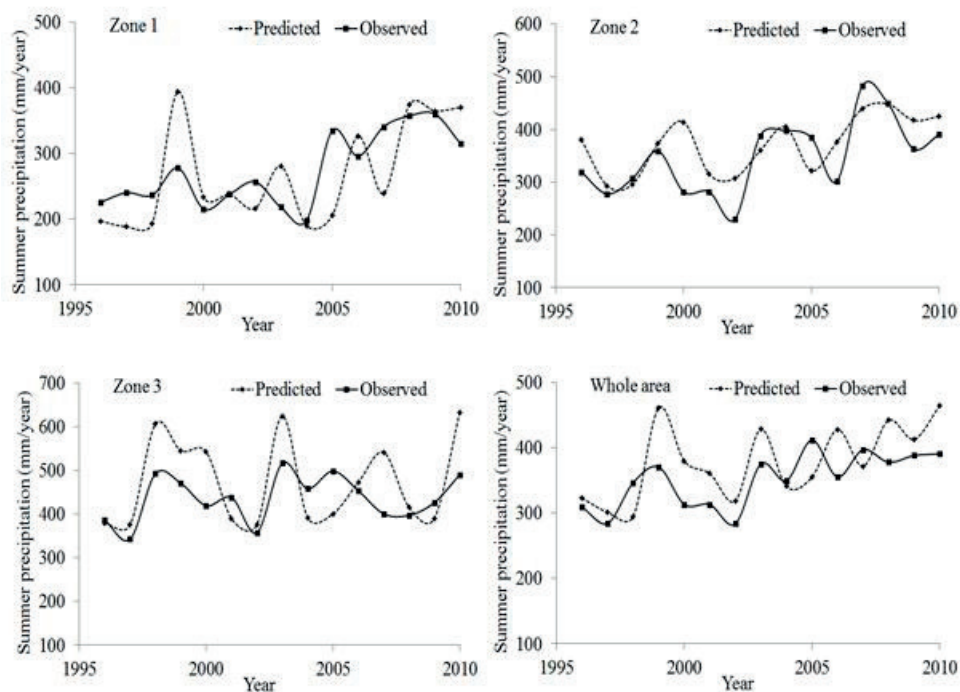434   indices) in the first mode of SVD.

435

436
437 Fig. 6 Observed and predicted summer precipitation for the validation period for the different

438 zones and the whole area

Paper IV

Modelling daily rainfall-runoff in the source region of the Yellow River using the Xinanjiang model

Feifei Yuan[1], Ronny Berndtsson[2], Lu Wang[3] and Linus Zhang[1]

[1]Department of Water Resources Engineering, Lund University, Box 118, SE-221 00 Lund, Sweden

Feifei.yuan@tvrl.lth.se

[2]Department of Water Resources Engineering and Center for Middle Eastern Studies, Lund University, Box 118, SE-221 00 Lund, Sweden

[3]Faculty of Civil Engineering and Geosciences, Delft University of Technology, Delft, Netherlands

Abstract The declining water availability caused by climate change in the source region of the Yellow is expected to have severe repercussions for the 110 million basin inhabitants. Thus, there is an urgent need to improve the understanding of the hydrological processes in the basin for integrated water resources management. In this respect, the performance of the Xinanjiang model for daily rainfall-runoff simulation in the source region of the Yellow River was evaluated. The Blaney–Criddle method was used to calculate the potential evapotranspiration as model input due to data scarcity of this area. The Monte Carlo method was used to optimize the sensitive model parameters. The resulting Pearson correlation coefficient between observed and simulated runoff for the calibration period was up to 0.87, and 0.85 for the validation period. Accordingly, the Xinanjiang model simulated the daily runoff series well in general. Thus, the Xinanjiang model can be a proper tool for further water resources management involving runoff simulation and flood forecasting in the source region of the Yellow River.

Key words: Rainfall-Runoff relationship; the Xinanjiang model; the source region of the Yellow River;

1 INTRODUCTION

The Yellow River is of immense importance to China. It is 5,464 km long, has a basin area of 752,440 km^2, and is the main source of surface water in northwest and northern China (Tang et al. 2008, Yang et al. 2008). The basin has more than 110 million inhabitants and 12.6 million ha cultivated land, representing about 8 and 13% of the national totals, respectively. The lower Yellow River has increasingly suffered from low-flow conditions and parts of the lower reaches have often been dry during the last 30 years. The situation has been exacerbated during recent years (Liu and Zheng 2004, Sato et al. 2008). The source region of the Yellow River contributes about 35% of the total water yield in the Yellow River basin (Lan et al. 2010). Consequently, it is an extremely important area in terms of water resources affecting agricultural productivity, municipal, and industrial water supply for the whole basin.

Comprehensive hydrological models are expected to be effective tools for flood simulation and forecasting. However, proper runoff simulation is often one of the most challenging tasks in theoretical and operational hydrology due to the lack of hydrologic observations (Yao et al. 2014). Data scarcity or inconsistency for the model input is one of reasons for high uncertainty in hydrological modelling (Sood and Smakhtin 2014). The source region of the Yellow River is an important area for water supply in the entire basin but with limited observational data. Hence, it is essential to evaluate suitable hydrological models in view of data scarcity to investigate the impact of climate change on regional water resources.

Several studies have dealt with the issue of the contribution of climate change to hydrological process in the source region of the Yellow River. Hu et al. (2011) investigated streamflow trends and climate linkages in the source region of the Yellow River during the last 50 years (1959-2008). Liu and Zheng (2004) attempted to detect trends associated with hydrological cycle components in the Yellow River basin using data from 1952 to 1997. Tang et al. (2008) presented an analysis of changes in the spatial patterns of climatic variables in the Yellow River basin from 1960 to 2000. Cong et al. (2009) used a distributed hydrological model to analyze hydrological trends in the Yellow River basin. Several of these studies have reported dwindling streamflow in the Yellow River during the latest years. Yuan et al. (2015) investigated the hydroclimatic trend and periodicity for the source region of the Yellow River. Zhang et al. (2013) reported substantially decreased annual flow of the Yellow River during recent years. However, daily rainfall-runoff relationships for the source region of the Yellow River has not yet been explored. It is important to quantify this relationship and develop

possible quantitative runoff prediction techniques using proper hydrological models. The Xinanjiang model had been widely used and modified to improve runoff prediction (Jayawardena and Zhou 2000, Ju et al. 2009, Li et al. 2009, Lin et al. 2014, Liu et al. 2009, Lu et al. 2013, Mao et al. 2013, Shi et al. 2011, Yang et al. 2011, Yao et al. 2012). In this study, a partly modified Xinanjiang model was applied to the source region of the Yellow River to simulate the rainfall-runoff relationships. The Blaney–Criddle method was used to calculate the potential evapotranspiration for the model input due to data scarcity in this area. The Monte Carlo method was used to optimize the sensitive model parameters.

2 STUDY AREA, DATA AND METHODOLOGY

2.1 Study area and data

The source region of the Yellow River is located on the northeast Qinghai-Tibet Plateau between 32º12´-35º48´N and 95º50´-103º28´E and includes the area upstream the Tangnaihai runoff observation station. The area is 12.2×104 km^2, occupying about 16% of the Yellow River Basin, and it has a great elevation change from 2670 m in the east to 6253 m in the west (Fig. 1). Grassland covers 80% of the catchment and it includes typical alpine swamp, steppe, and shrub meadows. In recent years, the alpine grasslands in this area have suffered from severe degradation (Zhou et al. 2005). The grassland degradation is thought to be a joint effect of long-term overgrazing and climate warming. The area of lakes and swamps is about 2,000 km^2. There is a permanent snowpack and glaciers in the southern Animaqing, Bayankala, and Northern Qilian mountains. The area has a comparably low population density with a total of about half a million inhabitants. The area is therefore regarded as relatively unaffected by human activities (Hu et al. 2011). Neither large irrigation projects nor large dams exist in the area even though the population increase of humans and domestic livestock is increasingly affecting the grass cover and soil erosion.

Climatologically the area belongs to the semi-humid region of the Tibetan Plateau sub-frigid zone and around 70% of the annual precipitation in this area fall during the wet summer season (June-September). The climate of the source region of the Yellow River is greatly influenced by the southwest monsoon and the East Asian summer monsoon (Ding and Chan 2005).The earliest onset of the East Asian summer monsoon occurs in the central and southern Indochina Peninsula. It displays a distinct stepwise northward and northeast-ward movement and then finally penetrates in to the upper Yellow River from the south of China

(Ding and Chan 2005). The effects of atmospheric circulation are in general different for the upper and lower Yellow River. The monsoon rain belt in the upper part is caused by south-easterly flow while the corresponding monsoon rain belt in the lower parts is influenced by south-westerly flow (Qian et al. 2002). This causes differences in spatial distribution of summer precipitation between the two parts of the Yellow River. The upper part of the Yellow River is characterized by low-temperatures, sharp day-night temperature contrasts, long-cold and short-warm seasons, and intense sunlight (Liang et al. 2010). Annual average temperature varies between -4 and 2°C from southeast to northwest. The precipitation in this region is generally of low intensity (<50 mm/day), long duration (10-30 days), and covers a large area (>100,000 km2) (Hu et al. 2011, Zheng et al. 2007). Snowfall is concentrated from November to March, when more than 78% of the total precipitation falls in the form of snow. However, total amount of annual snowfall accounts for less than 10% of the annual precipitation (Hu et al. 2011). The potential evaporation is 1300-1400 mm/year (Liang et al. 2010).
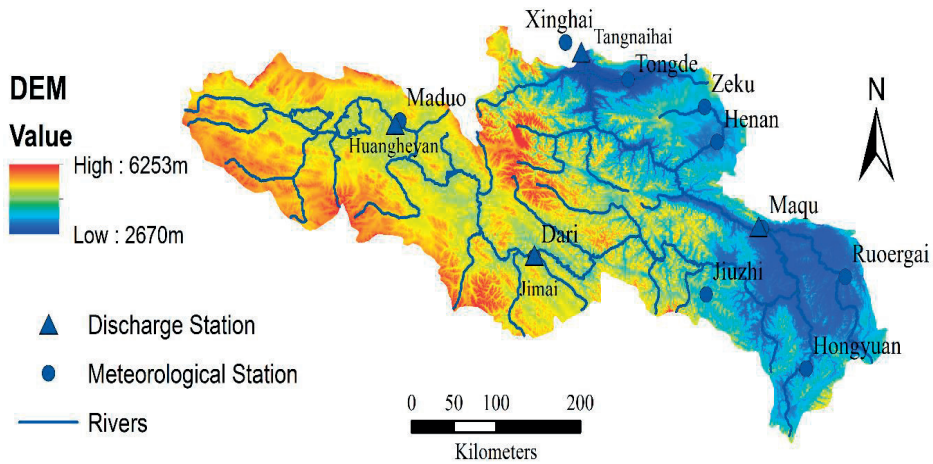

Fig. 1 The Yellow River source region topography, river network and hydroclimatic stations.

Daily precipitation observations from 1961 to 2009 collected at ten meteorological stations (Fig. 1); Xinghai, Tongde, Zeku, Henan, Maduo, Dari, Jiuzhi, Maqu, Ruoergai, and Hongyuan, were obtained from the China Meteorological Administration (CMA). The data quality has previously been checked by the CMA. Daily streamflow data from 1961 to 2009 at Tangnaihai runoff observation station were obtained from the Yellow River Conservancy Commission. The Shuttle Radar Topography Mission (SRTM) 90 m digital elevation data were downloaded from the Consortium for Spatial Information (CGIAR-CSI).

2.2 Methodology

Xinanjiang Model. The Xinanjiang model was originally developed by Zhao (1992). The model applied to the source region of the Yellow River consists of two components: a three-layer evapotranspiration component and a runoff generating component (Fig. 2). The input data are daily precipitation and potential evapotranspiration, and the outputs are discharge and actual evapotranspiration. The model parameters and their ranges are listed in Table 1. The parameters are usually defined by specifying lower and upper limits. These limits are chosen according to physical and mathematical constraints, information about physical characteristics of the system, and from modelling experiences (Cheng et al. 2006).

The evapotranspiration component acts on three vertical layers identified as upper, lower, and deeper soil layers. The upper layer refers to the vegetation, water surface and the very thin topsoil. The lower layer refers to the soil in which the vegetation roots dominate and the moisture transportation is mainly driven by the potential gradient. The deep layer refers to the soil beneath the lower layer where only the deep-rooted vegetation can absorb water and the potential gradient is very small (Jayawardena and Zhou 2000). Evapotranspiration takes place at the potential rate in the upper layer. On exhaustion of moisture content in the upper layer, evapotranspiration proceeds to the lower layer at a decreased rate that is proportional to the moisture content in that layer. Only when the total evapotranspiration in the upper and lower layers is less than a pre-set threshold, represented as a fraction of the potential evapotranspiration, does it further proceed to the deep layer to keep this pre-set minimum value (Jayawardena and Zhou 2000). Evaporation is first subtracted during the rainfall process, and the runoff generation is computed by considering the respective soil moisture states and the storage capacities of the three layers. The runoff is separated into three components: surface runoff, interflow, and groundwater flow. A more detailed conceptual hydrological process description is found in Zhao (1992).

Blaney–Criddle Method. The Blaney–Criddle method has been widely used to calculate the potential evapotranspiration as model input (Xu and Singh 2002, Kingston et al. 2009, Sperna Weiland et al. 2012). It is a temperature-based method that requires temperature as input variable. The Blaney-Criddle equation is:

ET = KP (0.46T +8.13)

where

ET = potential evapotranspiration from a reference crop, in mm, for the period in which p is expressed;

T = mean temperature in °C;

K= monthly consumptive use coefficient, depending on vegetation type, location and season. Here it was taken to be 1.

Table 1. Parameters of the Xinanjiang model. Parameters in bold indicate high sensitivity.

Parameter	Definition	Range
UM (mm)	Soil moisture storage capacity of the upper layer	0-50
LM (mm)	Soil moisture storage capacity of the lower layer	0-150
WM (mm)	Areal mean soil moisture storage capacity	50-300
B	Exponential parameter with a single parabolic curve representing the non-uniformity of the spatial distribution of the soil moisture storage capacity	0-1
IM (%)	Percentage of impervious and saturated areas	0-1
K	Ratio of potential evapotranspiration to pan evaporation	0-2
C	Evapotranspiration coefficient of deeper layer	0-0.5
SM (mm)	Free water capacity of the surface soil layer representing the maximum possible deficit of free water storage	0-200
EX	Exponent of the free water capacity curve influencing the development of the saturated area	0.5-2.5
KG	Outflow coefficient of the free water storage to groundwater flow	0.01-1
KI	Outflow coefficient of the free water storage to interflow	0.01-1
CG	Recession constant of the groundwater storage	0.5-1
CI	Recession constant of the lower interflow storage	0.1-1
CS	Recession constant in the lag and route method for routing through the channel system	0.01-1
L (d)	Lag time for runoff routing period	0-4

P= percentage of total daytime hours for the used period out of total daytime hours of the year; The daylight hours here are based on the calculation of sunset hour angels that depend on the calculation of solar declination. It can be calculated as N=M $(24/\pi)$, where M is the sunset hour angle in radians.

Monte Carlo Method. The process of model calibration is normally performed either manually or by using computer based automatic procedures. In this study, Monte Carlo method was used to generate 10000 sets of the 8 sensitive parameters for calibration. The other 7 parameters were pre-set as initial values and adjusted manually during the calibration process. The parameters for best fit between observed and simulated discharge were used for validation.

Model performance measure. The Pearson product-moment correlation coefficients r between observed and simulated discharge data were used to measure model performance. The normal distribution of observed and simulated discharge data were tested by the Kolmogorov-Smirnov test in Matlab.
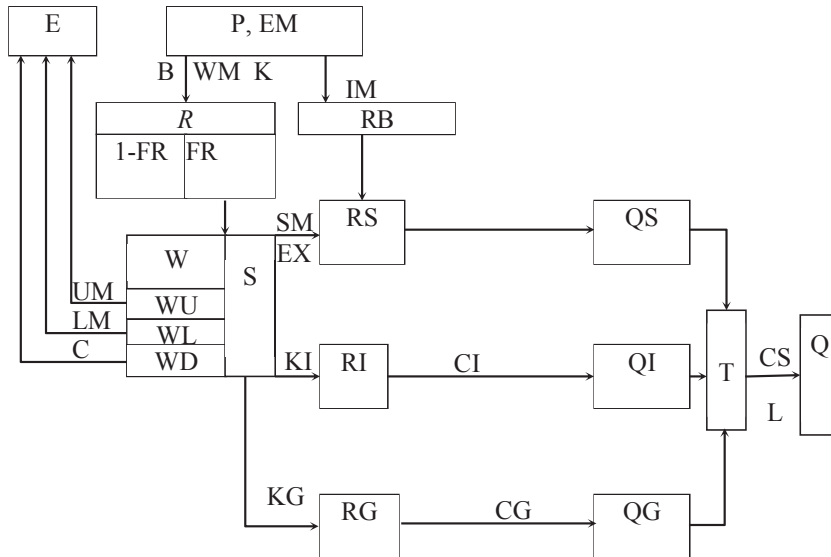

Fig. 2. Flowchart for the Xinanjiang model.

3 RESULTS

Interannual variability in streamflow mainly reflects catchment response to precipitation variability and is an important aspect of the hydrological regime for a catchment. Figure 3 shows the monthly precipitation and runoff depth in the source region of the Yellow River. It

is seen that precipitation in the summer monsoon period (June-September) accounts for about 72% of the annual total. The monthly runoff depth shows dual peaks in July and September. Calibration and validation of the Xinanjiang model for the source region of the Yellow River were carried out using daily rainfall-runoff data. The Thiessen polygon method was used to calculate the daily mean areal precipitation and temperature over the experimental area. The daily discharge at Tangnaihai station was used to evaluate the model results since Tangnaihai station is the outlet of the source region of the Yellow River. The data from 1961 to 1995 were used for calibrating the model and the data from 1996 to 2009 was used for validation. Table 2 shows the results of the calibrated model parameters. According to the table all parameter values are in a reasonable range.
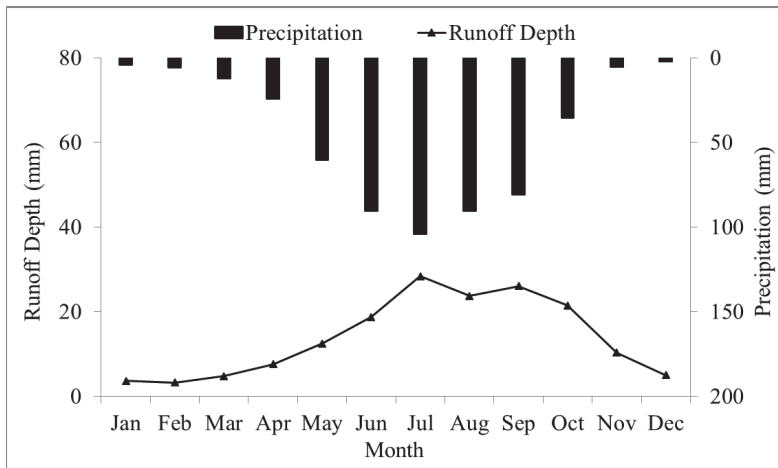

Fig. 3. Monthly precipitation and runoff depth in the source region of the Yellow River from 1961 to 2009

Figure 4 and 5 show the observed and simulated discharge for the catchment during calibration and validation period, respectively. It is seen that the Pearson correlation coefficient for calibration period is 0.87 and 0.85 for validation period. Consequently, in general, the Xinanjiang model simulates the daily runoff series well.

Table 2. Calibrated model parameters.

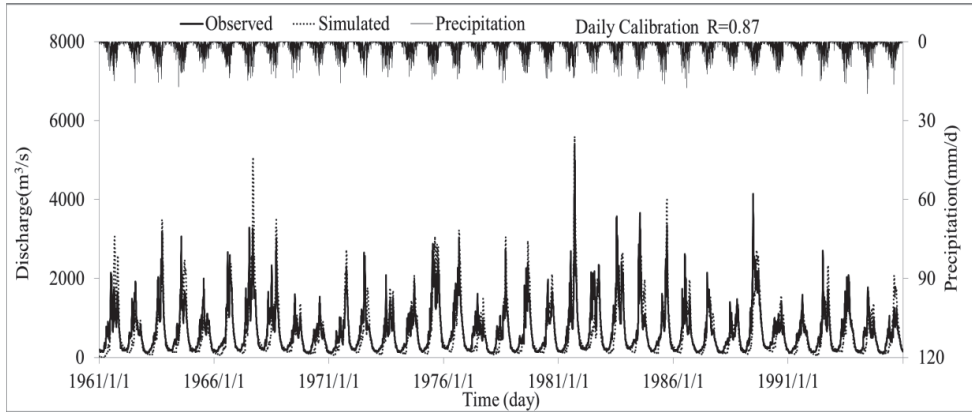| Parameter	K	SM	CS	CI	CG	KG	KI	B	C	EX	IM	L	UM	LM	WM
Value	0.48	193	0.79	0.90	0.99	0.13	0.23	0.5	0.46	1.25	0.01	1	40	100	220

Fig. 4. Observed and simulated discharge for the source region of the Yellow River during calibration period.
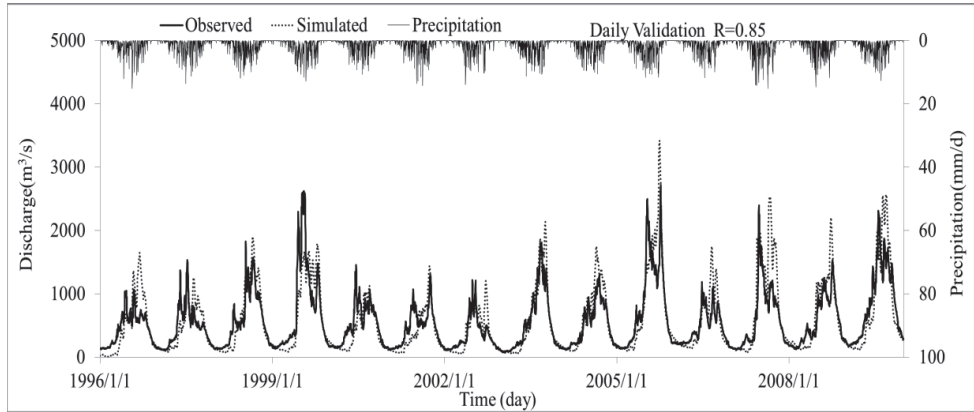

Fig. 5. Observed and simulated discharge for the source region of the Yellow River during the validation period.

4 DISCUSSION AND CONCLUSION

A partly modified Xinanjiang model was applied to the source region of the Yellow River for daily rainfall-runoff simulation. The Blaney–Criddle method was chosen to calculate the potential evapotranspiration for the model input due to data scarcity of this area. Monte Carlo method was used to optimize the sensitive model parameters. The good fit showed that the Xinanjiang model can be used for daily runoff simulation and flood forecasting in the source region of the Yellow River. The magnitude and variation of evaporative losses is required for efficient water resources management. It is, however, difficult to select the most appropriate

evaporation calculation method due to the wide range of data types needed in the various equations (Xu and Singh 2001).The Blaney-Criddle method only requires temperature to estimate the potential evaporation. For data scarce areas this may still be appropriate. The process of model calibration is normally performed either manually or by using computer-based automatic procedures. The process of manual calibration is generally tedious and time consuming (Cheng et al. 2006). Hence, the Monte Carlo method was used for automatic calibration. The investigated results showed that the Xinanjiang model could be a reasonable tool for daily runoff simulation and flood forecasting in the source region of the Yellow River. This has important implications for future water resource management in the Yellow River source region.

REFERENCES

Cheng, C. T*., et al.* 2006. Using genetic algorithm and TOPSIS for Xinanjiang model calibration with a single procedure. *Journal of Hydrology,* 316(1-4), 129-140.

Cong, Z. T*., et al.* 2009. Hydrological trend analysis in the Yellow River basin using a distributed hydrological model. *Water Resources Research,* 45(7), W00A13.

Ding, Y. H. and Chan, J. C. L. 2005. The East Asian summer monsoon: an overview. *Meteorology and Atmospheric Physics,* 89(1-4), 117-142.

Hu, Y. R*., et al.* 2011. Streamflow trends and climate linkages in the source region of the Yellow River, China. *Hydrological Processes,* 25(22), 3399-3411.

Jayawardena, A. W. and Zhou, M. C. 2000. A modified spatial soil moisture storage capacity distribution curve for the Xinanjiang model. *Journal of Hydrology,* 227(1-4), 93-113.

Ju, Q*., et al.* 2009. Division-based rainfall-runoff simulations with BP neural networks and Xinanjiang model. *Neurocomputing,* 72(13-15), 2873-2883.

Kingston, D. G*., et al.* 2009. Uncertainty in the estimation of potential evapotranspiration under climate change. *Geophysical Research Letters,* 36(20), L20403.

Lan, Y. C*., et al.* 2010. Response of runoff in the source region of the Yellow River to climate warming. *Quaternary International,* 226(1-2), 60-65.

Li, H. X*., et al.* 2009. Predicting runoff in ungauged catchments by using Xinanjiang model with MODIS leaf area index. *Journal of Hydrology,* 370(1-4), 155-162.

Liang, S*., et al.* 2010. Can climate change cause the Yellow River to dry up? *Water Resources Research,* 46(2), n/a-n/a.

Lin, K. R., Lian, Y. Q. and He, Y. H. 2014. Effect of Baseflow Separation on Uncertainty of Hydrological Modeling in the Xinanjiang Model. *Mathematical Problems in Engineering.*

Liu, C. M. and Zheng, H. X. 2004. Changes in components of the hydrological cycle in the Yellow River basin during the second half of the 20th century. *Hydrological Processes,* 18(12), 2337-2345.

Liu, J. T*., et al.* 2009. Coupling the Xinanjiang model to a kinematic flow model based on digital drainage networks for flood forecasting. *Hydrological Processes,* 23(9), 1337-1348.

Lu, H. S*., et al.* 2013. The streamflow estimation using the Xinanjiang rainfall runoff model and dual state-parameter estimation method. *Journal of Hydrology,* 480, 102-114.

Mao, Y. Y., Zhang, X. G. and Li, Z. J. 2013. Coupled Simulation of Xinanjiang Model with MODFLOW. *Journal of Hydrologic Engineering,* 18(11), 1443-1449.

Qian, W., Kang, H. S. and Lee, D. K. 2002. Distribution of seasonal rainfall in the East Asian monsoon region. *Theoretical and Applied Climatology,* 73(3-4), 151-168.

Sato, Y*., et al.* 2008. Analysis of long-term water balance in the source area of the Yellow River basin. *Hydrological Processes,* 22(11), 1618-1629.

Shi, P*., et al.* 2011. Evaluating the SWAT Model for Hydrological Modeling in the Xixian Watershed and a Comparison with the XAJ Model. *Water Resources Management,* 25(10), 2595-2612.

Sood, A. and Smakhtin, V. 2014. Global hydrological models: a review. *Hydrological Sciences Journal,* 60(4), 549-565.

Sperna Weiland, F. C*., et al.* 2012. Selecting the optimal method to calculate daily global reference potential evaporation from CFSR reanalysis data for application in a hydrological model study. *Hydrol. Earth Syst. Sci.,* 16(3), 983-1000.

Tang, Q*., et al.* 2008. A spatial analysis of hydro-climatic and vegetation condition trends in the Yellow River basin. *Hydrological Processes,* 22(3), 451-458.

Xu, C. Y. and Singh, V. P. 2001. Evaluation and generalization of temperature-based methods for calculating evaporation. *Hydrological Processes,* 15(2), 305-319.

Xu, C. Y. and Singh, V. P. 2002. Cross Comparison of Empirical Equations for Calculating Potential Evapotranspiration with Data from Switzerland. *Water Resources Management,* 16(3), 197-219.

Yang, S. T*., et al.* 2011. Coupling Xinanjiang model and SWAT to simulate agricultural non-point source pollution in Songtao watershed of Hainan, China. *Ecological Modelling,* 222(20-22), 3701-3717.

Yang, T*., et al.* 2008. A spatial assessment of hydrologic alteration caused by dam construction in the middle and lower Yellow River, China. *Hydrological Processes,* 22(18), 3829-3843.

Yao, C*., et al.* 2012. A priori parameter estimates for a distributed, grid-based Xinanjiang model using geographically based information. *Journal of Hydrology,* 468, 47-62.

Yao, C*., et al.* 2014. Improving the flood prediction capability of the Xinanjiang model in ungauged nested catchments by coupling it with the geomorphologic instantaneous unit hydrograph. *Journal of Hydrology,* 517, 1035-1048.

Yuan, F*., et al.* 2015. Hydro Climatic Trend and Periodicity for the Source Region of the Yellow River. *Journal of Hydrologic Engineering,* 0(0), 05015003.

Zhang, Q., Singh, V. P. and Li, J. F. 2013. Eco-Hydrological Requirements in Arid and Semiarid Regions: Case Study of the Yellow River in China. *Journal of Hydrologic Engineering,* 18(6), 689-697.

Zhao, R. J. 1992. The Xinanjiang Model Applied in China. *Journal of Hydrology,* 135(1-4), 371-381.

Zheng, H. X*., et al.* 2007. Changes in stream flow regime in headwater catchments of the Yellow River basin since the 1950s. *Hydrological Processes,* 21(7), 886-893.

Zhou, H*., et al.* 2005. Alpine grassland degradation and its control in the source region of the Yangtze and Yellow Rivers, China. *Grassland Science,* 51(3), 191-203.